Federal State Autonomous Educational Institution for Higher Education
« Peoples' Friendship University of Russia »

As a manuscript

MARYAM BAYAT

BIOSYNTHESIS AND CHARACHTERIZATION OF NANOPARTICLES AND EVALUATING THEIR PROSPECTIVE BIOTECHNOLOGICAL APPLICATIONS

Specialties: 4.1.3. Agrochemistry, agrosoil science, plant protection and quarantine; 1.5.6. Biotechnology

Thesis for the degree of candidate of biological sciences

Scientific supervisor:

Astarkhanova Tamara
Doctor of Agricultural Science, Professor, RUDN

Moscow 2022

ФЕДЕРАЛЬНОЕ ГОСУДАРСТВЕННОЕ АВТОНОМНОЕ
ОБРАЗОВАТЕЛЬНОЕ УЧРЕЖДЕНИЕ ВЫСШЕГО ОБРАЗОВАНИЯ
«РОССИЙСКИЙ УНИВЕРСИТЕТ ДРУЖБЫ НАРОДОВ» РУДН

На правах рукописи

МАРЬЯМ БАЯТ

БИОСИНТЕЗ И ХАРАКТЕРИСТИКА НАНОЧАСТИЦ И ОЦЕНКА ИХ ПЕРСПЕКТИВНОГО БИОТЕХНОЛОГИЧЕСКОГО ПРИМЕНЕНИЯ

Специальность: 4.1.3. Агрохимия, агропочвоведение, защита и карантин растений; 1.5.6. Биотехнология

диссертации на соискание ученой степени
кандидата биологических наук

Научный руководитель:

Астарханова Тамара Саржановна
профессор, доктор сельскохозяйственных наук,
профессор АТИ РУДН

Москва 2022

Table of Contents

INTRODUCTION

The relevance of research. Cultivation of cereal crops are associated with high risks of bacterial and fungal disease. Infection with different plant pathogens, significantly decreases the quality of cereal crops in agricultural systems. Plant pathogens accumulate in a latent form over several generations, which causes serious crop losses. Since, the new and modern strategy such as nontechnique will promote protecting crops against different plant diseases. Synthesis of metal-based nanoparticles (NPs) mainly mediates by physical or chemical methods. Physical methods need expensive equipment, high energy and large space area allocating for equipment. Chemical methods need costly and toxic chemicals, which may remain in the synthesized NPs and limit their application due to the toxicity of harmful residues. The use of chemicals is environmentally unfriendly and also hazardous for the person who deals with. To mitigate the problem of expensive equipment and toxic chemicals, green methods have been developed rapidly, presenting facile and cost-effective biosynthesis approaches [1].

Plant parts are the most preferred biosystem for this purpose as they contain exclusive phytochemicals which can participate in the reduction process during the biosynthesis of NPs. The rate of NP biosynthesis in plants is higher than in microorganisms; the obtained NPs would be more stable and diverse in size and shape [1]. Based on this, we used strawberry leaves as an economical material from agricultural waste to prepare an aqueous extract and use it for green synthesis of various NPs. There are no data in the literature on the use of strawberry leaves in green synthesis of NPs. After the biosynthesis of NPs, we studied their physical and chemical properties. To determine the positive or negative effect of biosynthesized NPs on plants, we chose two crops with a seed type of reproduction: wheat as the most demanded food crop and flax as the main industrial crop. Also, the task of our research was to evaluate the antimicrobial activity of biosynthesized NPs for

subsequent use as non-chemical plant protection products in the greening of agricultural production.

The degree of development of the topic. Plants are the most preferred source for biosynthesis of NPs because plant parts containing exclusive phytochemicals involve in reduction process of NPs biosynthesis. The rate of the biosynthesis in plant-mediated methods are more than microorganism-oriented one and the produced NPs are more stable and also more diverse in their size and shape. Plant extracts are widely applied in green synthesis of the metal-based NPs due to its the simplicity, ecofriendly and cost effectiveness for mass production of NPs and taking very less time. These features influence the potential scope and reproducibility of NP production.

After the synthesis of NPs, the chemical composition and crystalline structure of the biosynthesized NPs need to be investigated. Numerous experimental techniques are available to evaluate a variety of physical and chemical characteristics of biosynthesized nanoparticle samples such as size, shape, morphology, crystal structure as well as elemental composition.

Research goal and tasks: The biosynthesis and characterization of seven NPs based on zinc, magnesium, silver, copper and iron salts were the objectives of the present work, and then evaluating some biotechnological application for the synthesized nanoparticles and using them as the modern approach for protecting plants against different plant pathogens. The objectives of the research included:

1. To research on the use of an agro-waste materials, strawberry leaf, and extract its phytocomponents in water and use it instead of chemicals to develop a safe, cost effective and ecofriendly synthesis method for production of new materials with prospective application in agriculture such as using in plant protection or in fertilizers formulations

2. To develop a method with high production efficiency with no need to use high pressure, energy, temperature and toxic chemicals which could scaled up easily for synthesis in large scales in future industrial applications
3. Determine the possibility of synthesizing metal-based NPs based on Zn, Mg, Fe, Cu (micronutrients) and Ag during a green method
4. To characterize biosynthesized NPs using high-tech analytical instruments
5. To evaluate various applications of NPs in increasing growth and sustainability of crops
6. Evaluating the antibacterial and antifungal activity of synthesized NPs

Scientific novelty of the research. It is for the first time in my dissertation:

- The effectiveness of metal nanoparticles for their use as antibacterial, antifungal and growth-stimulating agents was studied.
- Bifunctional NPs (as growth regulators and pesticides) are proposed to be used as bactericidal additives to plant protection products.
- Strawberry leaf extracts were used in green NP synthesis (a method for obtaining metal nanoparticles from metal salts applying plant extracts as reducing and stabilizing agents).

Theoretical and practical significance. Developed and tested a new green method for biosynthesis of metallic nanoparticles which are more biocompatible than chemically synthesized ones and more ecofriendly than physically synthesized nanoparticles. Also, these nanoparticles were tested and investigated for their antimicrobial activities against different pathogens (*Pseudomonas aeruginosa*; *Botrytis cinerea*; *Pilidium concavum* (Desm.) Höhn. and *Pestalotia* sp.) and on seed germination and germination growth of wheat (*triticum aestivum*) and flax (*Linum usitatissimum*).

The results of the research were introduced into the educational process of the agro-biotechnological department of ATI PFUR and can be recommended in the industrial production of cereal crops.

Basic provisions for defense.

1. Synthesis of nanoparticles based on Zn, Mg, Fe, Cu (trace elements) and Ag in an environmentally friendly way (green synthesis).
2. Characterization of synthesized NPs
3. Evaluation of the effect of synthesized nanoparticles on various plant pathogens *Pseudomonas aeruginosa*, *Botrytis cinerea*, *Pilidium concavum* (Desm.) Höhn. and *Pestalotia sp*. to solve the problem of resistance to chemical pesticides
4. Evaluation of the effectiveness of biosynthesized NPs on germination of seeds and seedling growth of wheat (*triticum aestivum*) and flax (*Linum usitatissimum*).

Publication of research results. Upon the obtained results from dissertation research, 10 papers were published, including 5 articles in scientific journals indexed in the Web of Science and Scopus databases, 3 articles in peer-reviewed scientific journals in the list of VAK, and 2 abstracts of conferences.

Personal contribution of the author. The applicant participated in setting the goal and objectives of the study, collected and analyzed the material obtained, processed and interpreted the data, and also prepared publications in co-authorship.

Structure and volume of thesis. The PhD thesis consist of 157 pages in computer text, contains 22 tables, 83 figures. Thesis compounds are: introduction, literature review, materials and methods, results and discussion, conclusion, and recommendations. References included 124 authors.

CHAPTER 1. LITERATURE REVIEW

This section includes overview of the previous researches about biosynthesis, characterization and application of metal-based nanoparticles, which are close to this study's content.

1.1. Nanoscience and Nanotechnology

Nanoscience is the study of materials and structures at the scale of 10^{-9} m. When the dimensions of a material decrease from a large size, at first the properties remain the same, then small changes occur and finally, properties can dramatically change when the size drops below 100 nm [1].

Nanomaterials often represent different characteristics from their bulk counterparts because of nanomaterials' higher ratio of surface to volume which results in an exponential enhancement of the reactivity at the molecular level. These properties including optical, electronic, and chemical characteristics, while nanomaterials mechanical properties may also vary extensively and let them to be an object of intensive studies in attributed to their prospective technological applications in different areas [2-3].

Between various nanomaterials, metal-based NPs have been a focus of interest due to their remarkable characteristics and applications in different fields mainly in optoelectronics, catalysis, chemical sensing, cosmetics, and mostly in health industries [4-5]. Apart from mentioned applications, metal-based NPs have also been applied in agriculture practices in nano-fertilizers formulations and in protection of plants from different pathogens [6].

Several metal-based nanoparticles including C-ZnO, NC-ZnO, Zn, MgO, Ag, Cu and Fe have been biosynthesized in this research. The importance of each NP is briefly illustrated here. The only metal to have representatives in all six classes of

enzymes is the zinc (Zn). The fact that Zn was demonstrated to be involved in transcription and translation of genetic messages gave new importance to its known essentiality to life processes [7]. Zinc oxide (ZnO) and magnesium oxide (MgO) NPs are effective antibacterial and anti-odor agents. ZnO and MgO nanostructures are attractive antibacterial ingredient in many products such as wood, food and cosmetic products because their increased ease in dispensability, optical transparence and smoothness. Since such NPs are safe for plants and cause less environmental pollution in comparison to conventional chemicals, the use of them as nano-biopesticide and nano-fertilizer is more acceptable [8]. Silver nanoparticles (Ag NPs) have gained significance in last years as a result of their distinctive properties, including good conductivity, chemical stability, and catalytic and mainly antibacterial activity [9]. Copper nanoparticles (Cu NPs) are widely used in water treatment, food processing, in the electrical industries because of their conductivity and in chemistry as catalyst and lubricant [10]. The main potential of iron nanoparticles (Fe NPs) is their application in environmental remediation. Among various metallic nanoparticles, Fe NPs have promising advantages which could combat environmental pollution. Due to the reactivity of nanoscale iron having higher ratio of surface area to volume, the interest in nanoscale zero-valent iron in environmental remediation is increasing [11].

Today, the use of biological systems such as plants and microorganisms has emerged as a novel issue for the biosynthesis of various nanomaterials. These natural sources contain biological molecules such as polyphenols, terpenoids, flavones, carbohydrates, proteins, alkaloids, alcohol, phenolic acids and so on. The biosynthesis mechanism could be considered as electrostatic metal ions interaction and the functional groups of these biomolecules [9,12].

During the synthesis of NPs, extracted phytochemicals are added to metal salt solutions, reduce the metal ions and attach to the as-synthesized NPs acting as stabilizing or capping agents. These capping agents with “no toxicity” prevent NPs from aggregation. Moreover, as the kinetics of biological methods are slower than chemical methods, there is a better control over the growth of NP crystals [13-14].

1.2. Characterization of biosynthesized nanoparticles

Various experimental conditions can lead to the production of NPs with different properties such as color, size, shape and organic ligands binding to the surface of synthesized NPs. The mentioned features will affect potential applications and reproducibility of NPs formation. After the synthesis of the NPs, chemical composition and also the crystallin structure of the synthesized NPs should be investigated. A lot of different experimental approaches are available to evaluate a variety of chemical and physical properties of biosynthesized nanoparticle samples including size, shape, morphology, crystal structure and elemental composition [15-18].

Characterization techniques also help to conduct a reproducible synthesis method and study the influence of various environments on properties of synthesized nanomaterials. Moreover, appropriate characterization of nanoparticles gives useful information to the researchers who are investigating applications of NPs in different areas and also for regulatory bodies investigating impact of NPs on environment and healthcare [19]. Different techniques were used in this research for characterization of NPs including UV-Vis Spectroscopy, X-ray Diffraction (XRD), Field Emission Scanning Electron Microscopy (FESEM) coupled with Energy Dispersive X-ray Spectroscopy (EDS), Photon Cross-Correlation Spectroscopy (PCCS) and Fourier Transformed Infrared Spectroscopy (FT-IR).

1.3. Antimicrobial activity of nanoparticles

One of the big concerns of the recent years is bactericides or antibiotic-resistant organisms. Metal-based NPs, especially Ag and Cu NPs, are assumed as antimicrobial agents because in low doses they exhibit inhibitory activity and microbicidal activity against various bacteria, fungi and viruses. These NPs are used in bandages, wound healing ointments or creams biomedical and surgical devices as disinfectants, textiles coating, food packaging and storage, as a result of their effectiveness on resistant strains of microbial pathogens [4,20]. The nanoparticle-based composites or biosynthesized metal nanoparticles also could be used for plant diseases management against phyto-pathogens [21].

Copper-based antimicrobial products are regulated compounds with certain limit posed in the total dosage applied for preventing potential risks as a result of building up toxic levels in the environment. For instance, in many places of the world, copper sulfates are not recommended for use as sulfates are highly soluble and toxic to the spray applicators and the environment. Consequently, application of less-soluble Cu formulations, like Cu hydroxide and Cu oxychloride, are encouraged. Another novel approach is the use of nanoparticles in agriculture which has been proving very effective against plant pathogens [20].

Field and greenhouse trials have shown that silver NPs and zinc formulations are equally to or more efficient in comparison to copper-based antimicrobial formulations in reducing fungal and bacterial diseases on tomato and citrus. This is because most of the copper-based antimicrobial formulations applied in agriculture contain micron-sized insoluble metallic copper compounds, like copper oxide, copper hydroxide or copper oxychloride. Furthermore, fixed copper particles are hydrophobic, so they aggregate in water media and decrease the surface area of metallic particles thereby reducing their antibacterial activity. Vice a versa, NPs

have unique physical and chemical characteristics at the atomic, molecular and cellular levels. The smaller nano-sized compounds and their higher surface-to-volume ratio allow them to penetrate microbial membranes and release metal ions into the solution more efficiently in comparison to the micron-sized compounds conferring the nano-sized metallic compounds a higher antibacterial activity than micron-sized formulations. Also, nanoparticles size, shape, stability, and concentration affect their antimicrobial activity and prominently affected by the reaction condition of their synthesis [20-24].

The main action mechanisms of antimicrobial activity of the silver NPs on microbial cells could be mentioned as membrane breakage, oxidative stress, peptidoglycan damage, ribosome disassembly, proteins and DNA denaturation, enzyme inactivation, disruption of electron transport chain and proton motive force [13,25]. Another reason for silver's antimicrobial activity is Ag^{+} ions (released from Ag NPs) high affinity toward phosphorus, sulfur and nitrogen, which binding to amino and thiol groups, disrupting DNA and protein structure and finally affecting cell viability. The other mechanism is induction of the reactive oxygen species (ROS) by Ag NPs, leading to formation of free radicals and resulting oxidative stress and then a bactericidal action [13].

The antimicrobial properties of Cu NPs are due to the ions releasing from nanoparticles and their affinity to alternate between its oxidation states (Cu [I] and Cu [II]). Summarizing all of the researches, denaturing effect of copper ion on DNA, proteins and enzymes in microbes results in copper's antimicrobial properties [26-27].

There is a high interest to develop novel antimicrobial materials to overcome the problems of conventional antimicrobial agents such as microbial resistance and so

on. In last years, many different approaches have been developed for producing nano-scaled antimicrobial agents.

1.4. Effect of nanoparticles on germination of seed and seedling growth

Seed germination is a very important phenomenon in agriculture and also a crucial step in plant growth because it is considered as thread of life of plants which ensures its survival [28].

The interactions between nanomaterials and plants have not been fully elucidated. There have been various and sometimes conflicting reports on the absorption, translocation, accumulation, biotransformation, and toxicity of nanomaterials in different plant species. The effects of metal-based nanomaterials are still under investigation. The impact of NPs on various plants depends on the species, the concentration of nanomaterial, the experimental conditions (such as temperature and the duration) and method of the exposure. Recent researches have reported that a plant's response to nanomaterial, enhancement or inhibition of growth, depends on the dosage of nanomaterial. Exposure to different concentrations of NPs could enhance plant growth in comparison to the non-exposed plants, whereas lower and higher concentrations could affect plant growth negatively [29]. In the case of positive effect, nanomaterials may help to improve nutrient use efficiency due to their small size, higher surface area and also their slow rate of release, which could facilitate the plants taking up most of the nutrients without any waste [30].

In this study, we chose two important cereal crops, wheat and flax, for investigating the impact of synthesized NPs on seedling and seedling growth of their seeds:

Triticum aestivum L. commonly called as wheat is one of the most significant crops, the second most important consumables food crop all over the world, following rice. Unfortunately, due changing climatic conditions, yield of wheat crop has been

decreasing from many years. Therefore, it is the necessary to enhance the yield of major food of the world for the accomplishment of food requirements of the people using modern technologies [28].

Flax (*Linum usitatissimum L.*) is one of the oldest crops which is cultivated on a large area. Flax has a wide application range in food, textile and paint industries. It is also applied as medicinal remedy for cough, ageing, inflammation, diabetes, fatigue, cancers and cardiovascular abnormalities. It contains polyphenols, fatty acids, vitamins and cyclic peptides which are some examples of the medicinally significant compounds present in *L. usitatissimum* [31].

1.5. Biochemical synthesis of metal-based nanoparticles

There are important relations between the approach nanoparticles are synthesized and their potential applications. However, the use of toxic solvents and the resulted contamination from chemicals needed in production of the nanoparticles limit the potential of their use in biomedical applications. Therefore, a non-toxic "green" way for synthesis of metal-based nanoparticles is needed, allowing them to be applied in a wider range of industries. It could be achieved potentially by the use of biological approaches. Because of the developing popularity of green approaches, various researches had been done for synthesis of the metal-based NPs applying different sources such as fungus, bacteria, algae, plants and others [33].

Different parts of plant like root, leaf, stem, fruit, and seed have been applied for biosynthesis of metal-based NPs because of their exclusive phytochemicals content. Use of natural extracts of the plant parts is a very cheap and ecofriendly process, and also does not involve the use of any intermediate base groups. It does not involve application of costly equipment, takes very less time and gives a quantity enriched and highly pure product which is free from toxic impurities [12]. Bio-reduction includes the reduction of metallic ions with the help of existed phytochemicals in

plant such as polyphenolic compounds, polysaccharides, alkaloids, vitamins, amino acids, proteins and terpenoids. Orientation, size and physical properties of nanoparticles affects the reproducibility and the performance of a potential device, and then resulting the synthesis and design of shape and size-controlled nanocrystals an essential component for any practical usage. This need is motivating researchers for exploring various synthesis protocols [9].

For simple production of metallic NPs from plant, the most commonly applied approach is washing thoroughly the plant part, sterilizing it by double distilled water. The plant part is dried at room temperature, ground and weighed. The powder of plant part is mixed with distilled water according to a certain concentration. In the next step, the mixture is boiled under continuous heating and stirring using a magnetic stirrer for a while. The obtained solution is filtered using Whatman filter paper and the resulted clear solution will be used as extract of plant part. A concentration of the precursor salt's solution will be mixed with a specific volume of the obtained extract under definite temperature, stirring and other designed condition of the experiment. After formation of NPs, they will be centrifuged, washed for several times and then dried. After the drying step, the obtained NPs are being calcinated in some cases and in some other there is no calcination process for annihilation of the NPs [12].

1.6. Role of flavonoids and polyphenols in plant extracts as reducing, capping and stabilizing agents

Flavonoids are a large group of polyphenolic compounds containing different classes: flavonols, isoflavonoids, chalcones, flavones, and flavanones. These phytochemicals are able to reduce ionic metals into the nanoparticles, by actively chelating. As flavonoids contain different functional groups, they could cause nanomaterial formation "as chelating/caooing/reducing agent". Transformations of

the flavonoids from enol-form to keto-form lead to the release of a reactive hydrogen atom which will reduce metallic ions to metal nanoparticles. Some flavonoids are able to chelate metallic ions with their π-electrons or carbonyl groups. For instance, luteolin, quercetin and tryptophan flavonoids contain very strong chelating ligand which chelate metals through three positions; the carbonyl and hydroxyls positions and also the catechol. These groups are capable to chelate various metallic ions including Al^{+3}, Cr^{+3}, Pb^{+2}, Fe^{+2}, Fe^{+3}, Cu^{+2}, Zn^{+2}, and Co^{+2}. Stabilizing or capping agents applied for stabilization of the nanoparticles in the colloidal synthesis, lead to the protection of surface from aggregation and the control of particle morphology. Many plant species are studied for synthesis of nanoparticles in the form of leaf extracts, peel extracts, tissue culture extracts, essential oils, gum extracts, seed extracts, seedling extracts, whole-plant extracts, etc. [1].

1.7. Advantages of using plants over bacteria and fungi

Application of plants in production of nanoparticles has many benefits like being inexpensive, environmentally friendly, non-toxic, safe, no need for culture preparation and isolation maintenance, stable, easily scaled up for large-scale production and short production times [1].

1.8. Green synthesis of Zn-based NPs

In biosynthesis of Zn-based NPs, precursors of zinc oxide, hydrated Zinc nitrate, zinc sulfate and zinc acetate salts have been used. Many different plant extracts also have been used in this regard, like leaf extract of, aloe vera, neem, buchured clover, nochi, dog rose, Mexican mint, etc. [12].

The only metal which is found in all classes of enzymes (i.e., oxidoreductases, lyases, isomerases, transferases, hydrolases and ligases) and plays an important role in many integral metabolic processes as an essential micronutrient, is zinc. Zn can

also help in development of the biosynthesis of carotenoids and chlorophylls, and in increase of the photosynthetic system of plants. ZnO NPs have great potential to enhance productivity of agriculture due to their significant physical, optoelectrical, and antimicrobial properties. There are some researches which report considerable absorption abilities for many organic materials, heavy metals, zinc oxide and ZnO NPs. ZnO NPs have larger ratio of surface area-to-volume which results in a significant enhancement of being effective for blocking ultra-violet radiation in comparison with the bulk state [34]. Application of nanoparticles for modulating plants physiological response is a recent practice, as zinc is an important micronutrient that regulates various physiological responses in plant. The basis for its prospective application in agriculture for improving plant growth could be suggested by understanding physiological effect of Zn NPs on seed germination [35]. In the experiment carried out by Upadhyaya et al., the effect of Zn NPs was studied on rice and showed that the Zn NP treated seeds, showed better potential for germination [35].

Punjabi et al. [36] reported the biosynthesis of zinc nanoparticles which was carried out by *Pseudomonas hibiscicola*. Synthesized zinc nanoparticles were observed in TEM with the size of 60 nm and distinct morphology. Evaluating antimicrobial activity of Zn NPs revealed that it is mainly effective against Gram-positive bacteria like *Staphylococcus aureus* including its drug-resistant variant MRSA. Zn NPs were also active against *Mycobacterium tuberculosis* and its MDR strain with MIC of 1.25 mg/ml. The synergistic action of NPs studied in combination with the common antibiotic gentamicin (at the dosage of 590 mg/mg) applied for the treatment of different bacterial infections by Checker board assay. Zn NPs showed to have synergistic effect against MRSA, in combination of NPs with gentamicin. The MRSA, ESBL, and strains of *P. aeruginosa* showed MIC of 2.5 mg per ml

except VRE which was 10 mg/ml for Zn NPs. The obtained results show antimicrobial potential of Zn NPs against strains of community and hospital-acquired infections which are drug-resistant. This findings could open a new area of antimicrobials for clinical applications [36].

Ogunyemi et al. [37] used three plant extracts of chamomile flower (*Matricaria chamomilla* L.), olive leave (*Olea europaea*) and red tomato fruit (*Lycopersicon esculentum* M.) in green synthesis of non-calcinated ZnO NPs. According to the TEM micrographs, the zinc oxide NPs have cubic structures with the average size of 41 nm, 51 nm and 51 nm for ZnO NPs synthesized by *Olea europaea*, *Matricaria chamomilla*, and *Lycopersicon esculentum* respectively. The results exhibited that the inhibitory effect of the ZnO NPs against *Xanthomonas oryzae* enhanced with enhancement of the concentration. The maximum inhibition occured at 16.0 mg/ml for all the green synthesized ZnO nanoparticles. The highest inhibition zone of 2.2 cm was related to the ZnO nanoparticles synthesized by *Olea europaea* at 16.0 mg/ml which was significantly different from zinc oxide NPs synthesized by *Matricaria chamomilla* L., and *Lycopersicon esculentum M.*. All over, zinc oxide nanoparticles are potentail biocontrol agents which could be used to combat bacterial leaf blight diseases of rice [37].

In the study conducted by Dobrucka et al., calcinated zinc oxide nanoparticles which are biosynthesized using flower extract of *Trifolium pratense*. The synthesized zinc oxide NPs characterized using UV–Vis spectroscopy, X-ray diffraction, Fourier transform infrared spectroscopy, and scanning electron microscopy with Energy dispersive X-ray analysis. These methods revealed the presence of the ZnO nanoparticles in the size range of 60 to70 nm and the larger ZnO NPs are resulted from agglomeration of the smaller NPs. Moreover, according to this study, synthesized ZnO NPs showed antimicrobial efficacy against clinical

and standard strains of *S. aureus* and *P. aeruginosa* and standard strain of *E. coli*. The zinc oxide nanoparticles had high activity against *E. coli* ATCC 25922, *S. aureus* ATCC 4163, *P. aeruginosa* ATCC 6749, *S. aureus* and *P. aeruginosa* [38].

Green synthesis of zinc oxide nanoparticles in an extracellular approach (spherical shape with the size range of 23–57 nm) was done by reducing 0.025 M aqueous zinc acetate solution with a leaf extract of *Catharanthus roseus*. The synthesized ZnO NPs were tested for evaluating their antibacterial activity and also their maximum antimicrobial activity against *Pseudomonas aeruginosa* and *Staphylococcus aureus* [39].

Zinc oxide NPs (with the size of 15–40 nm) biosynthesized by flower extract of *Elaeagnus angustifolia*. The effect of various concentrations of ZnO nanoparticles and zinc sulphate on *Solanum lycopersicum* was studied. The authors observed an enhancement in germination rate and seedling vigor at the concentration of 1.2 mM in comparison with the control and zinc sulphate [34].

In the study conducted by Ates et al., it is reported that the Zn NPs' suspensions induced more toxicity comparing with nanoparticles of zinc oxide for *Artemia salina* larvae. The authors of the study suggested that this effect was related to the prominent release of free zinc ions from zinc NPs into the exposure medium. Furthermore, both ZnO and Zn NPs exhibited various toxic effects depending on their particle size, i.e., the smaller nanoparticles were more toxic [40].

Yuvakkumar et al. reported green synthesis of calcinated zinc oxide nanocrystals employing *Nephelium lappaceum* L., peel extract as a natural ligation and stabilizing agent. Biosynthesis of ZnO nanoparticles was done via formation of zinc-ellagate complex using rambutan peel wastes. The successful production of ZnO nanoparticles confirmed using standard characterization techniques. The prepared

zinc oxide NPs coated on a piece of cotton fabric and the antibacterial activity of them were analyzed. Coated cotton with ZnO NPs, had good antibacterial effect towards *Escherichia coli*, gram negative bacteria and *Staphylococcus aureus*, gram positive bacteria [41].

1.9. Green synthesis of MgO NPs

Magnesium oxide (MgO) is an important basic metal oxide with a wide range of functional properties which validates its usage as a catalyst, an additive in refractory materials, paints, a toxic waste remediation agent, and superconductors and also as a curative agent in the pharmaceutical industry. The important characteristics of MgO including low electrical conductivity, high thermal stability and catalytic behavior can be enhanced further at the nanoparticle level. With escalating interest in the application of MgO nanoparticles for biological and medical uses, including biocidal application, a curative for heart burn, bone regeneration and in cancer therapy, green synthesis approaches serve as important alternate methods to produce nontoxic MgO NPs for biological and medical applications [42].

Biosynthesis of magnesium oxide NPs reported by Jeevanandam et al., applying extracts of three various plant leaves: *Amaranthus tricolor*, *Andrographis paniculata* and *Amaranthus blitum*. The biophysical properties of the biosynthesized magnesium oxide NPs were investigated using different characterization methods. The UV-visible spectroscopy showed an absorbance peak at 320 nm indicating the formation of metal oxide nanoparticle. According to the FT-IR results, the functional groups are responsible for the formation of MgO NPs and the peak between 660 and 540 cm^{-1} is because of the presence of MgO. The TEM images exhibited the particulate size range of 18–80 nm. The method for formation of smaller MgO NPs also explained due to application of various precursors and leaf extracts. All over, in this approach potentials for development of highly stable MgO NPs are

demonstrated, resulting in small particle size distribution, using different plant materials for using in various areas such as biosensing and therapeutic development [42].

Biosynthesis and characterization of magnesium oxide nanoparticles using white button mushroom aqueous extract was studied by Jhansi et al. The application of biosynthesized MgO with particle sizes of 20, 18.5, 18, 16.5, and 15 nm on peanut seed germination was also studied. The MgO NPs with smaller size (15 nm) have been increased the seed germination and growth parameters in comparison with control and other sizes of magnesium oxide NPs. The MgO nanoparticles penetrates into peanut seeds and impact the seed germination and growth rate mechanism. Moreover, this germination is high in seeds rather than germination on selected soil plot magnesium oxide nanoparticles (0.5 mg/L stable concentrations) in comparison with different sizes of MgO nanoparticles and the control. Physicochemical approaches showed that the MgO nanoparticles can penetrate into the seed coat and support water uptake inside the seeds. Probably, this improving effect may result in the uptake of MgO nanoparticles by plants, as shown in the UV-Vis and SEM studies. As the smaller size of MgO nanoparticles (15 nm) stimulates improvement of the seedling and enhancement of growth, it clearly exhibits that the study can help in growing peanuts in large-scale agricultural production [43].

Another study focused on the green synthesis of MgO NPs using the extract of Neem leaves and the precursor salt of $Mg(NO_3)_2$. The method is eco-friendly and non-toxic. In this report, the Neem leaves extract acts as a reducing agent in the reaction. The obtained particles were characterized by different analytical methods such as UV-Vis, XRD, FT-IR, FESEM and PSA conforming the presence of MgO nanoparticles. The biosynthesized MgO nanoparticles used in to study the seed germination of *Cicer arietinum* and *Solanumlycopersicum.* According to the results,

after 3 days 90% seeds were germinated and roots and leaves were developed. The germinated seeds planted for investigation of the impact of MgO NPs on the plant growth and after measurement of the leaves' length (at the 10^{th} days) it was revealed that the process of germination was affected by MgO NPs in *Cicer arietinum* not in *Solanumlycopersicum* [44].

Dobrucka biosynthesized MgO nanoparticles with *Artemisia abrotanum* water extract. The biosynthesized MgO nanoparticles characterized using various characterization methods. XRD analysis showed that pure monoclinic crystallite MgO nanoparticles were prepared. The average particle size of MgO nanoparticles was 10 nm. EDS analysis confirmed the signal characteristic of Mg and O. According to the FT-IR studies, the active organic compounds are responsible for the stabilization of MgO nanoparticles. The biosynthesized NPs in the reduction of methyl orange showed good catalytic activity. MgO nanoparticles also showed very good antioxidant characteristics [38].

It was reported that MgO nanoparticles were rapidly boisynthesized by water extract of *Clitoria ternatea* as reducing and stabilizing agent and precursor of $MgCl_2.6H_2O$ which was confirmed by the initial color change of light yellow at optimized metal and plant extract concentration of 25 mM: 200 μg, at the temperature of 37 ^oC and pH of 12 and also with the UV–visible absorption peak position at 280 nm. The XRD analysis showed cubic shape of MgO nanoparticles. SEM and FESEM with EDS showed the average particle size of 50–400 nm. FT-IR spectra has exhibited the presence of organic functional groups in the plant extract, and also the peak at 521 cm^{-1} showed the characteristic absorption band of MgO. The biosynthesized MgO nanoparticles showed 65% inhibition activity by the *In vitro* antioxidant testing of the activity of MgO nanoparticles by DPPH and reducing power assay. The potential antioxidant activity of biosynthesized MgO nanoparticles

may be because of the presence of bioactive components in the plant extract. As the biosynthesized nanoparticles showed potential *in vitro* antioxidant activity, and further studies will be done to find *in vivo* antioxidant activity of MgO NPs [45].

MgO nano-flowers successfully biosynthesized using aqueous Rosemary extract without using any catalyst agent, at the temperature of 70 °C for 4 h, with a size less than 20 nm, which showed antibacterial activity against *Xanthomonas oryzae* pv. *Oryzae,* rice bacterial blight pathogen. The antibacterial activity of MgO NFs against *Xoo* strain GZ 0005 may be related to its inhibition on bacterial growth, biofilm formation, and motility due to the destruction of cell wall. Overall, the biosynthesis of MgO NFs is a safe approach that could be widely used in agricultural applications to overcome rice bacterial disease [46].

1.10. Green synthesis of Ag NPs

In numerous studies have been shown silver nanoparticles (Ag NPs) display antibacterial properties. For example, Ag NPs have been shown to be effective in growth inhibition of both Gram-negative and Gram-positive bacteria. With the grow of antibiotic resistance in last years and development of some new antibiotics, many researches have begun focusing on such antibacterial NPs as potential new medical materials. Ag NPs have also been applied as optical sensors in producing small molecule adsorbates [33].

Krishnaraj et. al reported that a plant which has the potential for reduction of Ag^+ is *Acalypha indica.* Aqueous extract of this plant's leaf was used for synthesis of silver NPs. The average size of silver nanoparticles was in the range of 20 to 30 nm, which is considerably homogenous. They also evaluated the synthesized Ag NPs' antimicrobial activity on *Vibrio cholera* and *Escherichia coli*. According to the results, silver nanoparticles showed bacterial growth inhibition at the concentration of 10 μg/ml [47].

Behravan et al. in another study illustrated a green synthesis method for production of Ag NPs using *Berberis vulgaris* root and leaf aqueous extract and tested its antibacterial activity. Ag NPs had spherical shapes and particle size of 30-70 nm, according to XRD and TEM results. In this study, the antibacterial effect of produced NPs was evaluated on *Staphylococcus aureus* and *Escherichia coli* bacteria using disk diffusion method and MIC (minimum inhibitory concentration) test. The results indicated that the antibacterial activity of silver nanoparticles on gram-negative bacteria (*E. coli*) is really more than gram-positive bacteria (*S. aureus*) and the complete bacterial growth inhibition happens by the concentration increasing and number of NPs. The smaller NPs are found to be more toxic because of their easier absorption and the larger surface area. Moreover, the potential release of Ag ions also has increased by reduction of NPs size [48].

The formation of silver nanoparticles by *Medicago sativa* seed exudates is reported by Lukman et al. Ag^+ reduced by mixing silver salt and the extract and in one minute, almost instantly silver NPs were observed. The shapes of the synthesized NPs were triangular, spherical or flower-like and a particle size of 5 to 108 nm. In contrast to the study of Krishnaraj et al.'s, Ag NPs synthesized by *M. sativa* seed extract were heterogenous in shape and size, and also did not show significant bacterial growth inhibition. However, it was suggested that the synthesized Ag NPs with the seed extract are able to act synergistically for elimination of bacteria [49].

Another study, using *Ligustrum lucidum* leaf extract in biosynthesis of silver nanoparticles was reported by Huang et al. The biosynthesized nanoparticles had a nearly spherical shape and an average particle size of 13 nm. The antimicrobial activity of silver nanoparticles was tested using the methods of conidia germination, colony growth, paper disk diffusion, and in vitro inoculation. The IC_{50} (50%

inhibition concentration) of Ag NPs against *Setosphaeria turcica* was 170.20 μg/mL (calculated by SPSS 13.0). Furthermore, it was shown that there is a significant synergistic antifungal activity when silver nanoparticles were combined with epoxiconazole with the ratios of 8:2 and 9:1 [50].

Kasthuri et al., reported the use of plant *Phyllanthus amarus* extract in biosynthesis of Ag NPs. This is an interesting study because they only applied a single component of the plant extract in the synthesis of Ag NPs, contrasting the other studies in which whole extracts of plants are applied. The concentrations of the extract have a key role in shape and size of the biosynthesized Ag NPs. At lower concentrations, the slowly formation of hexagonal and triangular Ag NPs was observed and at higher concentrations of the extract, greater levels of spherical Ag NPs produced, which was confirmed using UV-Vis spectroscopy and TEM analysis [51].

Song et al. talked about an extensive research on formation of silver nanoparticles using leaf extract of several different plants including Persimmon, Pine, Magnolia, Ginkgo and Platanus. They also compared their potential in formation of Ag NPs. According to the results, the Magnolia leaf extract showed the best results in reduction of Ag^+ ions. In 11 minutes, 90% of the Ag^+ ions reduced to Ag NPs. In this case, temperature needed to be controlled during the biosynthesis of NPs as it affected size and shape of the Ag NPs and the rate of the reaction. The effect of various reaction temperatures evaluated and found that at 95 °C, Ag^+ ions reduction was much higher in comparison with 25 °C. However, at higher temperatures the particle size of the Ag NPs reduced. It could be suggested that it is because of the enhanced turnover of the Ag NPs with reducing agent because it takes less time to build upon the pre-synthesised Ag NPs before starting biosynthesis of new ones [52].

Mahakham et al. in a very interesting study, talked about the application of biocompatible silver nanoparticles, which were biosynthesized in a green approach by the use of kaffir lime leaf extract, for increasing the seed germination of rice aged seeds. According to the results of characterization methods, silver nanoparticles were successfully formed, which were capped with phytochemicals existed in the plant extract. Rice significantly developed seed germination and seedling vigor of the seeds soaked in biosynthesized silver nanoparticle suspensions at 5 and 10 ppm in comparison with control and $AgNO_3$ treated samples. Treating seeds with silver nanoparticles could increase α-amylase activity, and results in higher amounts of soluble sugar for supporting the growth of seedlings. In addition, in germinating seeds, it also stimulated the up-regulation of aquaporin genes. However, more formation of ROS was observed in Ag NPs treated germinating seeds in comparison with the control and other treatments, indicating that both ROS and aquaporins have important roles in increase of seed germination. Various mechanisms were proposed which underly Ag NP-induced seed germination, such as rebooting ROS/antioxidant systems in seeds, generation of nanopores for enhanced water uptake, formation of hydroxyl radicals for cell wall loosening, and nano-catalyst for fastening starch hydrolysis [53].

1.11. Green synthesis of Cu NPs

Copper nanoparticles have functional decontaminating characteristics against different infectious microorganisms and the potential to be applied as bactericidal material. Cu NPs show antibacterial activity against common pathogenic bacteria *Escherichia coli*. The Cu NPs, biosynthesized by the use of stem latex of *Euphorbia nivulia*, showed toxic effects to human lung cancer cells (A549) suggessting their potential use in the field of cancer therapy [54]. In last years, copper nanoparticles have gained importance because of their multifunctional applications in medicine

industry. Meanwhile, other NPs, like iron oxide, gold, platinum, silicon oxides and nickel did not show bactericidal activity in other studies against *E. coli*. Cu and Ag NPs used for evaluation of their antibacterial activity on *E. coli* and *B. subtilis*, which revealed that copper NPs exhibited superiority over silver NPs [54].

Copper nanoparticles are widely applied as antimicrobial materials, sensors, heat transfer systems, and catalysts. Moreover, Cu and its compounds also have been used as antifungal, antiviral, and molluscicidal agents. The green synthesis of coper nanoparticles using various plants' extracts have been reported in many previous studies. Copper nanoparticles are naturally multifunctional and then find significant applications such as photoluminescent activities, photocatalytic degradation, catalytic degradation, anticancer activity, biofilm formation, nitrates removal, upshot against human pathogens, organic dye degradation catalysis, etc. Copper nanoparticles had good antimicrobial effect on *Bacillus spp.* and also significant fungicidal effect on *Penicillium spp*. microorganisms. Cu NPs also showed a greater inhibition on *E. coli* compared to *K. pneumoniae, P. aeruginosa*, *Propionibacterium acnes* and *Salmonella typhi*. Copper NPs antibacterial function may be related to the interactions of nanoparticles with -SH groups resulting to denaturation of protein. It was suggested that Cu nanoparticles exert effect on cell membrane because of their strong affinity towards carboxyl and amines groups which are present on the surface of organisms' cell such as *B. subtilis*. Copper NPs also bind with DNA molecules and then the helical structure disturbs by cross-linking within and between the nucleic acid strands.

Many previous researches represented that Cu NPs could be boisynthesised using most common precursor copper salts including copper sulfate ($CuSO_4$), cupric acetate ($(CH3COO)_2Cu$) and copper chloride ($CuCl_2$). Green synthesized copper nanoparticles produced with *Ginkgo biloba* L. leaf extract showed catalytic

application for Huisgen [3 + 2] reaction. Green synthesized Cu NPs produced from Z. *spina-christi* fruits extract were excellent nano-adsorbent for removing Crystal Violet from aqueous solution [55].

Gondwal et al. biosynthesized copper nanoparticles via a green approach using *C. occidentalis* leaf extract and precursor of cupric nitrate salt. The biosynthesized copper nanoparticles characterized using UV-Vis, TEM, XRD and SEM- EDX methods. The formation of Cu nanoparticles was confirmed by UV-Vis analysis due to the color change from yellow to brown. Crystallinity of the Cu NPs is revealed from sharp peaks of the XRD pattern. The copper nanoparticles also showed antibacterial effect on *E. coli* and *S. typhi*. The copper nanoparticles also have catalytic ability in reduction of 2-NP and 4-NP. The copper nanoparticles bioreduction process is an ecofriendly and economic simple method with one-step [4].

Murthy et al. reported the biosynthesis of copper nanopartices applying leaf extract of *Hagenia abyssinica* (*Brac*e) *JF. Gmel.* The biosynthesized copper nanoparticles characterized using different characterization methods. The maximum absorbance, was 403 nm which is as a result of surface plasmon resonance phenomena. FT-IR spectroscopy represented peaks attributed to the presence of tannins, polyphenols, and glycosides in the *Hagenia abyssinica* leaf extract. Also, the presence of peak at 740 cm^{-1} is the characteristic peak related to the interaction of Cu and extract's biomolecules. The XRD spectra confirmed that the biosynthesized copper nanoparticles were more crystalline. TEM and SEM micrographs revealed that the shape of Cu NPs is a mix of hexagonal, spherical, cylindrical, triangular and irregularly. By "imageJ" analysis the average size of copper NPs was 34.76 nm. The antibacterial effect of Cu NPs evaluated on *P. aeruginosa*, *E. coli*, *S. aureus*, and *B. subtilis* and had zone of inhibitions 12.7, 12.7,

14.7 and 14.2 mm, respectively, showing potentiality of Cu NPs in treatment of infectious diseases caused by above pathogens [56].

In a study reported by Kiranmai et al. Cu NPs synthesize from green tea (*Camellia sinensis*) and β-cyclodextrin extracts. Polyphenols which are presented in green tea extract are responsible for reduction of Cu ions to highly stable copper nanoparticles. The synthesized Cu NPs characterized by different analytical methods. Cu NPs' UV-Vis spectra showed an absorbance peak at 659 nm. Cu NPs also evaluated for antibacterial activity against Gram-negative and Gram-positive bacterial strains. In addition, synergistic activity of synthesized copper NPs was tested with amoxicillin, ampicillin, ciprofloxacilin, and gentamicin. According to the obtained results, the antibacterial effect of these antibiotics improved in combination with Cu NPs. Furthermore, the combination of NPs with antibiotics exhibits significant antibacterial activity, especially combination with ampicillin increased activity more than others [26].

Green synthesis of Cu NPs applying different plant extracts of *Psidium guajava*, *Ricinus communis, Ocimum tenuiflorum, Punica granatum, Eucalyptus globules, Tagetes sp,* and *Phyllanthus emblica* and $CuSO_4$ solution has been reported. Fruit rind extract of *Punica granatum* was the best one which yielded higher amount of copper nanoparticles. The particle size of biosynthesized Cu NPs also were found 56-59 nm, using SEM analysis. Agar well assay was applied for evaluation of antibacterial effect of the biosynthesized NPs were on Gram-positive bacteria *Staphylococcus aureus*. Results showed that Cu NPs had a strong antibacterial effect against *S. aureus* and could be act as an efficient antibacterial agent against antibiotic resistant infections of *S. aureus* [57].

Nagar et al. have studied green synthesis of copper nanoparticles by *Azadirachta indica* leaf extract. The absorbance peak of UV-Vis spectra at different steps of the

biosynthesis process confirmed the formation of Cu NPs. The synthesized copper NPs characterized using various methods and according to the results, the shape of the particles are cubic and NPs are crystalline, with the average particle size of 48 nm [24].

Today, green synthesis and application of metal-based NPs has become an important and significant branch in nanotechnology. In another study, it was reported that the biosynthesis of Cu NPs using *Moringa oliefera* leaf extract as reducing agent was carried out and the synthesized NPs' effects on germination of seeds and seedling growth was tested. Cu ions rapid reduction occurred with the exposure to leaf extract, leading to the formation of Cu NPs. The UV-Vis and XRD analysis confirmed the formation of copper nanoparticles. The effect of biosynthesized copper nanoparticles evaluated on seed germination and seedling growth of *Triticum aestivum* as an important crop. Treated seeds with various concentrations of copper nanoparticles (25, 50, 75 and 100 ppm) were tested against control. Maximum seed germination percentage was related to the seeds treated with lower Cu NPs concentrations. Also, root fresh and dry weight, root length and elongation significantly improved at lower concentrations of Cu NPs in comparison with the control. Meanwhile, a delay in seed germination and an inhibitory effect on seedling growth was observed in Cu NPs treated with concentrations above 75 ppm. Upon the results of the study, the use of copper nanoparticles increased the germination in wheat [28].

1.12. Green synthesis of Fe NPs

Magnetic nanomaterials are introduced as a new class of important nanomaterials because of their exceptional characteristics such as high coercivity, super-paramagnetism, and etc. Magnetic nanomaterials, have some limitations during synthesis by conventional approaches. For instance, zero-valent iron

nanoparticles, which are synthesized by chemical and physical methods, are naturally very reactive and have a great tendency for formation of aggregates, which ultimately lead to a decrease in reactivity. Another limitation is that the magnetic NPs synthesized by conventional approaches could not be applied in biomedical purposes where organic nonpolar solvents are used. In addition, as-synthesized iron oxide NPs after exposure to air, lose their dispersibility and magnetism [58].

Todays, iron NPs have been widely green synthesized by applying various plant extracts. Extracts of plants are considered as inexpensive reducing, capping and stabilizing agents. Synthesis of iron nanoparticles could be done by mixing metal salt solution with plant extract with a fixed ratio, at room temperature or using heat [58]. For instance, tea waste extract was applied in biosynthesis of iron NPs as a reducing agent. Biosynthesized iron NPs had an average size of 98.79 nm and applied for removing phenol red (PR) from aqueous solution. The FT-IR analysis of iron nanoparticles confirmed the presence of various functional groups which are responsible for adsorption of Phenol Red (PR). In this study, the effect of several different parameters was evaluated. For example, the kinetics of adsorption of PR on the iron NPs based on the initial dye concentration, the effect of adsorbent dosage, various temperature and pH were investigated. Obtained results showed that with increase of initial dye concentration and temperature, adsorption of PR decreased. The best result for PR removal achieved at pH 8.0 (94.9%) in comparison with the acidic and alkaline pH. UV-Vis spectra exhibit a sharp adsorption peak in the range of 190–250 nm. Efficiency of PR removal observed higher with the biosynthesized iron NPs in comparison with chemically synthesized NPs [59].

In another study conducted by Murgueitio et al., Fe NPs synthesized using *Vaccinium floribundum* extract. As-synthesized nanoparticles characterized by XRD, TEM, and FT-IR methods. The assessment of the removal of total petroleum

hydrocarbons (TPHs) from water and soil were conducted by laboratory experiments after treatment with synthesized iron nanoparticles. Produced nanoparticles have spherical shape and particle size in the range of 5 to 10 nm. After treatment with Fe NPs, water contaminated with TPHs (at concentrations of 9.32 ppm and 94.20 ppm) exhibited 85.94% and 88.34% removals respectively. Also, a contaminated soil with TPHs (at 5000 mg/kg concentration) treated with iron nanoparticles during 32 h reached a removal of 81.90%. The application of Fe NPs conducted to a strong reduction condition, and lead to acceleration of TPHs removal, suggesting that application of Fe NPs may be a promising technique in cleaning of TPHs contaminations from water and soil [60].

Fe NPs also have been synthesized by flower sheath extract of *Musa ornata*. The best concentration of precursor salt was 5 mM. The optimum pH of the reaction mixture was 9.0 and the optimum ratio of precursor salt and reducing agent was 7:3. The best time for synthesis of NPs were at 0^{th} h. The biosynthesized Fe NPs characterised by UV-Vis spectroscopy, XRD spectroscopy, FT-IR spectroscopy, AFM microscopy and particle size analyser. UV-Vis absorption spectra indicated a peak at 250-350 nm. FT-IR spectroscopy carried out for identification of possible organic functional groups such as carbonyl, CH and OH band. XRD analysis showed that the average size of magnetite nanoparticles was 43.69 nm. The biosynthesized iron NPs showed antibacterial effect on pathogenic bacteria such as *Streptococcus agalactiae*, *Staphylococcus aureus*, *Salmonella enterica* and *Escherichia coli* using well diffusion technique. This green synthesis method was a eco-friendly, cost effective and promising for applications in different fields [61].

Gottimukkala have reported the biosynthesis of Fe NPs using leaf extract of *Camellia sinensis* as reducing agent for conversion of Fe ions into Fe NPs at room

temperature. The biosynthesized iron nanoparticles characterized by SEM and FT-IR methods. The average particle size of synthesized Fe NPs was about 116 nm [62].

Ebrahimnezhad et al. for the first time, reported the biosynthesis of Fe NPs by the use of *Urtica dioica* aqueous leaf extract as a source of reducing and stabilizing agents, i.e., Fe NPs were produced and stabilized in a biologic coating. Synthesized iron nanoparticles characterized using various characterization methods. According to the results, the synthesized nanoparticles were completely composed of iron atoms without any impurities of iron oxides. The shape of the Fe NPs were spherical and the particle size ranged 21-71 nm with an average size of 46 nm. Nanoparticles were coated by a biological coating resulting in the production of complexes with the size of 117-605 nm. The high zeta potential value of -82.6 mV and also the presence of hydrophilic functional groups on the biologic capping led to a stable colloid system. Biosynthesized iron nanoparticles were amorphous (non-crystalline) and had a low magnetization value of 0.14 emu/g. The Fe NPs are potential of significant interest in different applications in scientific and industrial areas [63].

In recent years, there is a need for intensive researches in the field of nanotechnology on ultrafine nanoparticles which cause increase of yield and quality of agricultural products. Meanwhile, most of the studies are controversial and comparing doses of NPs and types of plants seems really difficult. In research reported by Mushinskiy et al., Cu NPs (50–110 nm), Fe NPs (90–110 nm) and Mo NPs (100–120 nm) were applied for treatment of potato tubers at four concentrations with a geometric progression. The results showed that treatment of *Solánum tuberósum* L. tubers with Fe NPs at the concentrations of 0.0125 to 0.025 M, improved the length of sprouts (55.1% and 21.4%), roots (34.4% and 12.5%) and chlorophyll a (57 - 98%). In addition, Cu and Mo NPs were not effective on plants significantly [64].

Fe NPs were synthesized by a chemical approach and studied by Ngo et al. XRD studies and TEM analysis of as-synthesized nanoparticles revealed that the Fe NPs were zerovalent with sizes of 20-60 nm. A very low nanoparticle concentration was used for pre-sowing treatment of soybean seeds, which does not have any adverse effect on the environment of soil, and reliably affect the biological parameters of the plant growth. The germination rates of treated soybean seeds with iron nanoparticles was 80%, while 55% was recorded for the control sample in laboratory experiments. The number of nodules enhanced by 20–49% and the chlorophyll index by 7–15% in comparison with the control sample. Also, the yield of soybean crop improved up to 16% compared with the control sample in the field experiment, [65].

A study carried out in Bangladesh for the first time for determination of the potentiality of Fe NPs for increasing germination and growth of BARI Gom 25. Fe NPs were synthesized and applied for seed priming and investigation of their effect on germination and growth of wheat seeds. In synthesis of Fe NPs, iron ions reduced in the presence of PVP surfactant under heating for several minutes in oil bath. Seedlings growth experiment carried out in a sand culture to evaluate nanoparticles uptake to wheat seedlings. The seeds treated with five concentrations of nanoparticles: 0, 1.0, 1.5, 2.0 and 2.5 ppm. Germination of seeds and seedlings growth were influenced by 1.0-2.0 ppm but reduced significantly at 2.5 ppm concentration of Fe NPs. According to the all results of this study, that optimum Fe NPs' concentration improve germination of seed and seedling growth of wheat seeds. Further studies are needed for exploration of the internal mechanism of Fe NPs uptake and mode of application for enhancing wheat yield [66].

CHAPTER 2. MATERIAL AND METHODS

Strawberry leaves were collected from a field near the Moscow, Russia. All the chemicals were of analytical grade purity.

2.1. Preparation of strawberry leaf extract

For preparation of plant extract, healthy and fresh strawberry leaves were collected, washed with tap water and then rinsed with distilled water for removing dust and other dirt particles, shade dried at room temperature, grounded and kept for further use. 20g of leaf powder was mixed with 200 ml of distilled water in a flask, boiled and stirred for 1 h. The mixture was cooled at room temperature and then filtered with a fabric filter and centrifuged for 20 min at 10000 rpm. The supernatant was filtered through paper filter to remove all solid particles. The obtained clear solution stored at 4 ^{o}C for further use. The extract was used for nanoparticles biosynthesis. Figure 1 represents the schematic procedure of the strawberry leaf extract preparation.

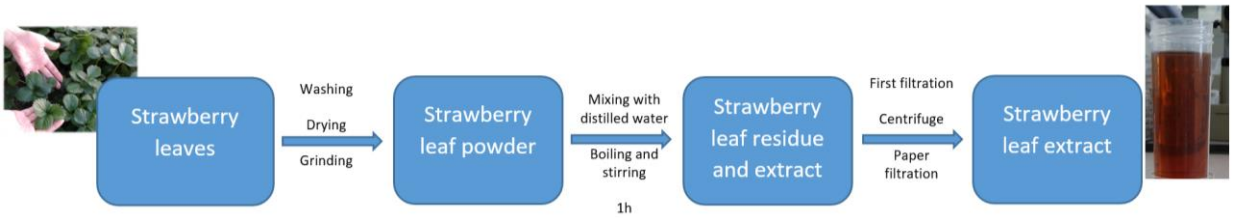

Figure 1. Schematic presentation of strawberry leaf extract preparation.

2.2. Preparation NPs

C-ZnO and NC-ZnO. Zinc acetate dihydrate, $Zn(CH_3COO)_2 \cdot 2H_2O$ and strawberry leaf extract applied for the synthesis of calcinated and non-calcinated ZnO nanoparticles. 10 mL of the extract added dropwise to the 100 mL 0.01 M solution of the zinc salt, which was stirring with magnetic stirrer and heated to 90 °C. As the reaction mixture became sturdy and brown showing the formation of NPs

and the process followed by addition of 2 M potassium hydroxide solution drop by drop to the pH of 11. After that, the reactant was centrifuged at 10,000 rpm for 25 min and washed several times until the supernatant became colorless. The obtained brown-color gel was dried at room temperature and ground very well to give a fine powder of non-calcinated ZnO (NC-ZnO) NPs. For production of calcinated ZnO NPs, the obtained NC-ZnO NPs was placed in furnace at 500 °C for 4 h. Finally, the white powder of calcinated ZnO (C-ZnO) was ground well and stored for further use.

Zn. Zinc acetate dihydrate, $Zn(CH_3COO)_2 \cdot 2H_2O$ salt used for the synthesis of the Zn NPs. 10 mL of the leaf extract was added drop by drop to the100 mL 0.01 M solution of the zinc salt under heating (90 °C) and stirring with magnetic stirrer. The color change of mixture into the cloudy brown indicated the formation of Zn NPs and then it was centrifuged at 10,000 rpm for 25 min and washed several times. The brown-color pelletlets dried at room temperature, ground and kept in a sealed container for further use.

MgO. Magnesium sulfate heptahydrate ($MgSO_4 \cdot 7H_2O$) was the precursor for the synthesis of MgO nanoparticles. 100 mL of the prepared 0.01 M solution of magnesium sulfate in distilled water was heated to 90 °C. 10 mL of the leaf extract was added drop by drop under continuous stirring and after that continued by addition of 2 M potassium hydroxide solution dropwise to the pH of 11. Addition of KOH resulted in formation of precipitation and turbidity of the solution, confirming the formation of NPs. The obtained solution centrifuged at 10,000 rpm for 25 min and washed several times. Resultant viscous dark brown gel was dried at room temperature and then ground perfectly, calcinated in furnace at 500 °C for 4 h to becomes a pinkish white powder of MgO NPs, then ground another time.

Ag. Silver nitrate ($AgNO_3$) used as the precursor for producing Ag NPs. Silver nanoparticles produced by reducing silver ions using strawberry leaf extract. 100 mL

of $AgNO_3$ 0.01 M solution was subjected to continuous stirring, heating to 90 °C and then addition of leaf extract drop by drop. By addition of the extract the color of the reaction mixture was changed to dark gray and became opaque which indicated the formation of Ag NPs. The solution was kept overnight at room temperature and then was centrifuged at 10000 rpm for 25 min and washed several times. Ag NPs was dried at room temperature and then ground to obtain very fine NPs.

Cu. The precursor of the synthesis of Cu NPs was copper (II) sulfate pentahydrate ($CuSO_4 \cdot 5H_2O$) salt. 10 mL of the leaf extract added dropwise to the 100 mL 0.01 M solution of the copper salt under the continuous magnetic stirring. A brown cloud of the Cu NPs appeared by the addition of extract solution. The resultant solution remained at room temperature overnight for completing the precipitation process. To collect the sample, the solution was centrifuged at 10,000 rpm for 25 min, washed several times, precipitant dried at room temperature and ground perfectly.

Fe. Iron (III) chloride hexahydrate ($FeCl_3 \cdot 6H_2O$) salt was used for the synthesis of the Fe NPs. 10 mL of the leaf extract was added dropwise to the 100 mL stirring 0.01 M solution of the iron salt. The color of the reaction mixture changed immediately from yellow to intense black, indicating the formation of Fe NPs. Then the mixture centrifuged at 10,000 rpm for 25 min and washed several times until the supernatant became colorless. The black-color precipitant was dried at room temperature and finally ground to result in a uniform and smooth powder.

2.3. Characterization of Biosynthesized NPs

UV-Visible absorption spectroscopy. A UV-Vis spectrophotometer model Varian Cary 50 (Palo Alto, U.S.) was employed in the range of 200 to 800 nm to confirm the production of NPs and explore the absorption spectra of NP suspensions. 1 mg/mL aqueous suspensions of the NPs were prepared freshly before the

spectroscopy and sonicated for 20 min. Distilled water was applied as the reference for all measurements.

Field emission scanning electron microscopy (FESEM) with energy dispersive X-ray spectroscopy (EDS). FESEM-EDS analysis was performed to obtain information about size, size distribution, shape heterogeneity and aggregation of the synthesized NPs and their elemental composition. TESCAN MIRA3 (Brno-Kohoutovice, Czech Republic) instrument was applied for FESEM-EDS analysis. In order to prepare samples for taking the FESEM images, samples were coated by a very thin layer of gold to improve the sample surface conductivity, prevent charge accumulation and obtain a better contrast. Analysis conditions are mentioned in Table 1.

Table 1. Analysis condition for FESEM-EDS reports

Accelerating Voltage (kV)	*15.0*
Beam Current (nA)	*10.000*
Magnification	*3000*
Live Time (s)	*30*
Preset Time (s)	*30*
Nb Channels	*4096*
Ev / Channel	*10*
Offset (keV)	*0*
Width (keV)	*41*

Data about mean size was obtained by measuring the particle size of about 100 nanoparticles. For analysis of SEM and FESEM images the software “imageJ” (1.53 e, Wayne Rasband and contributors, national institutes of health, Madison, USA) was used.

Photon cross correlation spectroscopy (PCCS). The hydrodynamic size distribution of the obtained NPs measured using a photon cross correlation spectroscopy (PCCS) applying a Nanophox particle size analyzer (Sympatec, Clausthal-Zellerfeld, Germany). Prior to measurement, 1 mg/mL aqueous suspensions of the nanoparticle were prepared and sonicated for 20 min at 25 °C. The measurements were performed at room temperature and repeated five times for each sample.

Fourier-transform infrared spectroscopy (FT-IR). To study peak patterns of leaf extract, and the bonding patterns of capping agents present in the extract of strawberry leaf and biosynthesized NPs, FT-IR studies were performed on BRUKER FT-IR Spectrophotometer (Billerica, U.S.). The spectra recorded in the range of 400 to 4000 cm^{-1} (mid-infrared region, MIR) and under the controlled atmospheric conditions.

X-Ray Diffraction (XRD) analysis. XRD analysis was applied to confirm the presence of synthesized NPs, identify the crystal structure, calculate the average particle size and detect the impurities. GNR XRD Explorer instrument (Novara, Italy) with cupper tube, and 40 kv, 30 Ma, 1.5460 Å set up used for X-ray diffraction analysis. The crystalline domain size was calculated using Scherrer equation, Equation (1) [19,67]:

$$D = \kappa\lambda/\beta \cos\theta \qquad (1)$$

in which θ represents for diffraction angle in radians, D is crystalline domain size and θ is the width of the peak at half of its height in radians. The Scherrer constant, κ, is the shape factor and typically considered to be 0.9. The X-ray wavelength (λ) depends on the type of X-rays used in the experiment (K_α =1.5460 Å).

2.4. In vitro evaluation of antibacterial activity of Ag and Cu biogenic nanoparticles

The method of broth dilution was applied for evaluation of antibacterial activity of NPs. Bacterium *Pseudomonas aeruginosa* isolated from potatoes tuber from Moscow region was used for this purpose. Lysogeny broth (LB) liquid medium was prepared for bacterial growth according to the Bertani (Bertani 1951) and LB agar medium prepared by addition of 3 g agar to 200 ml LB solution before autoclave.

The bacteria were cultured for 24 h in the LB medium before using for the tests. After that, 10 μl of this solution and different amounts of NPs powder added to the test tubes containing 2 mL of LB medium and incubated for 24 h at room temperature. Bacterial medium with no NPs was considered as negative control. The volume of 10 μl from the test tube were put in LB agar petri dishes, swabbed by L-shape rod and incubated for 24 h. The antibacterial activity for each NP was analyzed after taking an image of the plates and counting the number of grown colonies using the "imageJ" software (1.53 e, Wayne Rasband and contributors, national institutes of health, Madison, USA).

EC_{50}, MIC and MBC*:* EC_{50} or half maximal effective concentration, defined as the statistically derived median concentration of a substance (e.g. pesticide) which produce a certain effect in 50% on the test organisms like bacteria population or fungus mycelium and causing 50% growth inhibition after a specified exposure time. We calculated the EC_{50} values using linear curve graphs and the mathematical equations [68]. In this report, EC_{50} is the concentration of NPs at the point of 50% decrease of CFU.

MBC or minimum bactericidal concentration defined as the lowest concentration of an antimicrobial substance, which is needed to kill 99.9% of the final inoculum after incubation for 24 h under specific conditions. After broth macrodilution, MBC could be determined by sub-culturing samples from tubes, yielding a negative

microbial growth after incubation on the surface of non-selective agar plates to determine the number of colony forming units (CFU) after 24 h of incubation [69].

2.5. In vitro evaluation of antifungal activity of biogenic nanoparticles

Pathogenic fungi, *Botrytis cinerea* Pers., *Pilidium concavum* (Desm.) Höhn. and *Pestalotia sp.* applied in present study. *B. cinerea* (strain 19MFrR1) was isolated from the roots of strawberries grown in the Moscow region, and identified by cultural and morphological characters and by PCR, followed by sequencing of the species-specific site. *Pilidium concavum* (Desm.) Höhn. (strain 19FrPil1) *and Pestalotia sp.* (strain 19FrPest1)- donated by Yulia Yvetkova (All-Russian Plant Quarantine Center Federal State Budgetary Institution, "VNIIKR" FGBI).

Two different methods used for studying antifungal properties of NPs:

(I) Agar dilution method with slight modification was applied using oatmeal agar medium. Oatmeal agar was prepared according to Koneman [70] as oatmeal is a source of nitrogen, carbon, protein and nutrients and agar is the solidifying agent. Then the extract was divided into different volumes and agar was added to each volume (1.5 g per 100 mL solution), autoclaved and allowed to cool. NPs dispersed in sterile distilled water by sonication for 20 minutes at 25^{o}C. Proper amounts from the NPs suspensions with different concentrations were added to the molten agar under the laminar flow hood, swirled, poured into Petri dishes and allowed to become cool and solidify. Also, a NP free solution poured into the Petri dishes and allowed to solidify as control. To obtain reliable results, the experiment was carried out in triplicate.

The strains of *B. cinerea*, *P. concavum* and *Pestalotia sp.* were replicated and grown in culture media before using in the experiment. Agar disks of mycelial with 1 cm diameter cut from the fungal cultures of seven days' age, were put in the center of each Petri dish and incubated at room temperature. Diameter of each colony (the

average of the longest and the shortest diameter in mm) was measured every three days. Finally, the inhibition ratio of NPs calculated by the following equation (Equation 2) [71-72]:

$$\text{Percentage growth inhibition} = [\frac{C-T}{C}] \times 100 \qquad (2)$$

where C is the diameter of the control colony and T is the diameter of the treatment colony.

The fungi were maintained using the periodic replanting technique that enabled the cultures to survive over short periods of time. This technique is based on transferring the growth from the dry or old medium to a fresh one, providing optimum conditions for fungus growth. In this way, the high risk of contamination and variability of the characteristics of the strains which represent the main disadvantages are avoided.

(II) To determine the ability of *B. cinerea* spore's germination oatmeal agar medium was used with the addition of different concentrations of silver nanoparticles.

To produce fungal inoculums of *B. cinerea*, isolates were grown on oatmeal agar plates at 25 °C. Conidia were collected by scraping them with a sterile spatula, and then suspending in sterile distilled water. The spores were counted under light microscope and the suspension was diluted with sterile distilled water to obtain the final concentration (4.3 spore per µl). A volume of 20 µl of spore suspension placed on agar culture containing different amounts of the Ag NPs of 0 (as control) 1, 10, and 100 ppm. The plates incubated at laboratory condition and the presence of growth was observed. The number of the colonies is reported after observation of visible growth. To obtain reliable results, the experiment was carried out in triplicate.

2.6. Effect of NPs on seed germination and seedling growth of crop plants

Preparation of priming solutions: Different concentrations (50, 100, 150 ppm) of NPs (C-ZnO, NC-ZnO, Zn, MgO, $AgNO_3$, Cu and Fe) and also their counterpart metal salts ($Zn(CH_3COO)_2$, $MgSO_4$, $AgNO_3$, $CuSO_4$ and $FeCl_3$) prepared in distilled water and the NPs dispersed by ultrasonic vibrations for 20 minutes. All dilutions were freshly prepared before use.

Preparation of seeds: Seeds of wheat (*Triticum aestivum L.*) variety Firuza 40 and flax (*Linum usitatissimum*) variety of Semi Lini were used in this experiment. Each treatment consisted 30 randomly selected seeds with three replications. Seeds were kept in dry place at room temperature prior to use.

(a) Preparation of wheat seeds: Viability of seeds checked by suspending them in distilled water, discarding the seeds floating above were and selecting seeds settled at bottom of the water for further experiment. Seeds immersed in a 5% sodium hypochlorite solution and rinsed with distilled water after 10 min, for surface sterility of the seeds [73]. Then seeds soaked in a prepared NPs suspensions or metal salt solutions for approximately 12 h. A set of seeds was soaked in distilled water without providing any treatment as a control.

(b) Preparation of flax seeds: Seeds were checked visually for removing damaged seeds from the samples. Then seeds soaked in NPs suspensions or metal salt solutions for 12 h. A set of seeds was used without providing any treatment as a control and soaked in distilled water.

In vitro germination of seeds: One piece of filter paper was placed into a Petri plate (10 cm in diameter), and for wetting the paper, 5 ml distilled water was added using a Pasteur pipette. Then 30 nano-primed seeds were transferred onto each the filter paper. The Petri plates incubated at room temperature for 7 days.

Measurement of physiological indexes: Germination percentages, shoot length, root length, seedlings length, root-shoot ratio, seedling vigor index (SVI), shoot length stress tolerance index (SLSI) and root length stress tolerance index

(RLSI) were calculated at 2nd and 7th days. Means and standard deviations were derived from measurements on three replicates for each treatment and controls.

A seed was considered germinated after the emergence of radicles or plumules from the seed coat [6]. The length of the roots and shoots were measured using a ruler with centimeter scale (fig. 2).

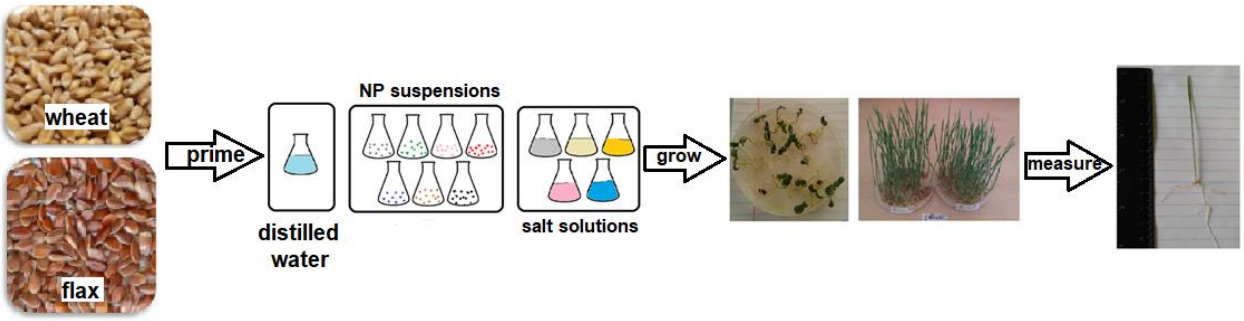

Figure 2. Graphical summary of the experiment

(a) Shoot length and root length: At 2nd and 7th days of the experiment, 10 seedlings from Petri plate randomly selected to measure shoot and root lengths [30].

(b) Seedling length: is considered as the sum of shoot length and root length [30].

(c) Germination percentage: The final germination percentage was calculated based on the total number of germinated seeds at the end of experiment. Germination parameters calculated using the following equation (Equation 3) [74]:

$$\text{Germination percentage (\%)} = (\text{average number of germinated seeds/total number of seeds}) \times 100 \quad (3)$$

(d) Root-Shoot Ratio: The root to shoot ratio for each seedling was calculated as follows (Equation 4) [74]:

$$\text{Root to Shoot Ratio} = \text{average root length/ average shoot length} \quad (4)$$

(e) Seedling Vigor Index (SVI): The seedling vigor index was computed by adopting the method suggested by Abdul-Baki and Anderson (1973) and expressed as an index number (Equation 5) [75]:

Seedling Vigor Index (SVI) = [average root length (cm) + average shoot length (cm)] × average germination percentage (5)

(f) Shoot length stress tolerance index (SLSI) calculated using following equation (Equation 6) [6,74]:

SLSI (%) =average shoot length of treated seedlings/average shoot length of control seedlings ×100 (6)

(g) Root length stress tolerance index (RLSI) calculated as follow (Equation 7) [6,74]:

RLSI (%) =average root length of treated seedlings/average root length of control seedlings ×100 (7)

2.7. Statistical analysis

The obtained data were statistically analyzed using Microsoft Excel software (version 2019), SAS and MSTAT-C statistical programs. Two-way analysis of variance (ANOVA) applied for performing statistical analysis and p-value <0.05 considered as significant. Means and standard deviations obtained from measurements on three replicates for controls and each treatment. Mean comparison performed by Least Significant Different (LSD) test. Values are presented as the mean ± SD. of the three replications in each experiment.

CHAPTER 3. RESULTS AND DISCUSSIONS

3.1. Biosynthesis of NPs

In this investigation, for the first time, we used *Fragaria ananassa* (strawberry) leaf extract as a source of natural reducing, capping or stabilizing agent to develop an eco-friendly, cost-effective and safe process for the biosynthesis of metal-based nanoparticles including calcinated and non-calcinated zinc oxide, zinc, magnesium oxide, silver, copper and iron nanoparticles.

Strawberry leaf extract. A complete water mediated extraction method with no solvent or chemical addition was used to extract phytochemicals from strawberry leaf. During the biosynthesis of metal-based nanoparticles, the leaf extract was added to different precursors at specific procedures related to each precursor.

A reduction in the color intensity of the extract was observed during the process for all of the different samples. The observed color change demonstrates the degradation of phytochemicals in the mixture which were reducing agents for synthesis of nanoparticles. Minerals and biomolecules of strawberry leaf extract are responsible for the biochemical reactions wherein biological molecules react with the metallic precursors leading to formation of the NPs (Figure 4).

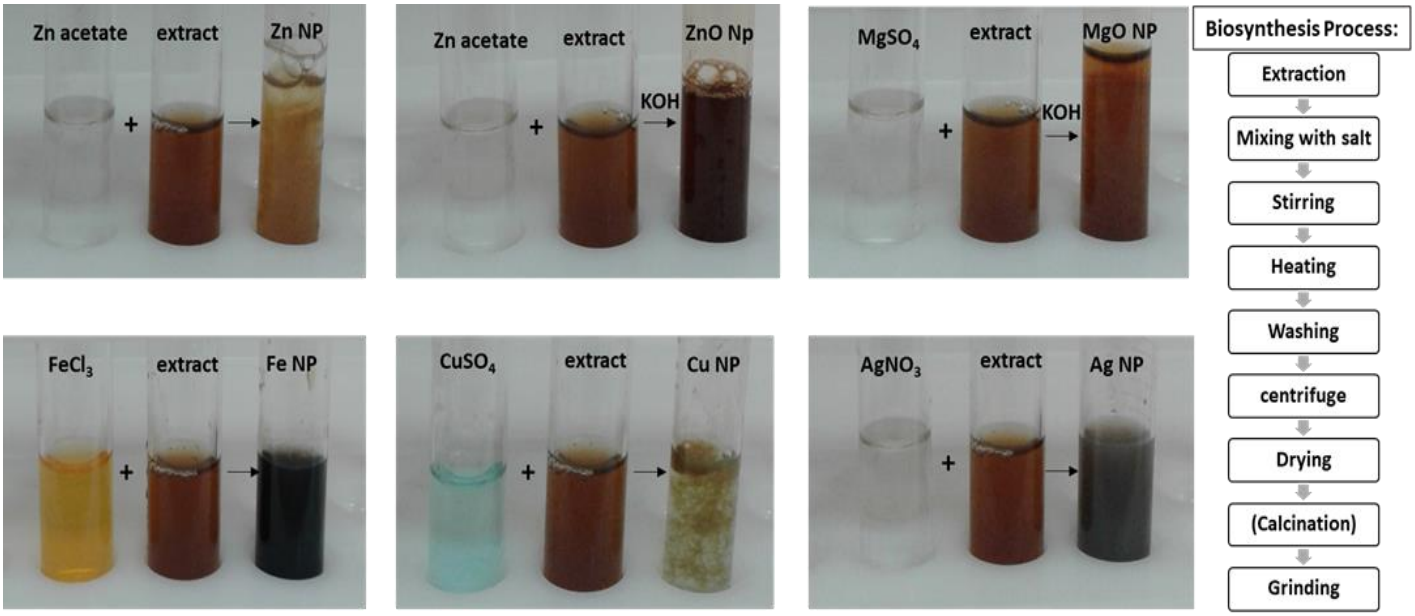

Figure 4. Schematic representation of biosynthesis of NPs and color changes due to the formation of nanoparticles.

Green synthesis of Calcinated-ZnO nanoparticles. For the first time, in present investigation, the biosynthesis of zinc oxide nanoparticles was carried out by a novel, ecofriendly, cost effective, biocompatible, safe approach using strawberry leaf extract as a natural reducing and capping agent. It is obvious that the synthesis of ZnO nanoparticles in a green method is much environmentally friendly and safer comparing to the chemical methods [76-77]. The reaction mechanism of C-ZnO NPs formation could be illustrated as bio-reduction of zinc ions by various plant metabolites or phytochemical components of the plant extract, including terpenoids, polyphenols, sugars, flavonoids, etc., which results in complexation and then formation of ZnO NPs after addition of KOH. These phytochemicals also act as capping agent or stabilizer for nanoparticles by chelating effect to control the growth of them and preventing them from aggregation. The synthesis of zinc oxide by strawberry leaves results in an end product of light brown precipitate. The final step is calcination and decomposition reaction to yield C-ZnO NPs, a yellowish white powder.

Moreover, the strawberry leaf extract has significant potential due to its polyphenols and have an easy electron losing capacity which results in the green zinc complex formation. The obtained zinc complex on heat treatment by calcinating at 500 °C yields zinc oxide nanocrystals.

The reaction mechanism for the formation of C-ZnO NPs is as a result of the reaction of the zinc ions present in the solution with the polyphenols such as the tannins, glycosides, and flavonoids in the plant extract forming complexation. This is followed by hydrolysis reaction to form zinc hydroxide by interaction of the hydroxyl group in the polyphenol. Calcination and decomposition reaction shortly follows to form zinc oxide nanoparticles. Also, the synergistic reaction of all the phytochemical components presents in the extracts (terpenes, flavonoids, saponins, tannins, glycosides/carbohydrates, and alkaloids) act as both reducing/stabilizing agent by reducing Zinc to the zero valence state [37]. Similarly, Chikkanna et al. successfully biosynthesized C-ZnO NPs using agro-waste materials and zinc sulphate precursor [77].

Green synthesis of NC-ZnO nanoparticles. In the synthesis of NC-ZnO nanoparticle, with drop wise addition of the leaf extract of strawberry to the colorless 0.01 M zinc acetate solution followed by the addition of KOH at 70 ^{o}C the color of the extract changes from clear brown to a turbid one, confirming the formation of ZnO nanoparticles.

Gupta et al. reported the green synthesis of ZnO NPs (noncalcinated) using leaf extract of *Catharanthus roseus* (*C. roseus*) [78].

Green synthesis of Zn nanoparticles. Synthesized Zn NPs are known in the solution by the formation of brown particles in the zinc acetate solution after addition of extract droplets. This is due to metal ion reduction and capping of stabilizing agent. The color change can be easily identified by the naked eye. It clearly indicates the formation of well reduced and stabilized Zn NPs.

Green synthesis of MgO nanoparticles. In biosynthesis of MgO nanoparticle, strawberry leaf extract added drop wise to the colorless 0.01 M magnesium sulfate solution. It followed by drop wise addition of KOH at 70 ^{o}C. The color of the reaction mixture changed to a turbid one, which is due to the formation of $Mg(OH)_2$ (magnesium hydroxide) nanoparticles. The phytochemicals present in the leaf extract function as a reducing, capping and stabilizing agent towards the biosynthesis of these NPs. The formation of nanoparticles is confirmed by the visible color change and the UV-Vis spectroscopy response. The calcination process, converts $Mg(OH)_2$ nanoparticles to the MgO NPs.

Green synthesis of Ag nanoparticles. Silver nanoparticles were prepared from a drop wise addition of aqueous strawberry leaf extract to the $AgNO_3$ solution of 0.01 M. The observed color changed to dark brown in reaction indicating the formation of silver nanoparticles using water extract of strawberry leaf.

The reduction of the silver ions is moderately rapid at ambient conditions. This is innovative and interesting to the field of material, science the evaluated leaf biomass was found to have the capability to reduce metal ions at ambient circumstances [79]. However, according to the literature, the rate of synthesis of Ag NPs increases with an increase in temperature (30–90 ^{o}C) and encourages the production of small-size NPs [14]. Furthermore, the biomass handling and processing is less rigid since, it does not involve boiling for long hours or successive treatment [79].

Leaf extract of pine, alfalfa, magnolia, persimmon, and many other plant's leaf extract were successfully applied by other researchers for synthesis of Ag NPs [9].

Green synthesis of Cu nanoparticles. After adding the extract to the copper sulfate solution drop by drop, the color of the copper sulfate changed immediately from light blue to dark brown, which was due to the synthesis of the copper nanoparticles. The formation of copper NPs was possibly facilitated by reduction of

metal ions by phytochemicals present in the extract of the strawberry leaves. The formation of Cu NPs takes place via the following steps:

(1) Complexation with copper metal salts, (2) simultaneous reduction of copper metal, and (3) capping with oxidized phytochemicals. The use of the extract for synthesis of NPs some advantageous is taken over other biological processes because it can be suitably scaled up for large-scale nanoparticles synthesis [5]. Some other green methods for synthesis of Cu NPs have been reported, using extract of different plant leaves such as leaves of *Euphorbia esula L* [5], *Eclipta prostrata* [23] or *Azadirachta indica* [24].

Green synthesis of Fe nanoparticles. The leaf extract plays a double role in the process of NP synthesis; it reduces the iron salts to Fe NPs and acts as stabilizing agents hindering the aggregation of the synthesized NPs. The light yellow color of the reaction mixture (iron choloride 0.01 M) changes to black on drop wise introducing of the leaf extract, indicating the formation of Fe nanoparticles. The leaf extract of may reduce Fe^{3+} to Fe^{0} [80]. The green synthesis of Fe NPs using extracts of waste tea [59] and mortiño berry (*Vaccinium floribundum*) [60] have been reported.

3.2. Characterization of Biosynthesized NPs

In order to investigate the main characteristics of the biosynthesized nanoparticles, they were characterized using UV-Vis Spectroscopy, Field Emission Scanning Electron Microscopy (FESEM) coupled with Energy Dispersive X-ray Spectroscopy (EDS), Photon Cross-Correlation Spectroscopy (PCCS), Fourier Transformed Infrared Spectroscopy (FT-IR) and X-ray Diffraction spectroscopy (XRD). Table 2 represents a summary of the possible information derived from using various characterization techniques which were applied in this research.

Table 2. Summary of the applied techniques for characterization of nanoparticles which were featured in this thesis [3].

Technique	The main derived information
XRD	Composition, structure of crystal, grain size of crystal
FT-IR	Composition of the surface, binding of the ligands
UV-Vis	Optical characteristics, size, agglomeration state, concentration, points on shape of NPs
FESEM-EDS	Elemental analysis, precision, morphology and dispersion of NPs in matrices/supports like cells
PCCS	Hydrodynamic size, size distribution, detection of agglomerates

3.2.1. UV-Visible Absorption Spectroscopy

The most widely used method for a preliminary analysis of metallic nanoparticle formation is UV–Vis absorption spectroscopy. Metal nanoparticles' optical properties is one of the most interesting properties of them which changes proportional to the shape and size of nanoparticles [17,18]. The optical absorption spectra of metal NPs and their intense color in water arise from phenomenon of surface plasmon resonances (SPR). SPR phenomenon is responsible for the color change of reaction mixture because of SPR vibrations and reduction of metallic ions (Figure 4). SPR vibrations are affected by different parameters such as temperature, pH, concentration, size and shape of synthesized NPs [5,41]. Therefore, the peak maximum position and sharpness changes proportional to the size and shape of NPs and move towards longer wavelengths, with the increase in particle size [48,79,81]. The more spherical NPs will have the sharper peaks [79]. Based on the UV-Vis spectra, properties of NPs in terms of their shape and size can be determined.

According to Mie theory, light absorbance is directly proportional to the particulate size of metal nanoparticles, as metal nanoparticles are conductors and possess surface plasmon resonance. Although in most cases, X-ray photoelectron spectroscopy is used to analyze metal-based nanoparticles, UV-visible spectroscopy is sufficiently effective as a preliminary analysis of metallic NP formation [42].

Metal-based NPs intense colors in water is due to the dipole oscillation arising when an electromagnetic field in the visible range is coupled to the collective oscillations of conduction electrons. It is an established fact that metal nanoparticles ranging from 2 to 100 nm in size demonstrate broad surface plasmon peak. The optical absorption spectra of metal nanoparticles that are governed by surface plasmon resonances (SPR), move towards elongated wavelengths, with the increase in particle size. The absorption band position is also strongly dependent on dielectric constant of the medium and surface-adsorbed species [79]. The amount of light absorbed by the material, as a function of the wavelength, obtained for the extract and each NP, illustrated in following.

Extract. The UV-Vis spectrum of aqueous extract of strawberry leaf (Figure 5) shows peak maximum at 250 nm due to the π/π^* transitions strongly confirming the presence of aromatic compounds inside the plant extract [5].

C-ZnO. Synthesized C-ZnO NPs were subjected to UV-Vis spectrophotometer for confirming the formation of ZnO NPs at the first step (Figure 6). The UV-Vis spectra of C-ZnO NPs indicated an absorption band at 355 nm, which is in the characteristic wavelength range of zinc oxide NPs and is consistent with previous studies [37,77].

NC-ZnO. The existence of biosynthesized NC-ZnO NPs also confirmed by the UV-Vis absorption spectroscopy. The spectra exhibited a strong absorption band at 345 nm presented in (Figure 7) which is because of the surface plasmon resonance. The result is in agreement with other reports [37,77,81].

Zn. In order to make sure that the Zn NPs were successfully synthesized, the UV-Vis spectroscopy was used. As shown in Figure 8, there are two peaks of UV-Vis spectrum in the range of 200–800 nm. The peak maximum was observed at 270 nm, which is attributed to the Zn NPs.

MgO. UV–Vis spectra of pinkish colored biosynthesized MgO sample confirmed the formation of nanoparticles in the initial stage (Figure 9). Various peaks were observed under UV region, at about 200 to 300 nm, which are in accordance with previous studies [82-83].

Ag. The UV-Vis measurements showed that the Ag NPs exhibit one peak in the UV-Vis region centered at 457 nm, which is in accordance with earlier published results (Figure 10) [14,81].

Cu. The UV-Vis absorption spectra of Cu NPs showed an absorption band of around 270 to 370 nm (Figure 11). The Cu NPs exhibit a dark brown color in aqueous solution due to the SPR excitation in UV-Vis spectrum depending upon the particle size. The similar absorption bands for Cu NPs have been reported in this range [4,22].

Fe. The UV-Vis spectra of Fe NPs (Figure 12) showed prominent absorbance maximum at 270 nm and another low intense peak at 318 nm, thereby confirming the production of Fe NPs. These peaks were because of the excitation of SPR vibrations in the Fe NPs, which is consistent with the results of other researchers [59].

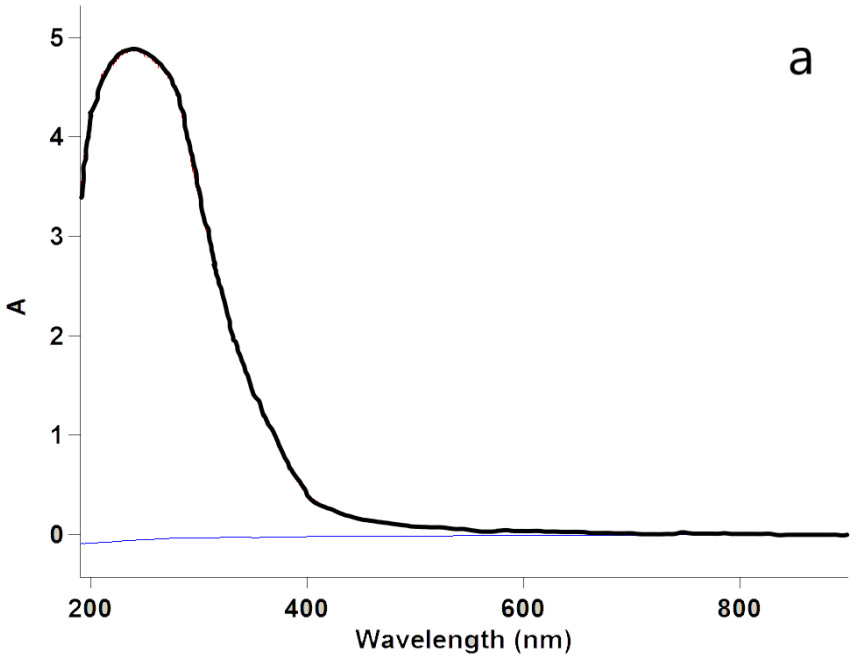

Figure 5. UV-Vis spectra of the strawberry leaf extract

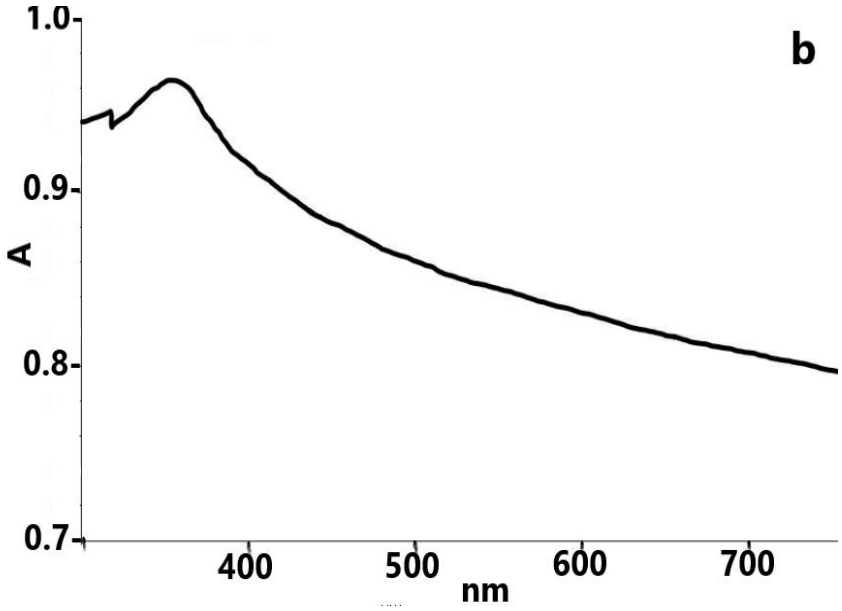

Figure 6. UV-Vis spectra of biosynthesized calcinated zinc oxide nanoparticles (C-ZnO NPs)

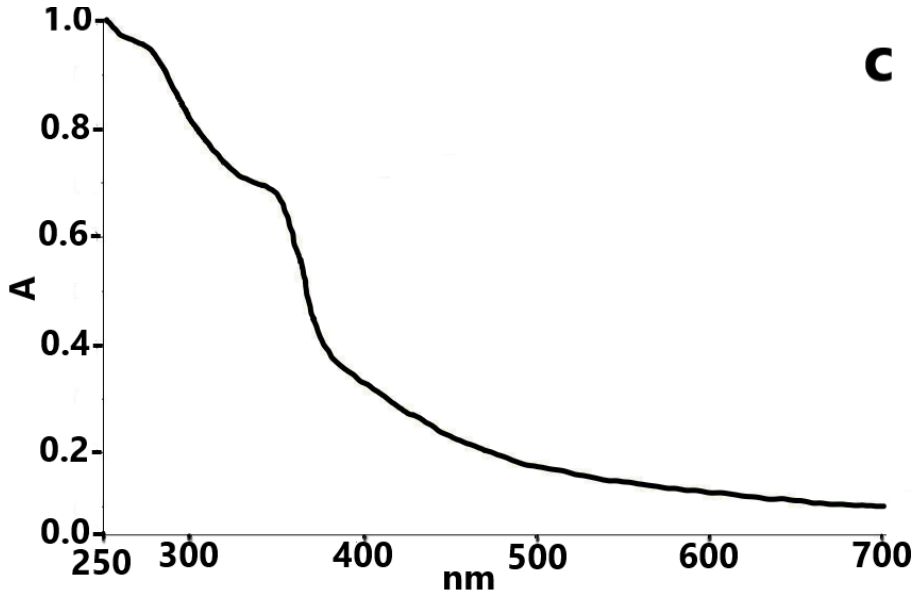

Figure 7. UV-Vis spectra of biosynthesized non-calcinated zinc oxide nanoparticles (NC-ZnO NPs)

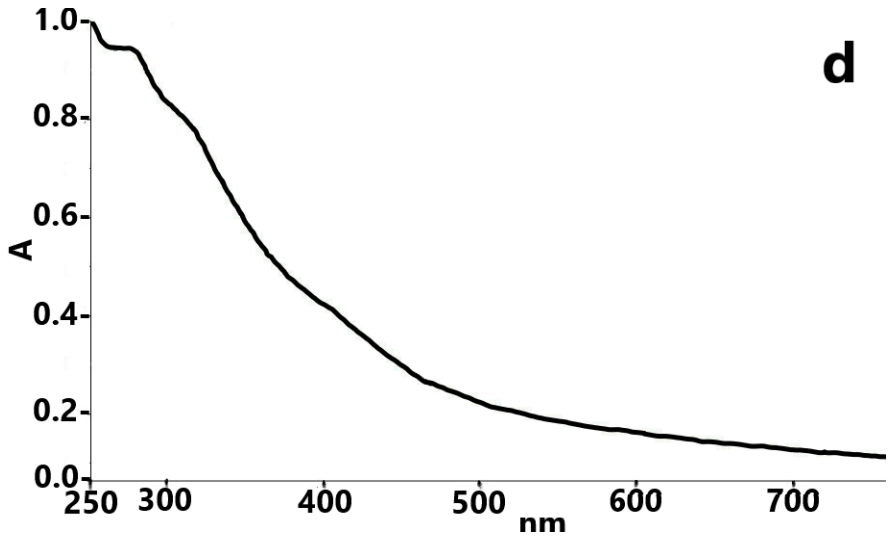

Figure 8. UV-Vis spectra of biosynthesized zinc nanoparticles (Zn NPs)

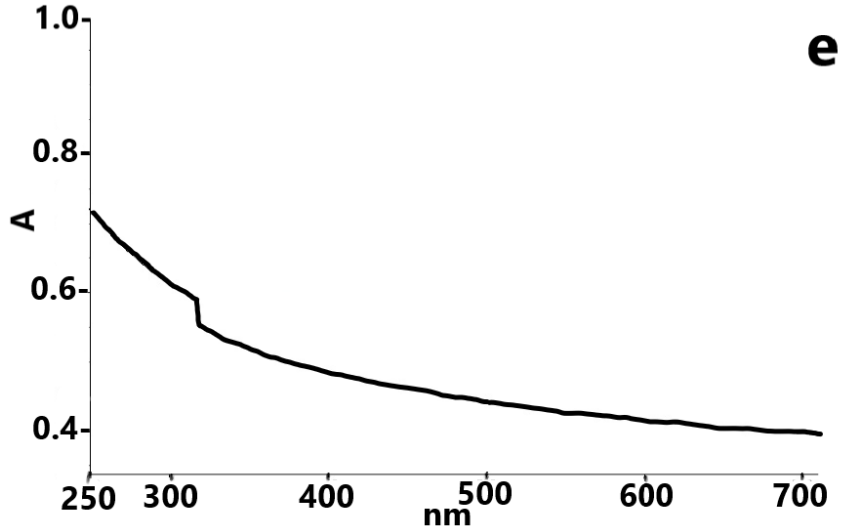

Figure 9. UV-Vis spectra of biosynthesized magnesium oxide nanoparticles (MgO NPs)

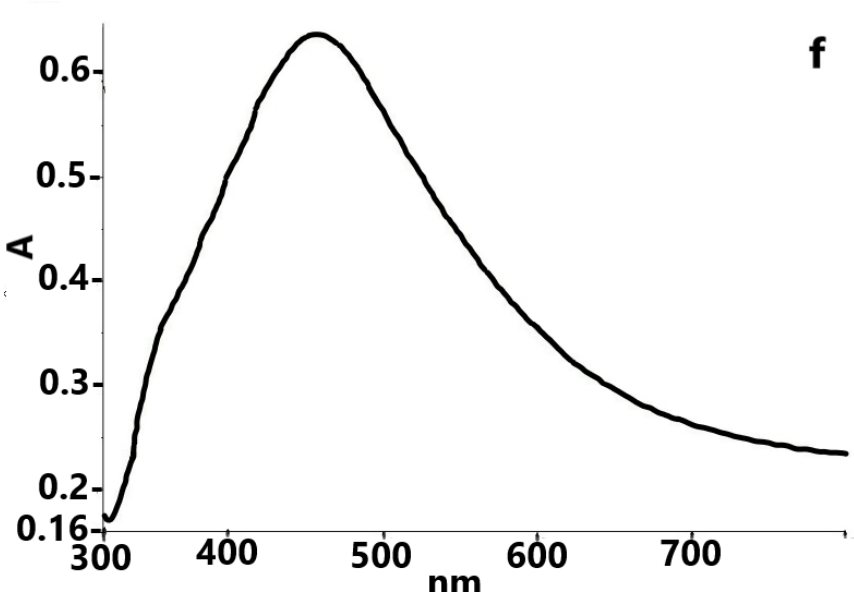

Figure 10. UV-Vis spectra of biosynthesized silver nanoparticles (Ag NPs)

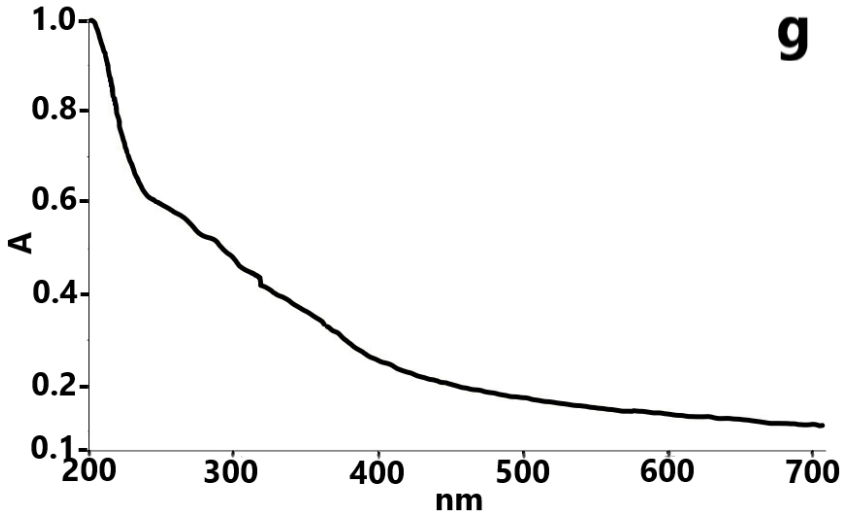

Figure 11. UV-Vis spectra of biosynthesized cupper nanoparticles (Cu NPs)

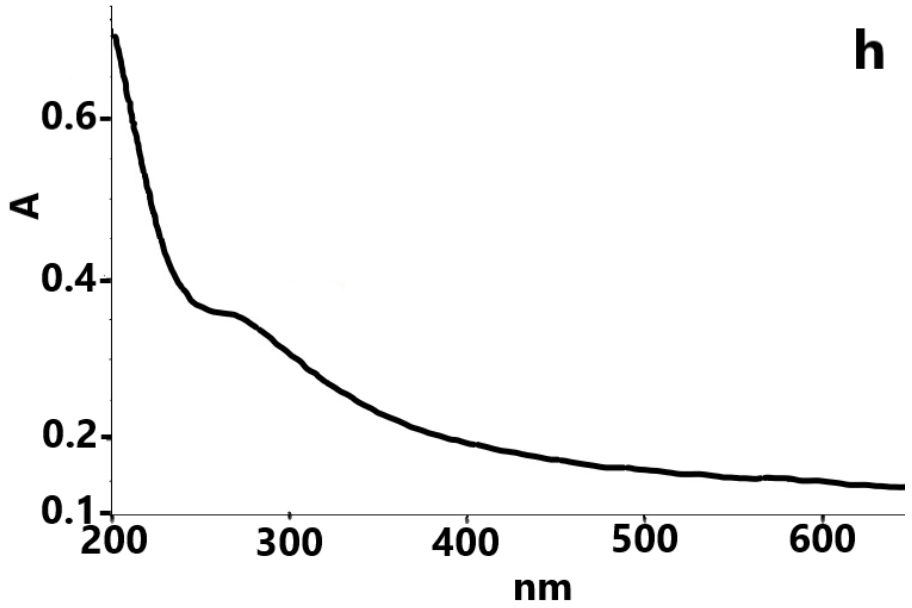

Figure 12. UV-Vis spectra of biosynthesized iron nanoparticles (Fe NPs)

3.2.2. Field Emission Scanning Electron Microscopic (FESEM) Images Analysis

The two most important parameters which are studied in characterization of NPs are “size” and “shape”. Size and size distribution of nanoparticles may affect other characteristics and their possible applications. [2]. After confirming the biosynthesis of nanoparticles firstly by color change and then by UV-Vis spectroscopy, the morphology of nanoparticles was investigated by FESEM, which gives information about structural properties such as size, size distribution, shape, shape heterogeneity and aggregation of NPs.

All of the biosynthesized NPs had sizes in the nanometer range, while some of them had nearly homogenous structure and yet others had heterogeneous structures (Table 2). Some nanoparticles were well separated from each other while most of them were present in agglomerated form. As a nanoparticle is defined as a particle with at least one dimension in the range of nanometer, these FESEM results confirmed the nanostructure behavior of the synthesized particles [3]. The results are in agreement with previous reports, although with some slight differences due to chemical composition and synthesis conditions.

C-ZnO. Representative FESEM micrographs of the biosynthesized C-ZnO NPs are displayed in (Figure 13). FESEM images show that the NPs have homogeneous spherical shape and the mean particle size is 40 nm. It is also visible that the particles have agglomerated into larger clusters due to the attractive forces which bring them together into groups. The results are comparable with the results of 400–124 nm reported by Ogunyemi et al. [37].

NC-ZnO. FESEM image of the NC-ZnO NPs (Figure 14) clearly demonstrated the presence of nano-scaled spherical shaped particles with average size of 25 nm which are agglomerated into larger clusters. It can be concluded from the FESEM

studies that the calcinated product brings larger values of particle size (Table 2). The results are better than some previously published works and the particles sizes are considerably less than that (40–120 and 60–130 nm) [77].

Zn. FESEM images of biosynthesized Zn NPs (Figure 15) show that the Zn NPs were sheets with irregular shape and the average size of 100 nm in diameter and 20 nm in thickness (Table 2). They also showed a small amount of agglomeration.

MgO. FESEM results of MgO NPs confirmed the nano range of the biosynthesized MgO nanoparticles with average size of 65 nm and quasi-spherical agglomerated nano-scaled particles (Figure 16). Jeevanandam et al. reported similar results (18–80 nm) in their report [42].

Ag. Representative FESEM micrographs of the biosynthesized Ag NPs contains particles with uniform spherical shapes in the size diameter range of 50 nm and also depicts agglomerated Ag nano-crystals. These agglomerates easily dispersed in water with ultrasonic vibrations (Figure 17). The obtained results are similar to the results of previous reports [4].

Cu. Based on the obtained images of FESEM (Figure 18), the biosynthesized Cu NPs are in the nanometer range and it is obvious that the morphology of crystals showed some non-uniform distribution. Their structure is in the form of sheets with average diameter of 180 nm and thickness of 30 nm (Table 2). Some nanoparticles were well separated from each other while most were present in agglomerated form. The results are in agreement with previous reports [84], although with few differences due to the synthesis condition.

Fe. FESEM micrographs of the synthesized Fe nanoparticles were shown in Figure 19. The images represent nanoparticles of irregular shape like sheets with

average diameter of 130 nm and thickness of 20 nm (Table 2) and the surface morphologies in the form of assemblies of nanoparticles.

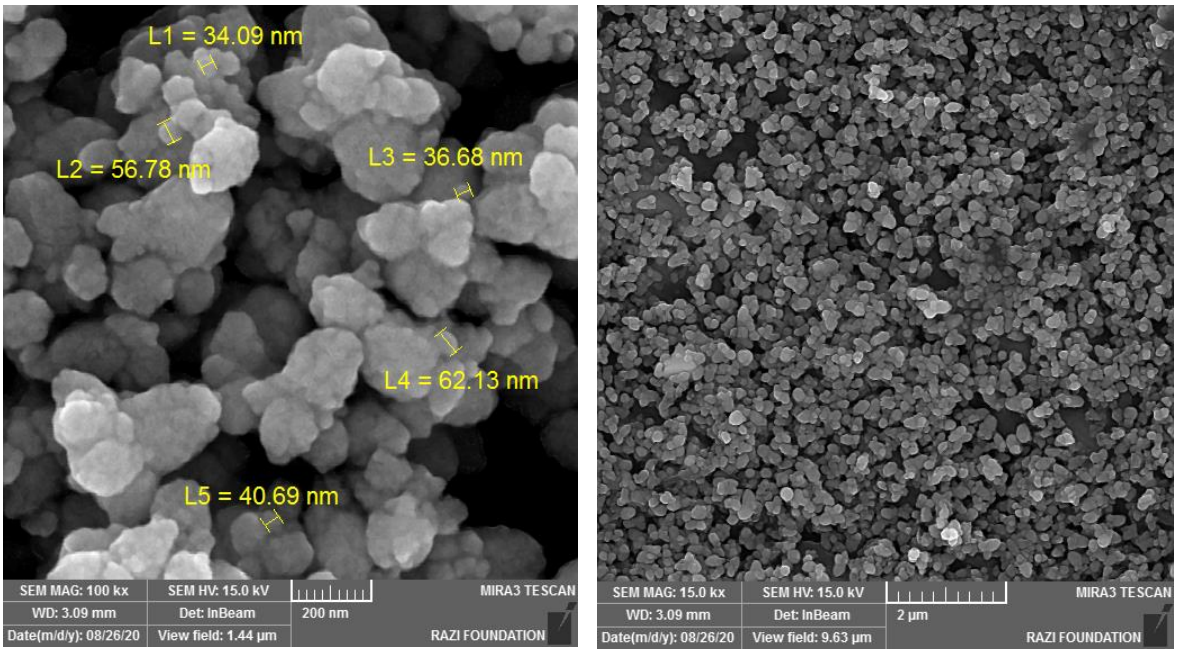

Figure 13. FESEM images of biosynthesized calcinated zinc oxide nanoparticles (C-ZnO NPs)

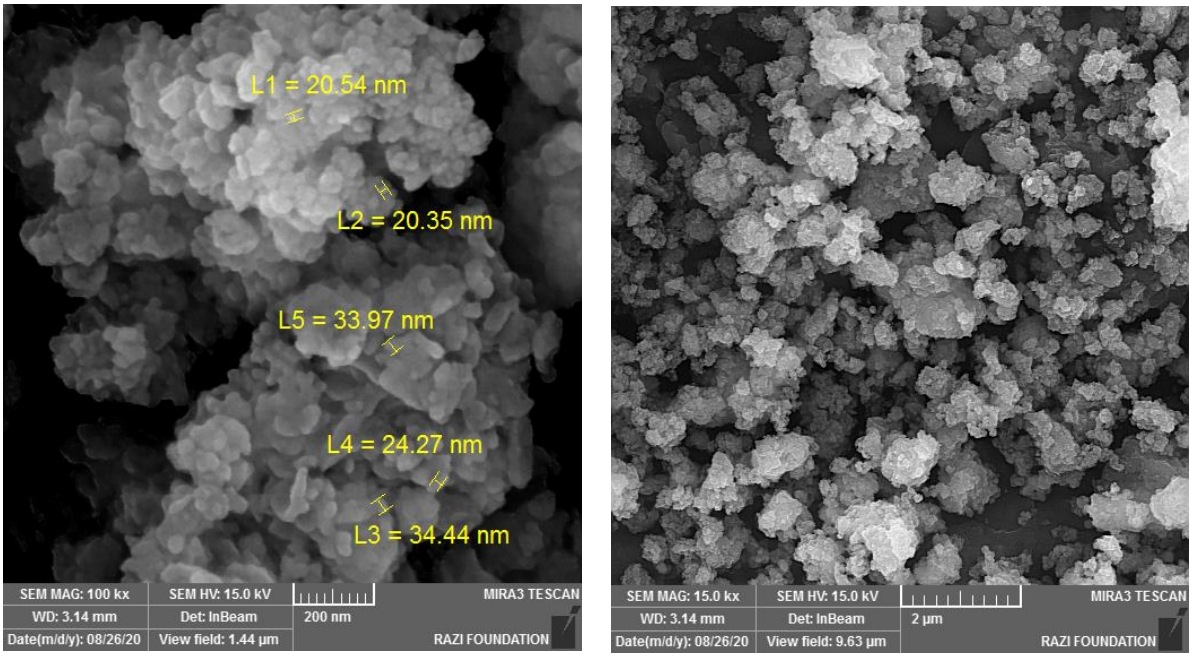

Figure 14. FESEM images of biosynthesized non-calcinated zinc oxide nanoparticles (NC-ZnO NPs)

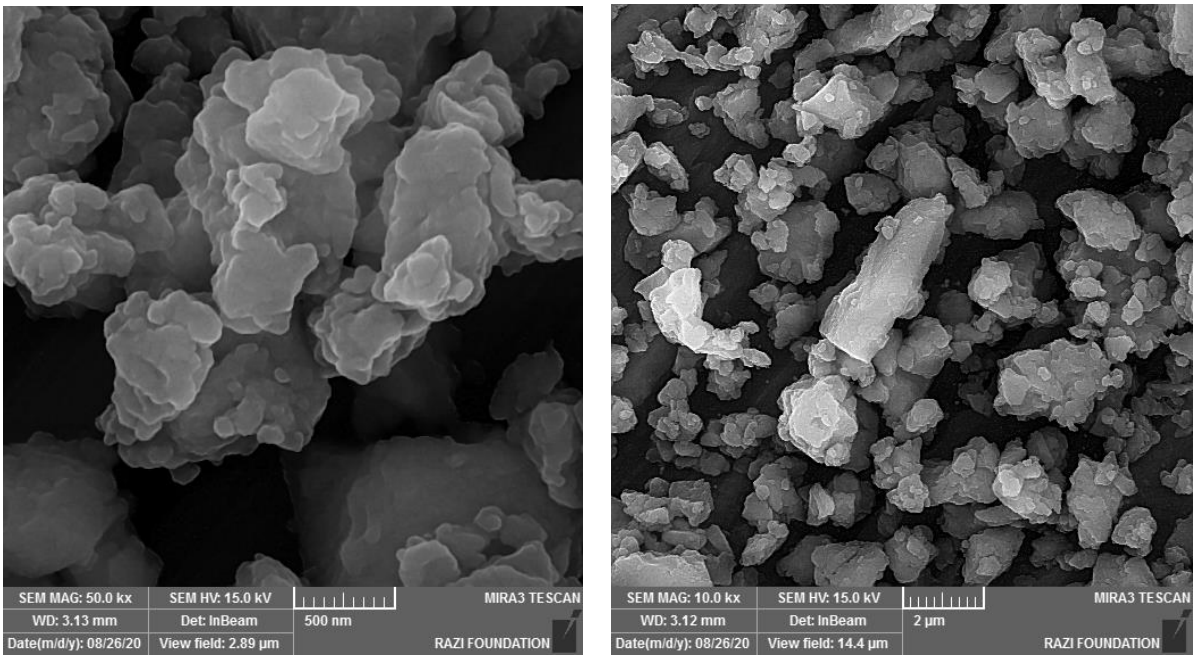

Figure 15. FESEM images of biosynthesized zinc nanoparticles (Zn NPs)

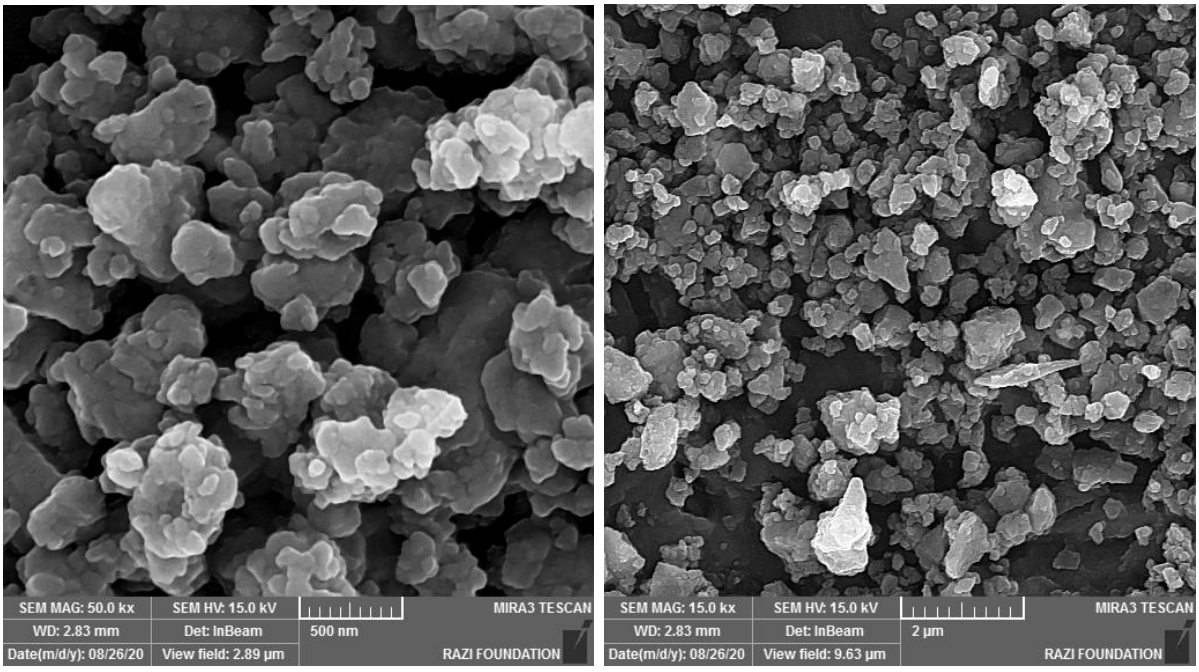

Figure 16. FESEM images of biosynthesized magnesium oxide nanoparticles (MgO NPs)

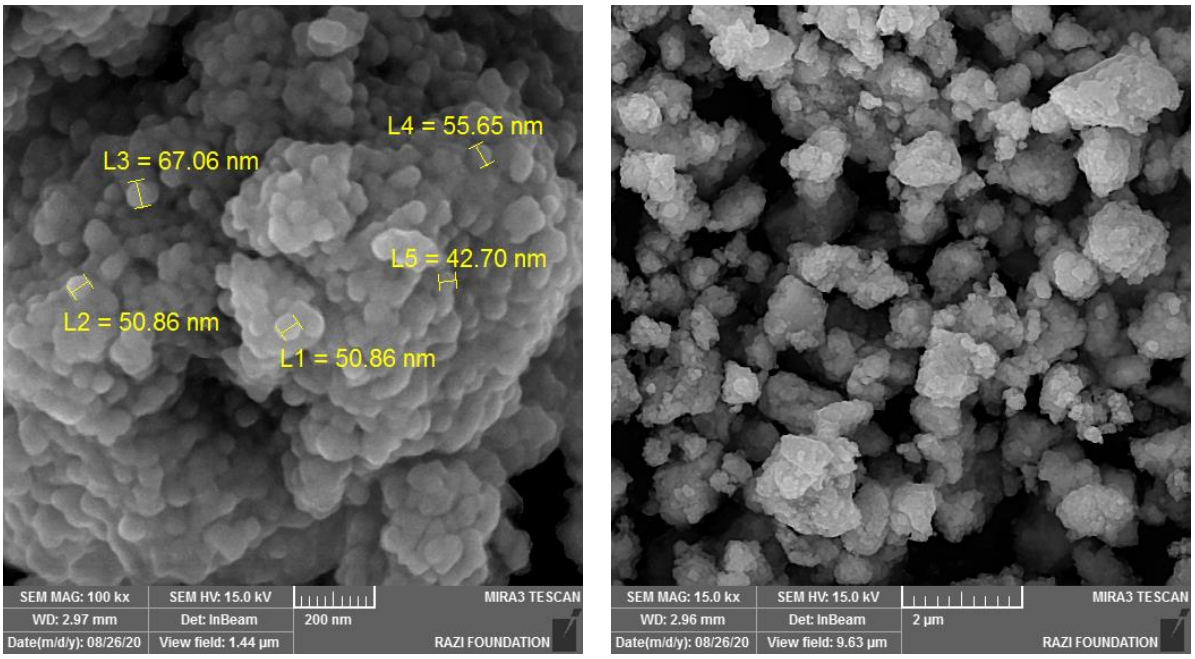

Figure 17. FESEM images of biosynthesized silver nanoparticles (Ag NPs)

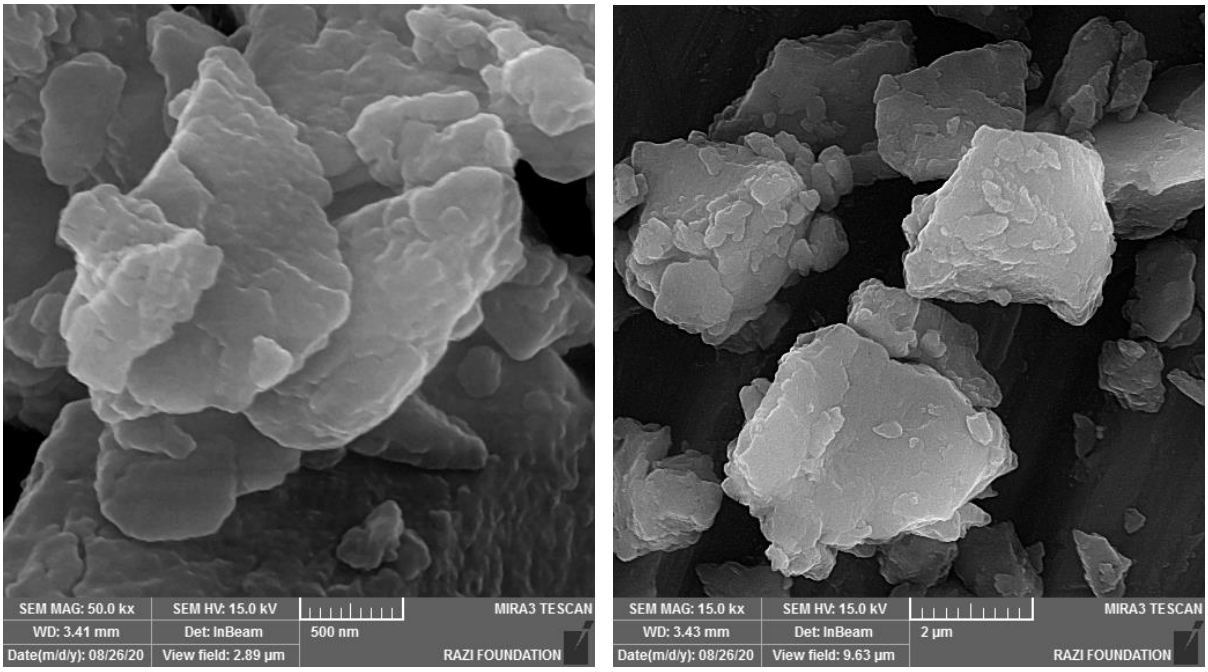

Figure 18. FESEM images of biosynthesized cupper nanoparticles (Cu NPs)

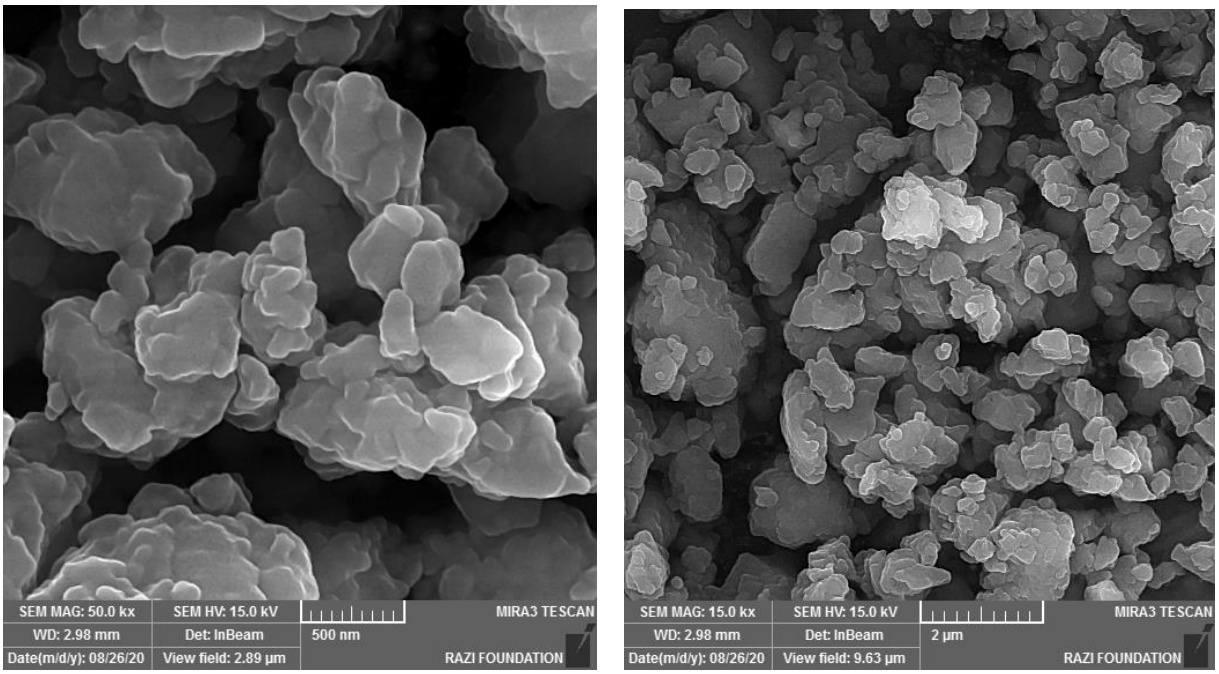

Figure 19. FESEM images of biosynthesized iron nanoparticles (Fe NPs)

Table 3. Average shape and size of the synthesized nanoparticles.

NP	C-ZnO	NC-ZnO	Zn	MgO	Ag	Cu	Fe
Shape	Spherical	spherical	Small sheets	Semi-spherical	spherical	sheets	Small sheets
Diameter (nm)	40	25	100	65	50	180	130
Thickness	-	-	25	-	-	30	20
Standard deviation	9	5	24	36	4	51	29
Homogeneity	yes	yes	no	yes	yes	no	no

3.2.3. Energy Dispersive X-ray Spectroscopy (EDS) Analysis

EDX is a powerful technique allowing elemental analysis of the surface of solid samples such as synthesized nanoparticles. The EDS analysis shows the optical absorption peaks as a result of SPR phenomenon. In EDS analysis the presence of

each element is defined by the normalized weight percentage, which is the percentage in weight assuming that the chosen elements represent the total composition of the sample [85].

C-ZnO. The EDS pattern of C-ZnO NPs (Figure 20, Table 4) showed the peaks of zinc and oxygen elements. According to the elemental percentage analysis, the major element of zinc comprises more than 50% of total constituents, along with oxygen, which clearly confirms formation of pure zinc oxide NPs. The EDS analysis shows that the samples contained pure zinc oxide nanoparticles which are in agreement with other researchers [37,77].

NC-ZnO. EDS pattern of non-calcinated zinc oxide NPs was shown in Figure 21 and Table 5. The obtained elemental percentage of zinc and oxygen elements were 74.58% and 22.95%, respectively, and 2.47% potassium impurity. The EDS analysis are in accordance with Gupta et al. [78] and Dobrucka and Dugaszewska [38].

Zn. The EDS analysis profile of biosynthesized Zn NPs shows zinc (Zn), carbon (C), phosphorus (P) and oxygen (O) that confirms the paticipation of plant phytochemical groups in the process of metal ion reduction and the stability of Zn NPs. EDS spectrum represents two peaks relevant to zinc and oxygen (Figure 22, Table 6). The EDS pattern of Zn NPs is in agreement with Hosseini Koupaei et al. [86].

MgO. EDS spectrum reveals presence of Mg and O elements in biosynthesized MgO NPs (Figure 23, Table 7). It is released from the EDS analysis that the MgO NPs are composed of Mg, O and a small amount of Ca as impurity. The molecular ratio of Mg:O was found to be nearly 1:1, which shows the purity of the NPs. Mentioned result was in agreement with previous reports [83,43,44].

Ag. The EDS spectrum presented in Figure 24 and Table 8 show the three characteristic peaks of silver around 3 keV due to SPR. According to the elemental profile, silver abundance is about 98.05% normalized mass percent. The other element is Cl with 1.95% relative abundance, which is related to the impurities of the precursor. This result was in good agreement with Masoud Hussein et al. [87].

Cu. The EDS spectra of biosynthesized Cu NPs is shown in Figure 25 and Table 9. It is clear from the spectra that the EDS pattern confirmed successful formation of Cu NPs, as the EDS peak positions were consistent with copper. The presence of other elements such as oxygen (O) and carbon (C) in the Cu NPs is related to the biomolecules of the extract attached to the surface of the Cu NPs [24]. These findings are in close agreement with the previous studies [37], but with slight difference due to variations in synthesis condition.

Fe. Figure 26 and Table 10 show the elemental profile of biosynthesized Fe NPs, which shows an intense signal indicating the presence of elemental Fe in examined samples. The elemental analysis of the Fe NPs revealed strong signals of O (48.75%), C (36.85%) and Fe (12.43%) along with weak signals of P (1.97%), as the impurities come from extract biomolecules. This result was in accordance with Sylvia Devi et al. [80].

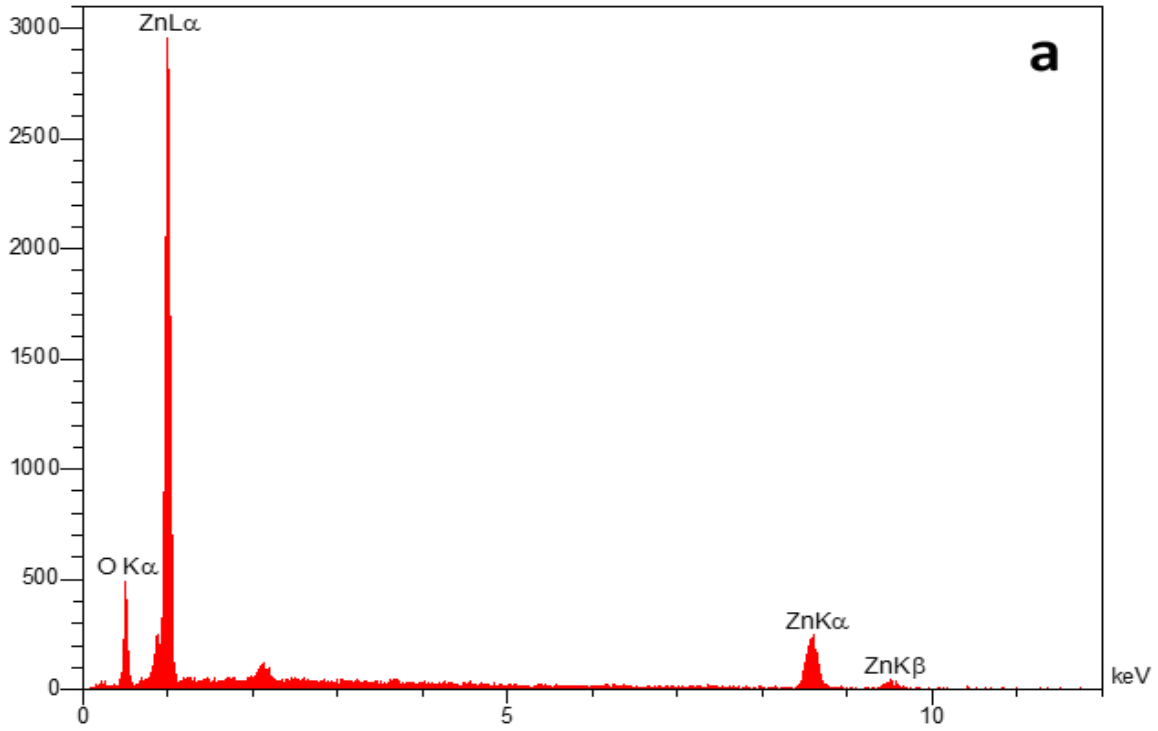

Figure 20. EDS spectrum of biosynthesized calcinated zinc oxide nanoparticles (C-ZnO NPs)

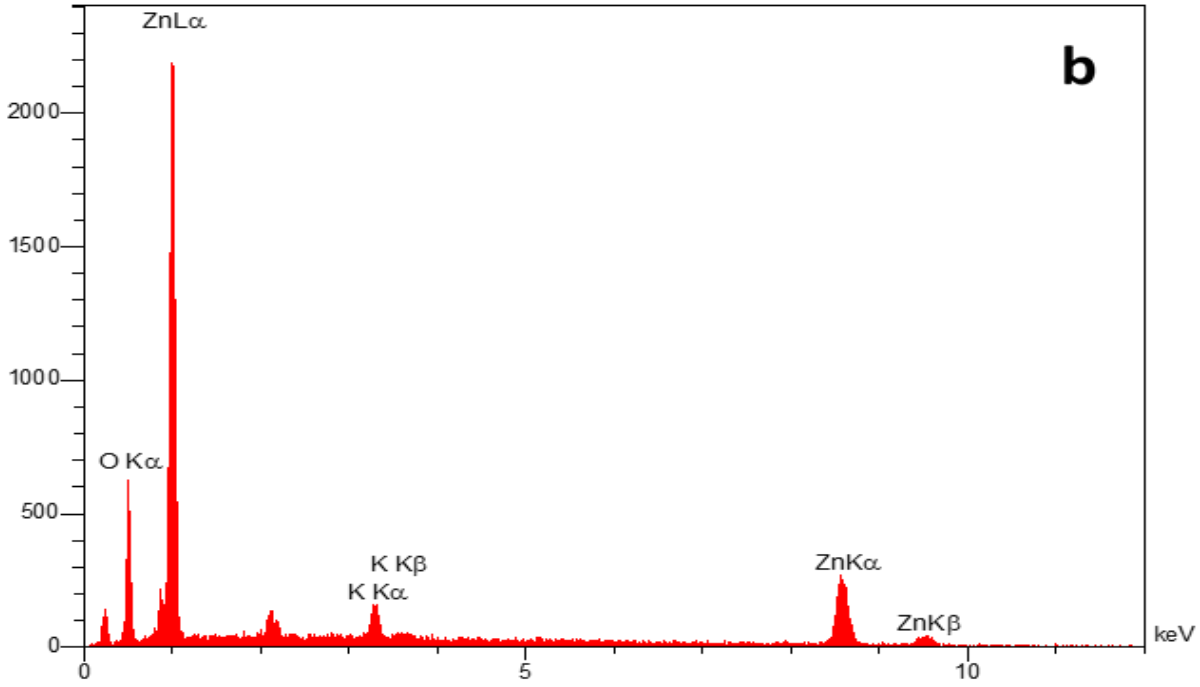

Figure 21. EDS spectrum of biosynthesized non-calcinated zinc oxide nanoparticles (NC-ZnO NPs)

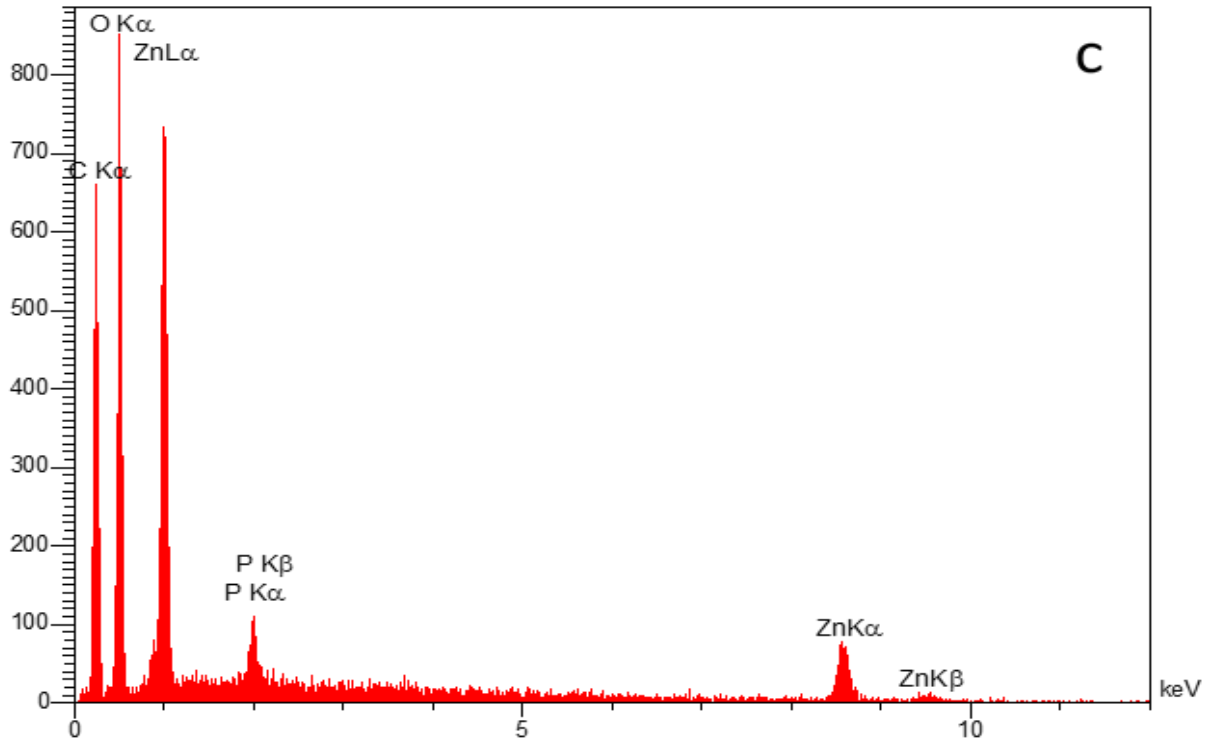

Figure 22. EDS spectrum of biosynthesized zinc nanoparticles (Zn NPs)

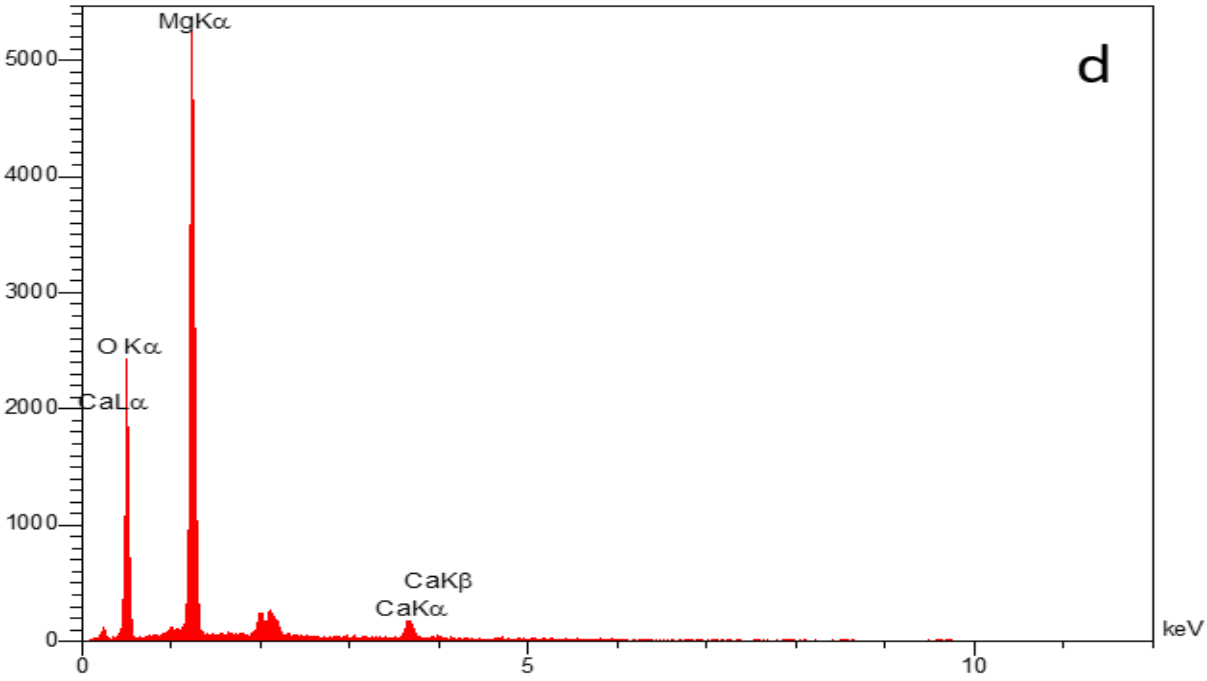

Figure 23. EDS spectrum of biosynthesized magnesium oxide nanoparticles (MgO NPs)

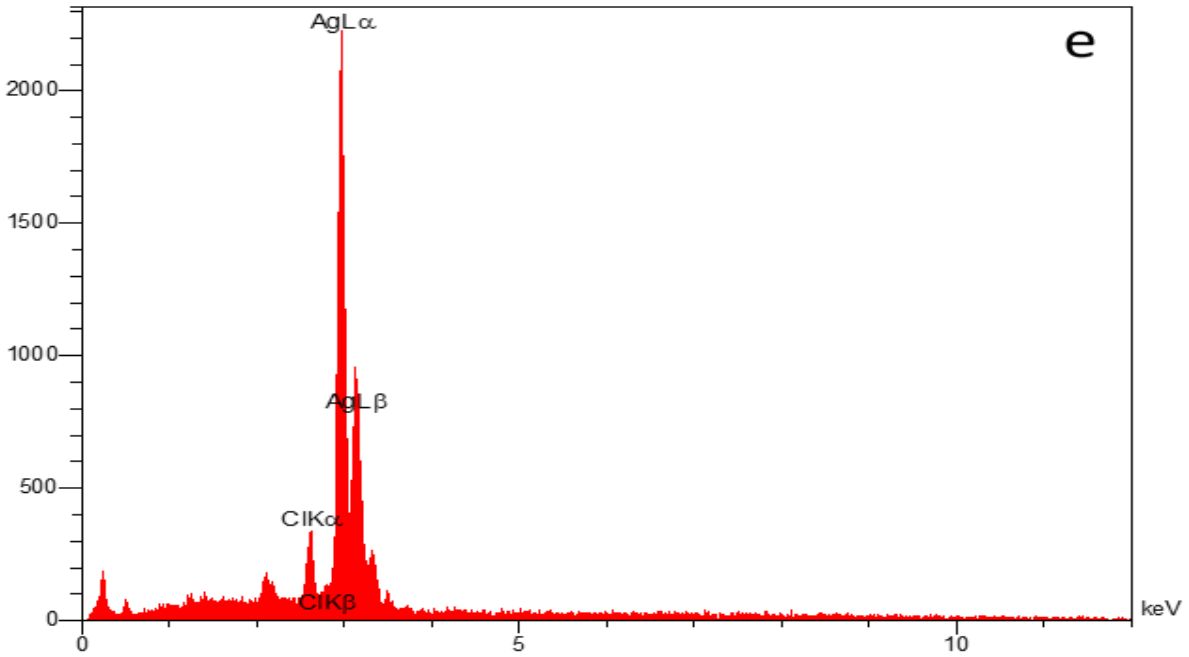

Figure 24. EDS spectrum of biosynthesized silver nanoparticles (Ag NPs)

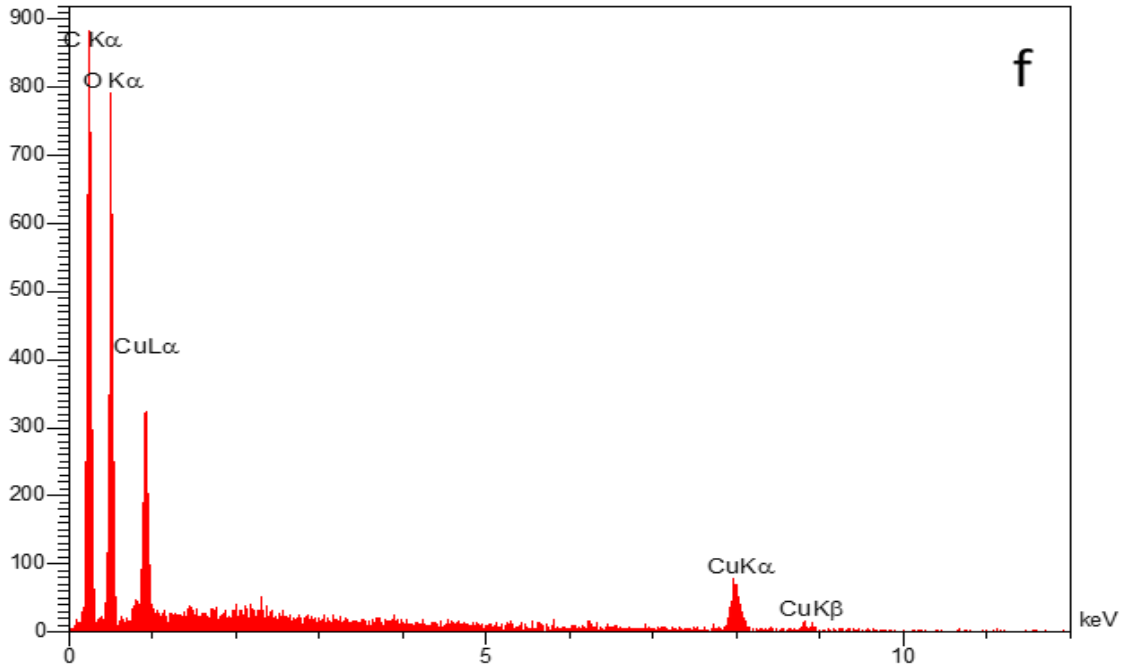

Figure 25. EDS spectrum of biosynthesized cupper nanoparticles (Cu NPs)

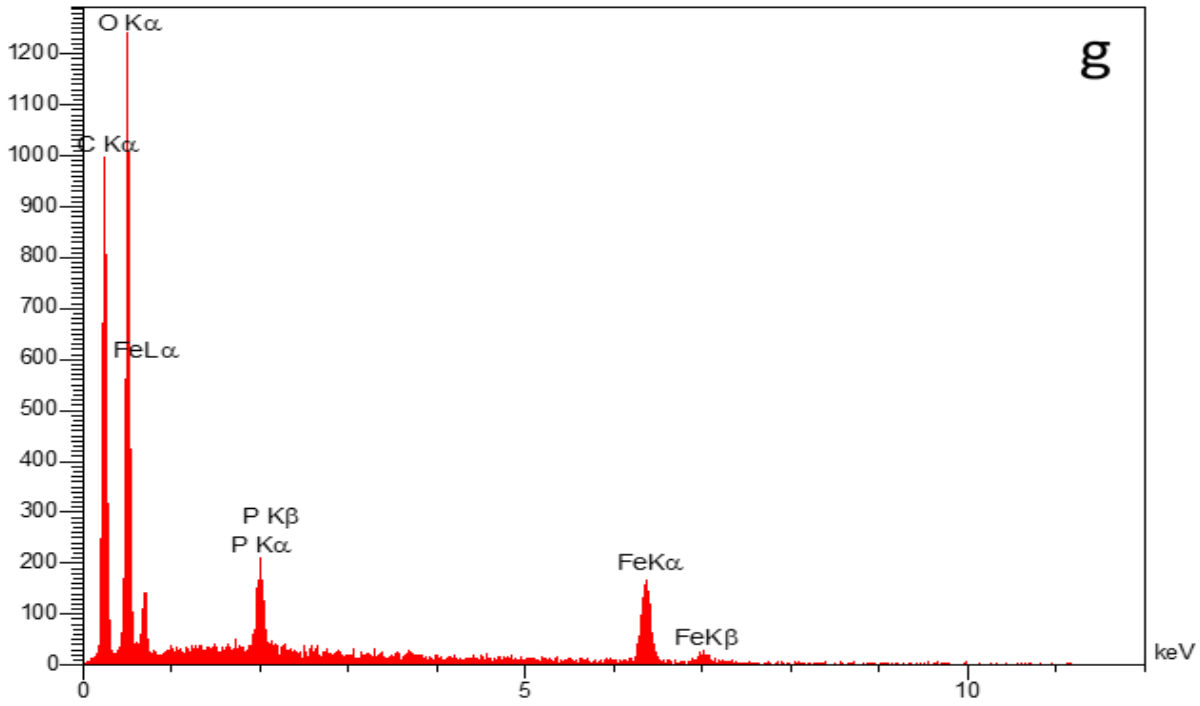

Figure 26. EDS spectrum of biosynthesized iron nanoparticles (Fe NPs)

Table 4. EDS analysis of C-ZnO NPs

Element	Line	Int	Error	K	Kr	W%	A%	ZAF	Pk/Bg
O	Ka	142.3	3.3054	0.1235	0.1049	20.12	50.72	0.5213	17.44
Zn	Ka	226.1	0.7333	0.8765	0.7445	79.88	49.28	0.9321	21.83
sum				1.0000	0.8494	100.00	100.00		

Table 5. EDS analysis of NC-ZnO NPs

Element	Line	Int	Error	K	Kr	W%	A%	ZAF	Pk/Bg
O	Ka	113.3	1.8504	0.1394	0.1149	22.95	54.37	0.5004	25.32
K	Ka	38.6	0.6599	0.0284	0.0234	2.47	2.39	0.9477	4.61
Zn	Ka	151.5	0.7848	0.8322	0.6859	74.58	43.24	0.9196	21.02
sum				1.0000	0.8241	100.00	100.00		

Table 6. EDS analysis of Zn NPs

Element	Line	Int	Error	K	Kr	W%	A%	ZAF	Pk/Bg
C	Ka	66.3	32.8819	0.2938	0.1265	36.77	50.95	0.3441	47.10
O	Ka	150.8	33.9689	0.3274	0.1410	41.63	43.30	0.3386	52.76
P	Ka	18.7	0.4167	0.0160	0.0069	0.90	0.48	0.7642	4.18
Zn	Ka	37.4	0.7385	0.3629	0.1563	20.70	5.27	0.7548	11.18
sum				1.0000	0.4306	100.00	100.00		

Table 7. EDS analysis of MgO NPs

Element	Line	Int	Error	K	Kr	W%	A%	ZAF	Pk/Bg
O	Ka	427.8	16.4339	0.5041	0.3195	55.00	65.62	0.5808	95.84
Mg	Ka	1143.5	9.1103	0.4535	0.2874	41.93	32.92	0.6853	74.05
Ca	Ka	54.0	0.5517	0.0424	0.0269	3.06	1.46	0.8773	6.23
sum				1.0000	0.6337	100.00	100.00		

Table 8. EDS analysis of Ag NPs

Element	Line	Int	Error	K	Kr	W%	A%	ZAF	Pk/Bg
Cl	Ka	53.5	3.0067	0.0225	0.0224	1.95	5.71	1.1461	6.10
Ag	La	1003.5	4.2683	0.9775	0.9707	98.05	94.29	0.9900	37.51
sum				1.0000	0.9931	100.00	100.00		

Table 9. EDS analysis of Cu NPs

Element	Line	Int	Error	K	Kr	W%	A%	ZAF	Pk/Bg
Cu									

C	Ka	94.8	42.7664	0.4569	0.2021	42.46	54.31	0.4759	63.72
O	Ka	135.6	44.1801	0.3204	0.1417	44.23	42.48	0.3203	71.15
Cu	Ka	28.4	1.0080	0.2227	0.0985	13.31	3.22	0.7402	9.45
sum				1.0000	0.4422	100.00	100.00		

Table 10. EDS analysis of Fe NPs

Element	Line	Int	Error	K	Kr	W%	A%	ZAF	Pk/Bg
C	Ka	102.9	42.5900	0.3712	0.1699	36.85	47.93	0.4610	66.06
O	Ka	216.2	43.9979	0.3822	0.1749	48.75	47.60	0.3588	95.34
P	Ka	49.4	2.1489	0.0344	0.0157	1.97	0.99	0.7982	8.10
Fe	Ka	73.4	0.6569	0.2123	0.0972	12.43	3.48	0.7817	17.74
				1.0000	0.4577	100.00	100.00		

3.2.4. Photon Cross Correlation Spectroscopy (PCCS) Analysis

PCCS analysis gives the radius of a particle and an estimation of the average hydrodynamic particle size. The average size distribution of the hydrated particles of the NPs synthesized by employing the present novel green strategy is presented in Figures 27-33, and the details are summarized in Table 2. As an example, the average hydrated particle size was 133 nm for Ag NPs. The observed results obviously revealed that the size obtained from PCCS was not correlated with FESEM observations because these results are related to hydrated aggregations of NPs, not single ones. The size analysis suggests that Ag NPs with the average size of 133 nm were comprised of nanocrystals with an average size of about 50 nm. The biosynthesized NPs existed as agglomeration of small individual nano sized particles, as there is a considerable tendency to form non-uniform sized and shaped agglomerates [81].

The polydispersity index (PDI) indicates the heterogeneity of a sample based on size and can occur due to size distribution in a sample or agglomeration of the sample. As Equation 9:

(PDI) = the square of the (standard deviation / mean diameter) (9)

PDI value ranges from 0–1 and 0–0.08 indicate good mono-dispersity of the sample, 0.08 to 0.7 are mid-range and values more than 0.7 show very broad distribution of particle sizes [14]. The values of PDI for the biosynthesized NPs are presented in Table 11.

Table 11. The average hydrated particle size of biosynthesized NPs and the particle size obtained from FESEM, SD: standard deviation, Ave: average hydrodynamic particle diameter of the agglomerates, PDI: polydispersity index, polymodal distribution of NPs**.**

NP	C-ZnO	NC-ZnO	Zn	MgO	Ag	Cu	Fe
Ave size (nm)	995	210	525	1551	133	795	559
Ave size (nm) of FESEM	40	25	100	65	50	30×180	20×130
SD	1026	15.16	37.84	278.9	4.47	59.50	31.53
PDI	1.06	0.005	0.005	0.32	0.001	0.005	0.003
Size distribution condition	High polydipersity	Good monodispersity	Good monodispersity	Mid-range monodispersity	Good monodispersity	Good monodispersity	Good monodispersity

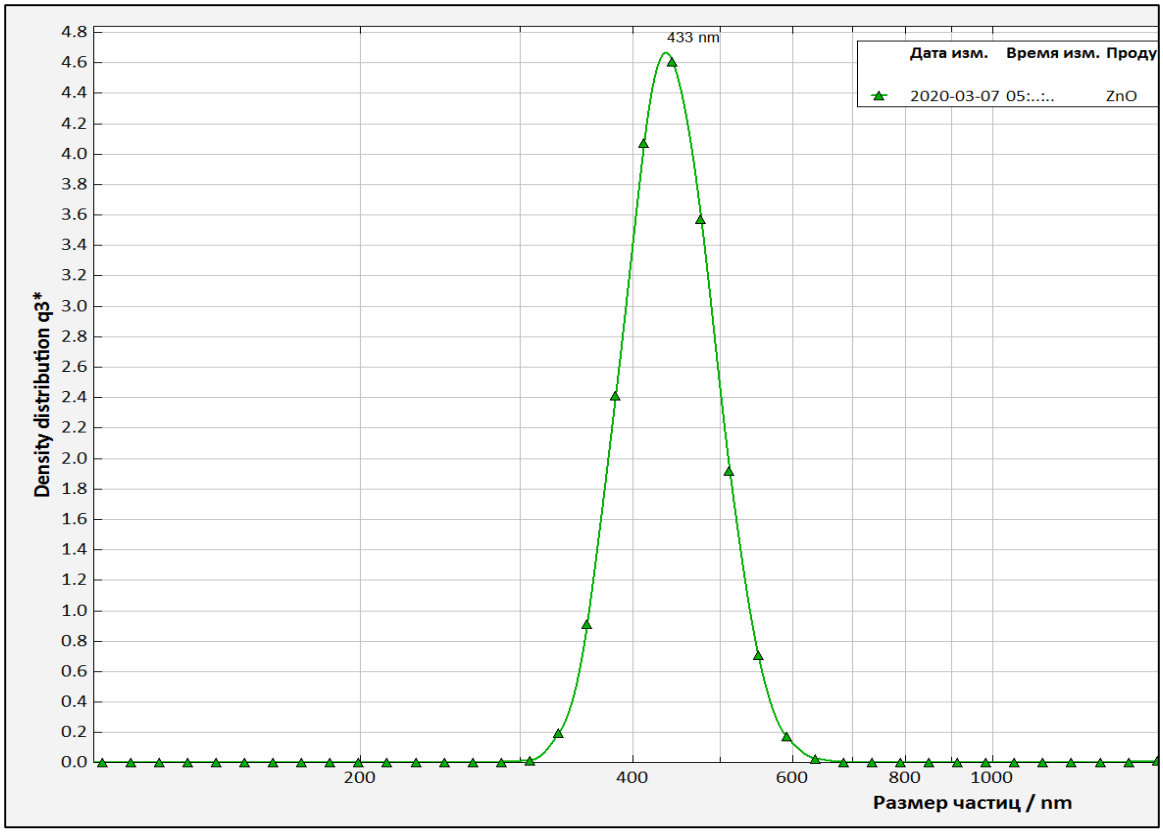

Figure 27. particle size distribution of C-ZnO NPs

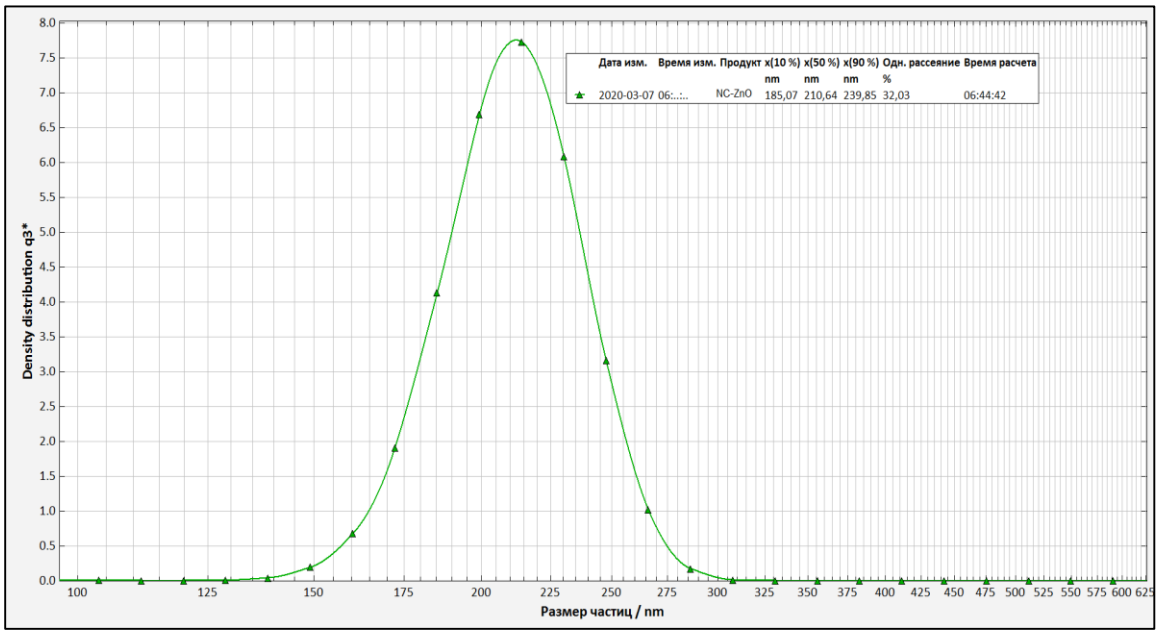

Figure 28. particle size distribution of NC-ZnO NPs

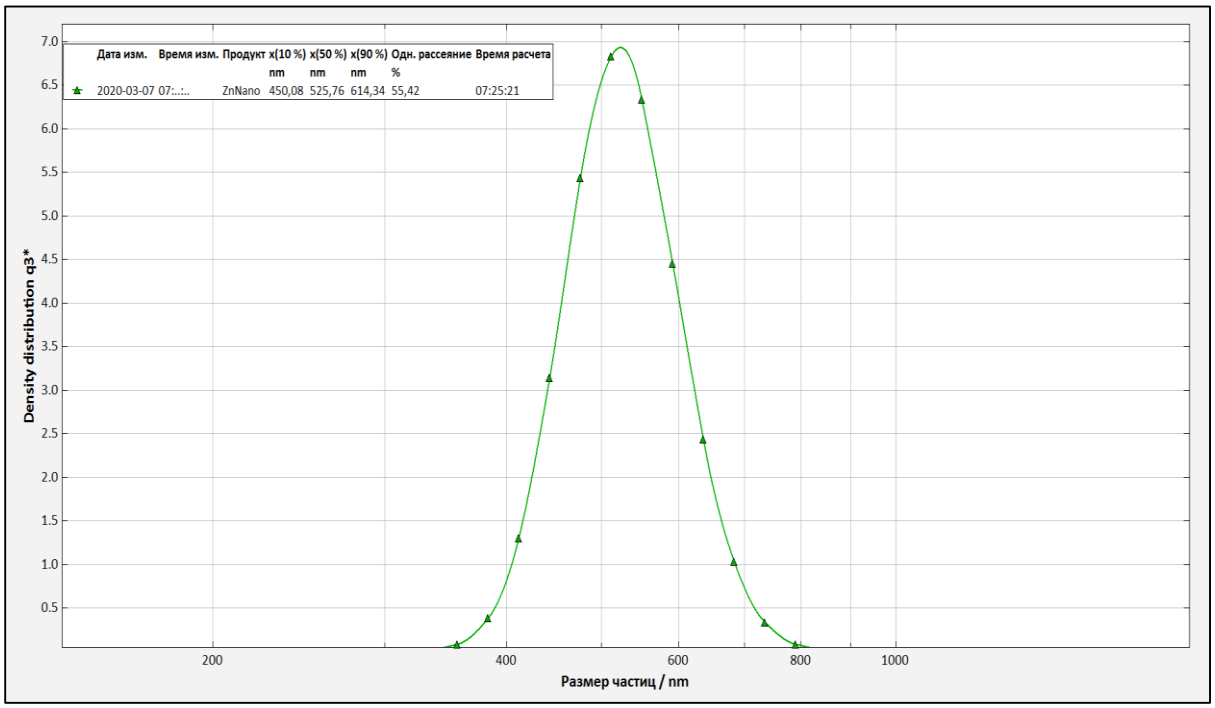

Figure 29. particle size distribution of Zn NPs

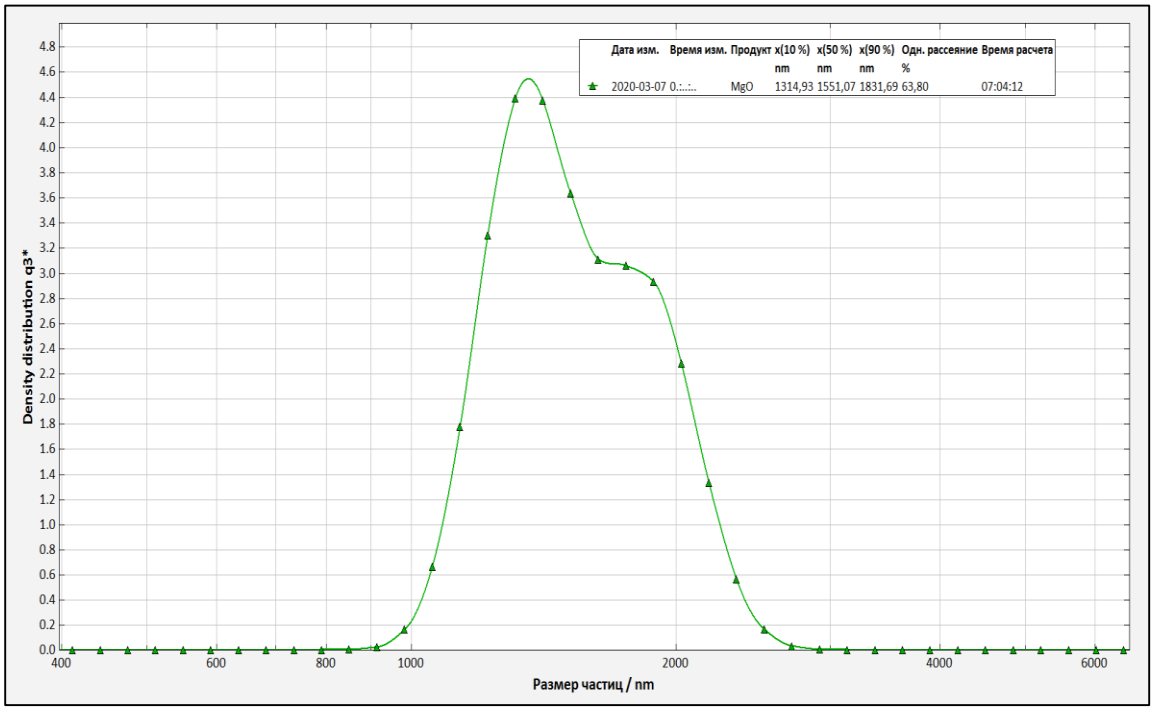

Figure 30. particle size distribution of MgO NPs

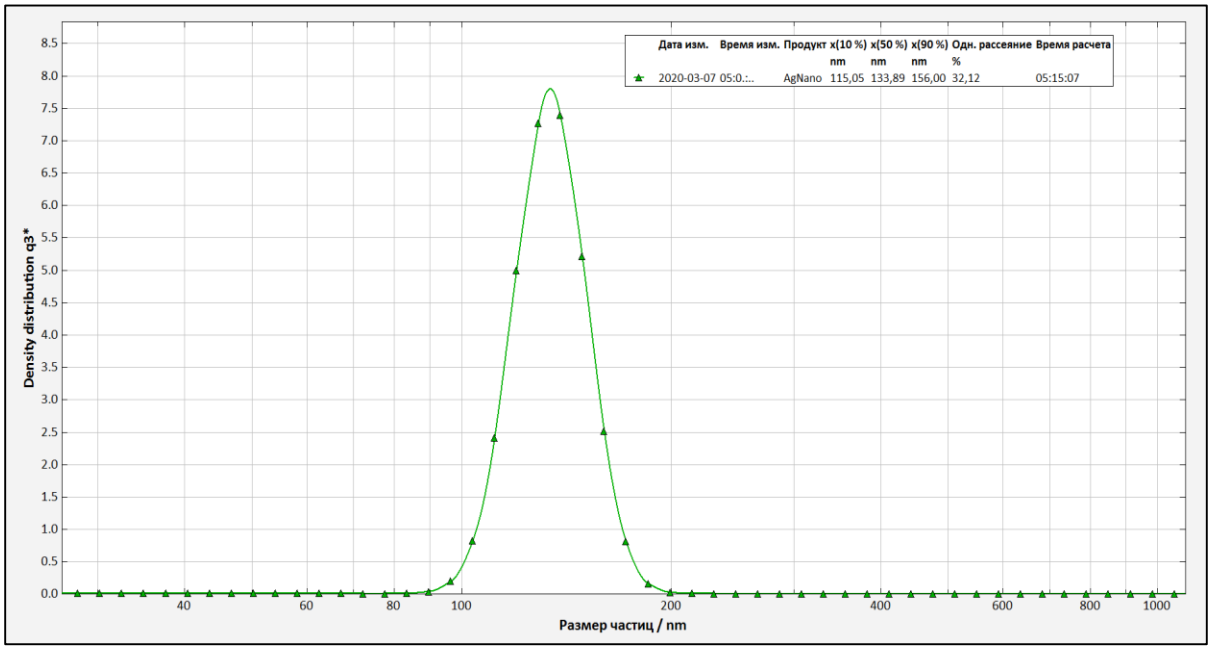

Figure 31. particle size distribution of Ag NPs

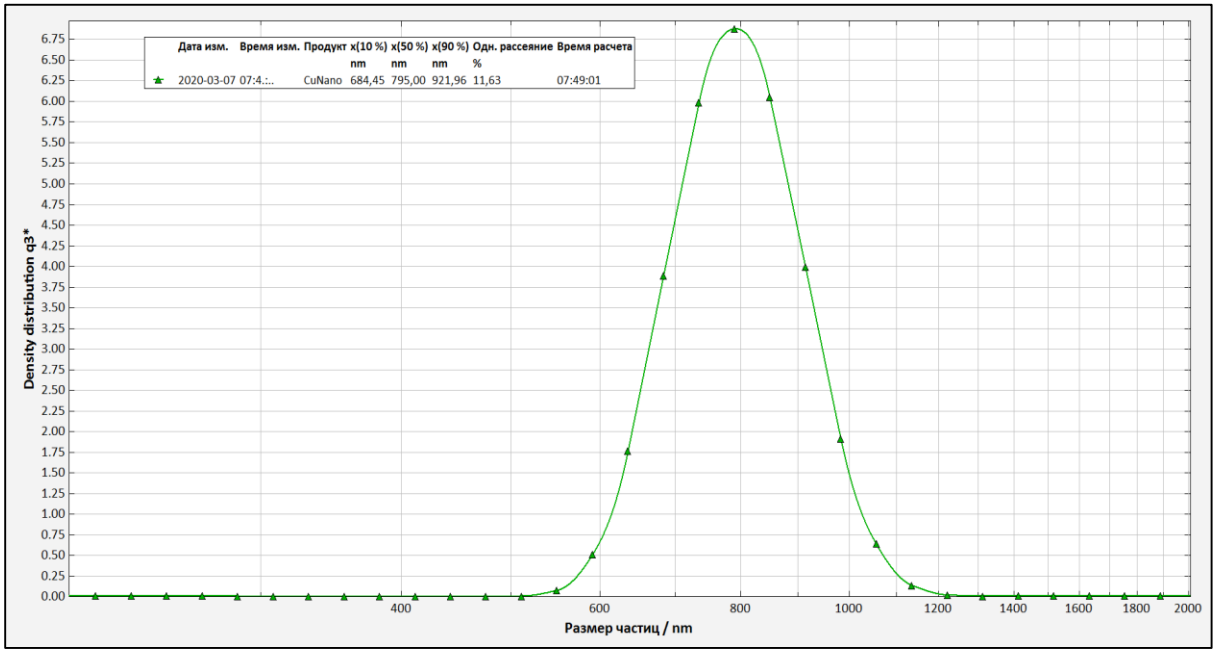

Figure 32. particle size distribution of Cu NPs

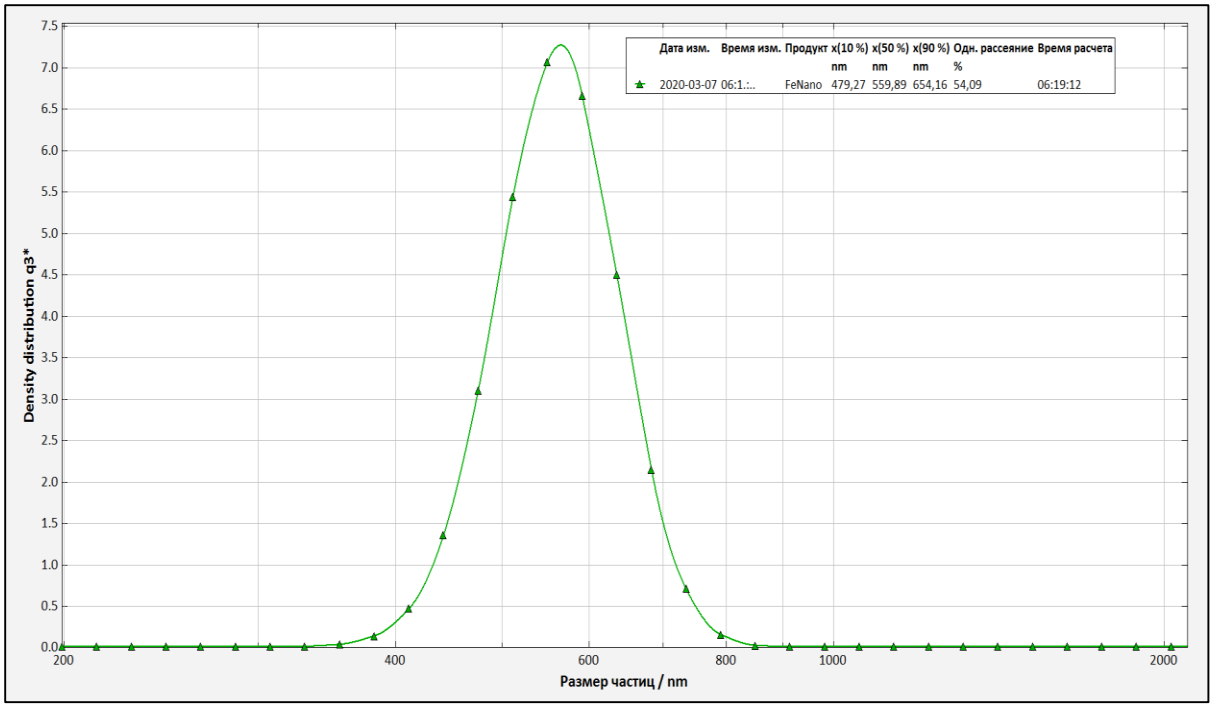

Figure 33. particle size distribution of Fe NPs

3.2.5. Fourier-Transform Infrared Spectroscopy (FT-IR)

The FT-IR spectra were analyzed in the range of 0–4000 cm^{-1}, and recorded using KBr pellet method to recognize the functional organic groups, organic, inorganic, biomolecule residues along with nanoparticle formation. These materials may come along via reducing agent on to the surface of synthesized NPs generated by strawberry leaf extract and interaction of NPs with capping agents. The obtained FT-IR spectra confirmed the interaction of biomolecules with synthesized nanoparticles. Aliphatic and aromatic compounds contain a wide variety of functional groups, *e.g*., cyano (–CN), mercapto (–SH), carboxylic acid (–COOH) and amino (–NH2), known to have a high affinity for functionalization of noble metallic NPs, and thus are useful as surface-protective functional groups [9].

Table 12 summarizes the absorption bands of all spectra obtained from the extract and NPs.

Extract. The FT-IR spectrum of the strawberry leaf extract (Figure 34) indicates absorption bands at 3927 cm^{-1}, 3539 cm^{-1}, 3392 cm^{-1}, 2028 cm^{-1}, 1624 cm^{-1}, 1084 cm^{-1}, 770 cm^{-1}, 621 cm^{-1}, 474 cm^{-1} and 423 cm^{-1} (Table 12). Intense peaks at 3539 cm^{-1} and 3392 cm^{-1} may be due to the N–H stretching frequency of peptide linkages or O–H stretching vibrations. The peak at 2028 cm^{-1} was assigned to the C-H aromatic. The band at 1624 cm^{-1} most probably refers to C=O or C=C aromatic ring stretching vibrations and 1084 cm^{-1} indicates the frequencies of C-O or C-N amine. At 770 cm^{-1}, a weak peak appears which may be related to the alkane, alkene or aromatics C-H band or C-S thiol or thioether [88]. The results indicate the presence of different biomolecules in strawberry leaf extract and most probably polyphenols, carboxylic acid, amino acids and proteins [88,89]. In the present study, the interaction of NPs with biomolecules of the extract showed intense peaks and relative shift in position and intensity distribution (in comparison to extract) which were confirmed with FT-IR.

C-ZnO. Figure 35 shows the FT-IR spectrum of the calcinated ZnO NPs. Absorption bands occurred at 418 cm^{-1}, 481 cm^{-1}, 623 cm^{-1}, 1079 cm^{-1}, 1424 cm^{-1}, 1513 cm^{-1}, 1621 cm^{-1}, 2030 cm^{-1}, 3238 cm^{-1}, 3415 cm^{-1}, 3480 cm^{-1}, 3553 cm^{-1} (Table 12). The intense broad bands at 3553 cm^{-1}, 3480 cm^{-1} and 3415 cm^{-1} were assigned to O–H stretching of flavonoids, polyphenols and C–O and N–H groups on the surface of ZnO NPs [77]. 3238 cm^{-1} indicates the frequencies of aromatic or alkene C–H groups [78]. The intense peak at 2030 cm^{-1} indicates the C–H of aromatic ring. The peak at 1621 cm^{-1} corresponding to C=C stretch in the aromatic ring or C=O group. Peaks at 1513 and 1424 cm^{-1} refer to N-O nitro, C = C or amine N–H stretching of the aromatic compound which is observed after calcination process. Bands at 1079 cm^{-1} indicates the stretching vibration related to C–N of an amine or C–O. Absence of 1395 cm^{-1} sharp peak (in comparison with NC-ZnO in

the following section) due to antisymmetric stretching vibration of O–H in the $Zn(OH)_2$. These findings show the presence of organic functional groups absorbed on the surface of C-ZnO nanostructures, which may present in strawberry leaf extract. The results are in accordance with previous reports [37,77-78].

NC-ZnO. According to FT-IR spectrum of the C-ZnO NPs (Figure 36), the bands are at 3553 cm^{-1}, 3475 cm^{-1}, 3411 cm^{-1}, 3237 cm^{-1}, 2028 cm^{-1}, 1620 cm^{-1}, 1395 cm^{-1}, 1069 cm^{-1}, 623 cm^{-1}, 482 cm^{-1}, and 418 cm^{-1}. The band at 3553 cm^{-1} 3475 cm^{-1} and 3411 cm^{-1} are due to stretching vibrations of O–H groups or N-H amine group (Table 12). The C–H stretch in alkene showed broad absorption bands at 3237 cm^{-1}. The absorption band at 2028 cm^{-1} is characteristic of the aromatic C–H stretching vibrations. The small peak located at 1620 cm^{-1} could be assigned to the C=O stretching in the carboxyl or C=C stretch in aromatic ring. The sharp band at 1395 cm^{-1} refers to the N=O vibrations of nitro compound which is formed during the calcination process. The peak at 1069 cm^{-1} is due to C–O stretching in amino acid and vibration of (NH)–C=O group. It may conclude that the biomolecules which are responsible for reduction of metallic ions remain on the surface of ZnO NPs for their stabilization.

Zn. The FT-IR spectra of Zn NPs (Figure 37) displays a number of absorption peaks explained in Table 12. The broad peaks of 3553 cm^{-1}, 3479 cm^{-1} and 3416 cm^{-1} could be attributed to N-H stretching of the aliphatic primary amine, or O–H stretching alcoholic or phenolic groups or different carboxylic acids of the extract. The C–H stretch in alkene showed broad absorption bands at 3239 cm^{-1}. The absorption band at 2039 cm^{-1} is relevant to the vibrations of the aromatic C–H stretching. Sharp peak which is located at 1620 cm^{-1} could be due to the C=C ring stretching vibrations in polyphenols or asymmetric stretching vibrations of COOH, and that around 1148 cm^{-1} corresponded to the C–N amine or C–O stretching

frequency [90]. FT-IR analysis of this compound suggested the presence of organic components from strawberry leaf extract [38,86].

MgO. The FT-IR spectrum of MgO NPs is shown in Figure 38 and summarized in Table 12. The broad absorption peaks at 3554, 3482, 3417 cm^{-1} are attributed to stretching vibrations of N-H stretching of the aliphatic primary amine, or O–H stretching alcoholic or phenolic groups or different carboxylic acids of the extract. The peak at 3233 cm^{-1} may related to the C–H stretch in alkene. The absorption at 2362 cm^{-1} most probably refers to the CO_2 molecules released in the calcination process. The absorption band at 1996 cm^{-1} is for aromatic C–H stretching vibrations. The peak at 1621 cm^{-1} could be related to the C=C ring stretching in polyphenols or stretching vibration of carboxyl group. Peak at 1549 cm^{-1} corresponded to N-O nitro compound, which is produced during calcination process. At 1078 cm^{-1} an absorption band occurred which could be related to the C–N amine or C–O stretching frequency [44].

Ag. The FT-IR spectra of Ag NPs (Figure 39, Table 12) confirms the presence of residual capping agent with the biosynthesized Ag NPs. The bands observed at 3552, 3479, 3416 cm^{-1} in the spectra correspond to the amine N-H and O–H stretching vibration indicating the presence of alcohols, phenolic-related species and proteins. The band detected at 3239 cm^{-1} is related to the C–H stretching of alkene compound. The peak at 2090 cm^{-1} can be assigned to the C–H stretching vibrations of aromatic compound and the strong band that appeared at 1622 cm^{-1} corresponded to the C=O or C=C aromatic ring vibration. The band at 1151 cm^{-1} could be relevant to the C-O or C-N amine, suggesting the presence of proteins. The band at around 621 cm^{-1} is assigned to the C-H alkyne bond or O-H out of plane bending vibration. Such detected functional groups have been also reported in previous investigations

[87,90]. It can be concluded from the FT-IR observations that the surface of Ag NPs is covered by organic species of the extract.

Cu. FT-IR spectra of Cu NPs presented in Figure 40 and Table 12 shows strong absorption bands at 3553, 3479 and 3416 cm^{-1} related to the amine N-H and O–H stretching vibrations indicating the presence of alcohol, phenolic-related species and protein. The peak at 3239 cm^{-1} is relevant to the C–H stretching vibrations of the alkene compounds and 2923 cm^{-1} may refer to the C-H, secondary amine or amine salt. The peak at 2039 cm^{-1} is related to the C-H aromatic vibrations and 1622 cm^{-1} is attributed to binding of C=O or C=C aromatic ring to metal ions. The sharp band at 1327 cm^{-1} refers to the S=O vibration of the sulfate substrate remaining from copper sulfate using in synthesis of Cu NPs. Another peak at 1151 cm^{-1} may refer to the C-O or C-N amine functional group. The peak at 621 cm^{-1} is related to the C-H alkyne bond or O-H out of plane bending. These findings are in good agreement with previous reports [4].

Fe. The obtained FT-IR spectrum of synthesized Fe NPs is represented in Figure 41 and Table 12. Intense bands at 3523, 3479 and 3416 cm^{-1} may refer to the N–H or O–H stretching and the band at 3239 cm^{-1} could be related to the C-H alkene. The peak at 2922 cm^{-1} is due to the C–H and CH_2 vibration of aliphatic hydrocarbons, secondary amine or amine salt. At 2039 cm^{-1} the peak may arise from C-H aromatic band, and at 1622 cm^{-1} may be relevant to the C=O or C=C aromatic ring stretching vibrations. The absorption band at 1144 cm^{-1} may related to the C-O or C-N amine, and finally absorption bands at around 622 cm^{-1} refer to C-H alkyne bond or O-H bending. Comparison of the IR spectrum of extract with the Fe NPs, shows a band shift towards higher frequencies from 3392 to 3416 cm^{-1} (O–H stretching vibrations), 2028 to 2039 cm^{-1} (aromatic C–H) and 1084 to 1144 cm^{-1} (C-OH bending) along with the presence of 1622 cm^{-1} (C=C stretching vibrations), which

indicates the possible attachment of the polyphenolic compounds of the extract in the reduction step through the hydroxyl group and attaching to the Fe NPs through the carbonyl groups.

Table 12. the absorption peaks of extract and synthesized NPs as obtained from FT-IR spectrophotometer and their corresponding functional groups**.**

Absorption Peak Position (cm^{-1})								Functional Group
Extract	**C-ZnO**	**NC-ZnO**	**Zn**	**MgO**	**Ag**	**Cu**	**Fe**	
3539	3553	3553	3553	3554	3552	3553	3523	O-H alcohol and phenol N-H primary amine
-	3480	3475	3479	3482	3479	3479	3479	
-	3415	3411	3416	3417	3416	3416	3416	
3392	-	-	-	-	-	-	-	N-H aliphatic primary amine
-	3238	3237	3239	3233	3239	3239	3239	C-H alkene
-	-	-	-	-	-	2923	2922	aliphatic C-H/ secondary amine/ amine salt
-	-	-	-	2362	-	-	-	CO_2
2028	2030	2028	2039	1996	2090	2039	2039	C-H aromatic
1624	1621	1620	1622	1621	1622	1622	1622	C=O/C=C aromatic ring
-	1513	-	-	1549	-	-	-	N-O nitro/C=C
-	1424	-	-	-	-	-	-	N-H aromatic amine
-	-	1395	-	-	-	-	-	Sulphate S=O
-	-	-	-	-	-	1327	-	
1084	1079	1069	1148	1078	1151	1151	1144	C-O/ C-N amine/C-OH bending
-	-	-	-	871	-	-	-	C-H Alkane/ alkene/aromatics/
770	-	-	-	-	-	-	-	C-S thiol or thioether
621	623	623	621	626	621	621	622	C-H alkyne/O-H alcohol (out of plane bend)
474	481	482	480	486	479	479	480	Organometalics/
423	418	418	418	-	418	-	418	S-S sulphides (stretch)

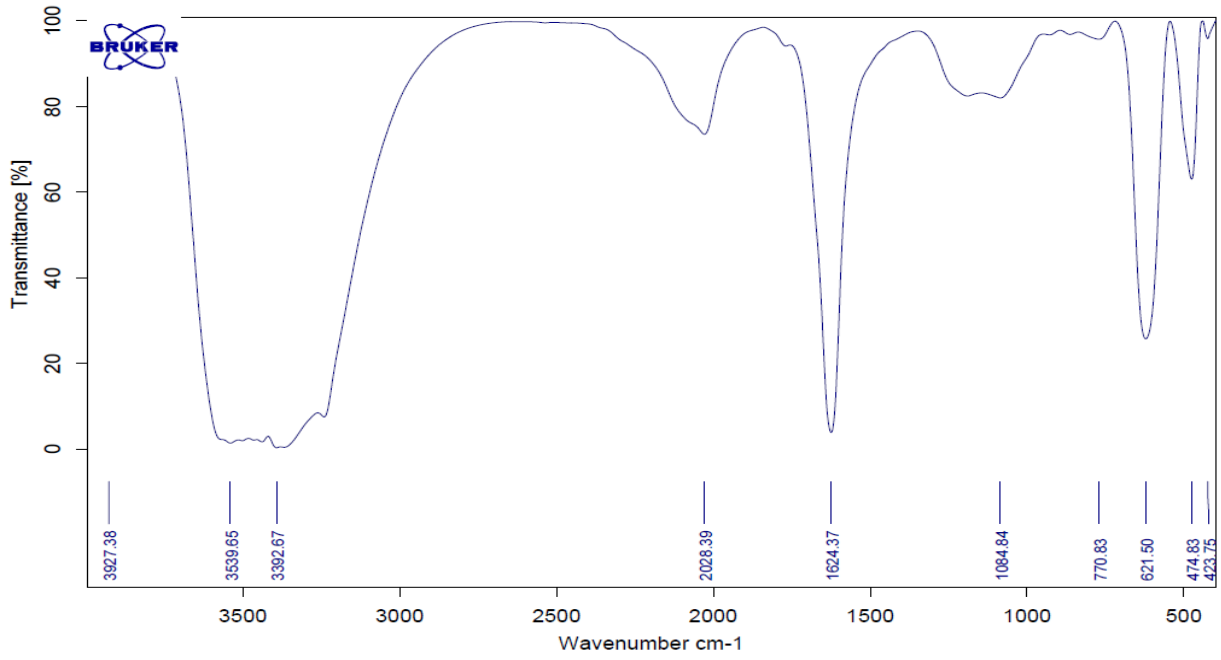

Figure 34. FT-IR spectrum of strawberry leaf extract

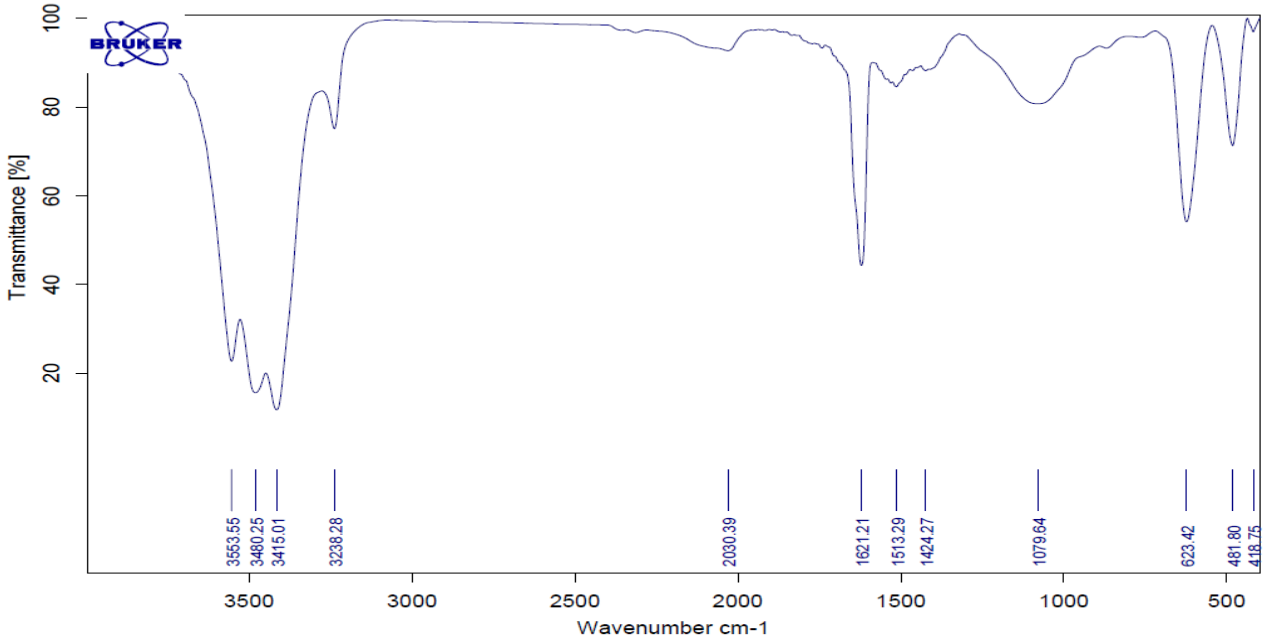

Figure 35. FT-IR spectrum of calcinated zinc oxide nanoparticles (C-ZnO NPs)

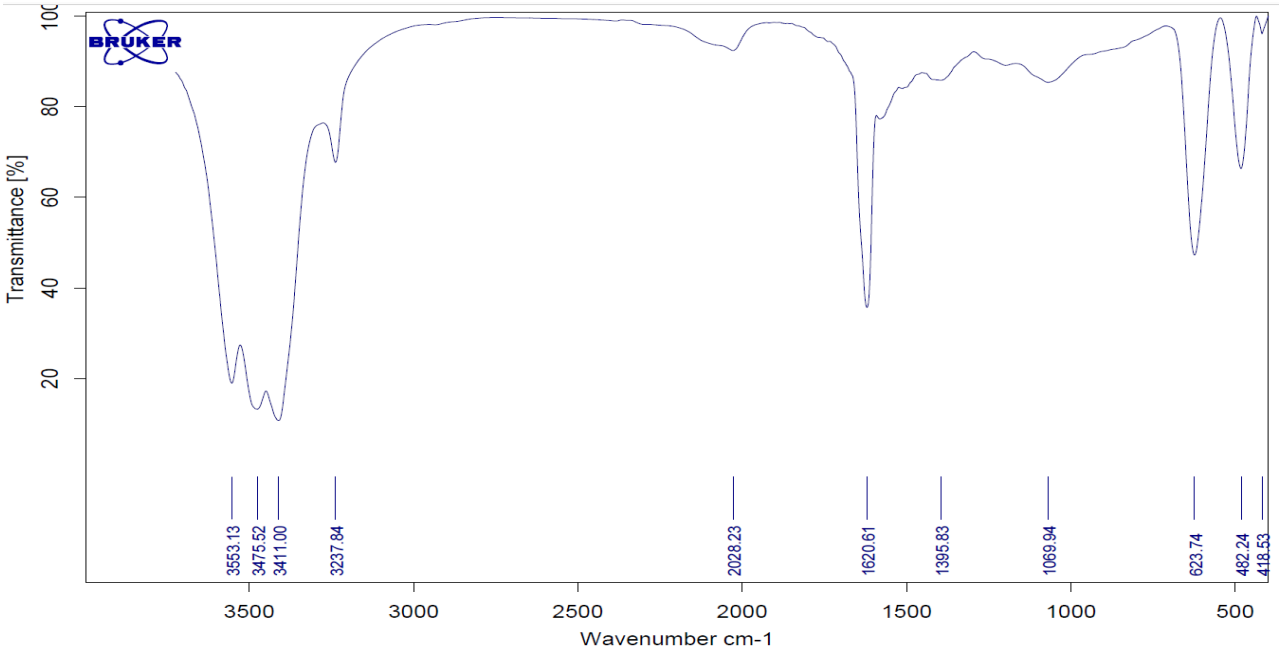

Figure 36. FT-IR spectrum of non-calcinated zinc oxide nanoparticles (NC-ZnO NPs)

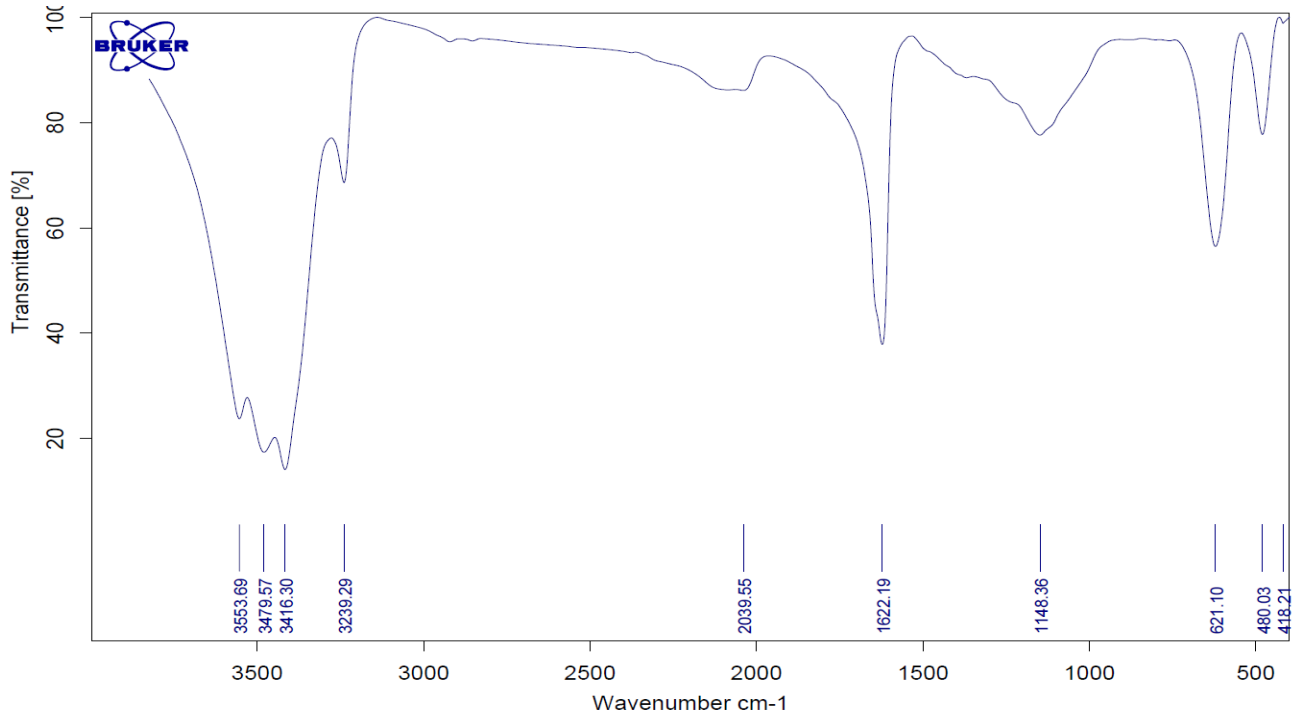

Figure 37. FT-IR spectrum of zinc nanoparticles (Zn NPs)

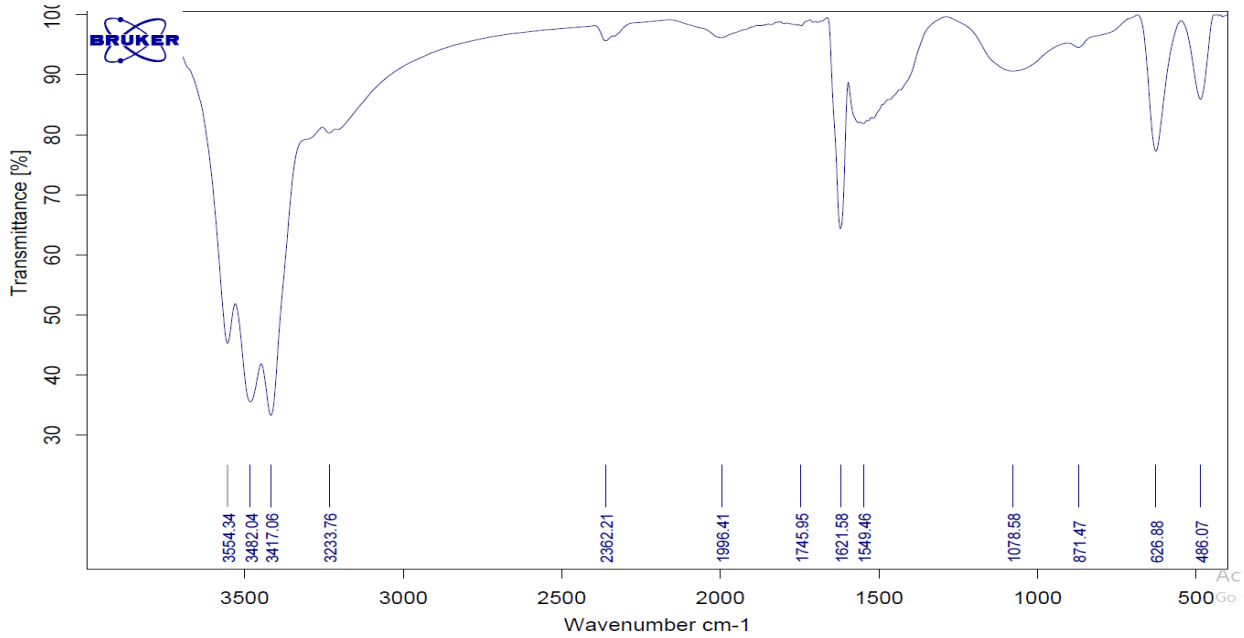

Figure 38. FT-IR spectrum of magnesium oxide (MgO NPs)

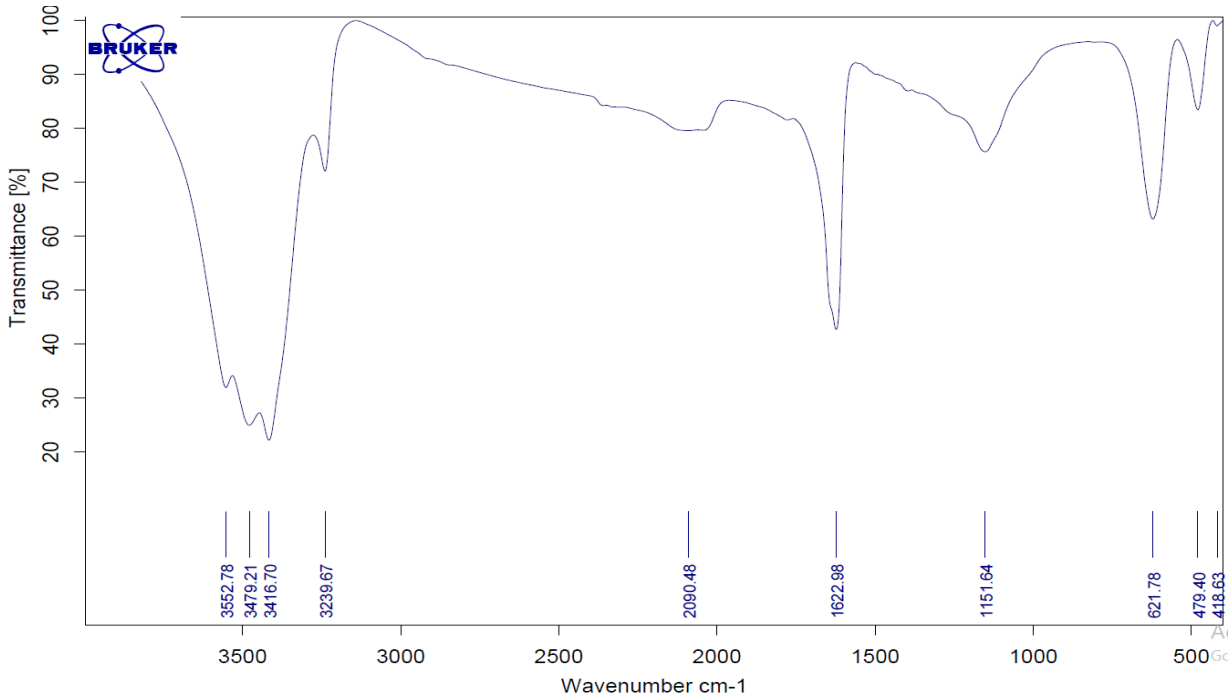

Figure 39. FT-IR spectrum of silver nanoparticles (Ag NPs)

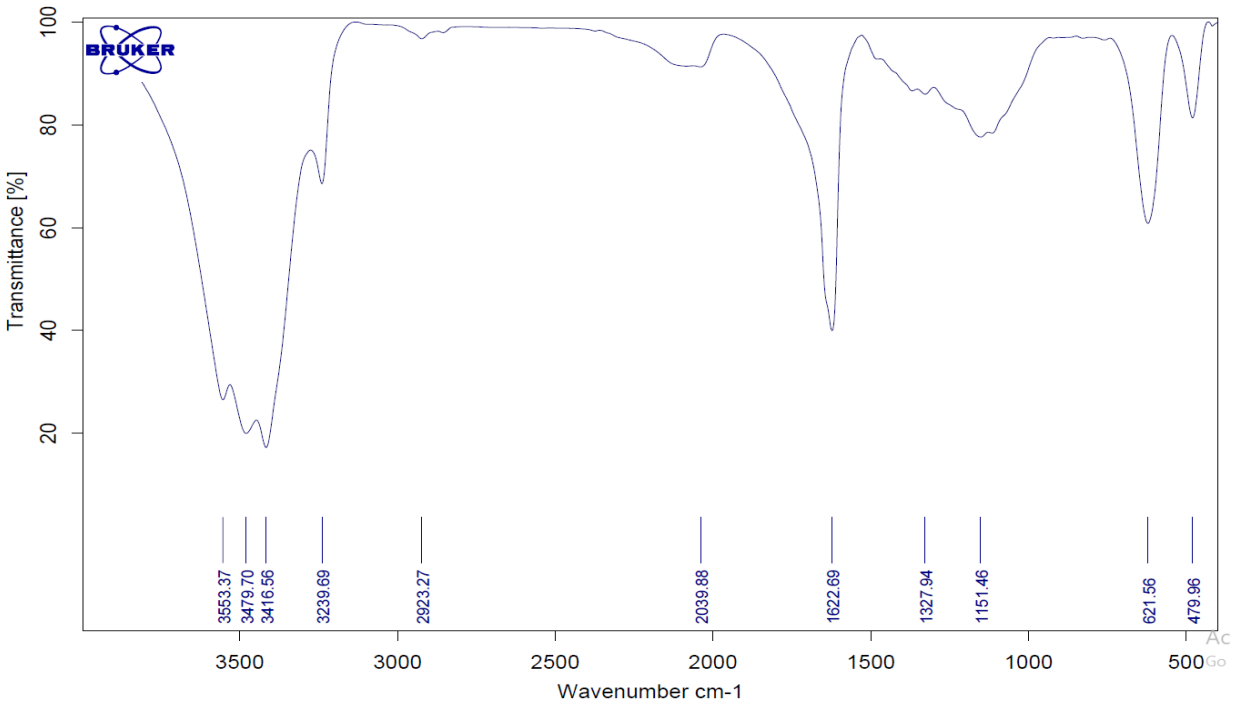

Figure 40. FT-IR spectrum of cupper nanoparticles (Cu NPs)

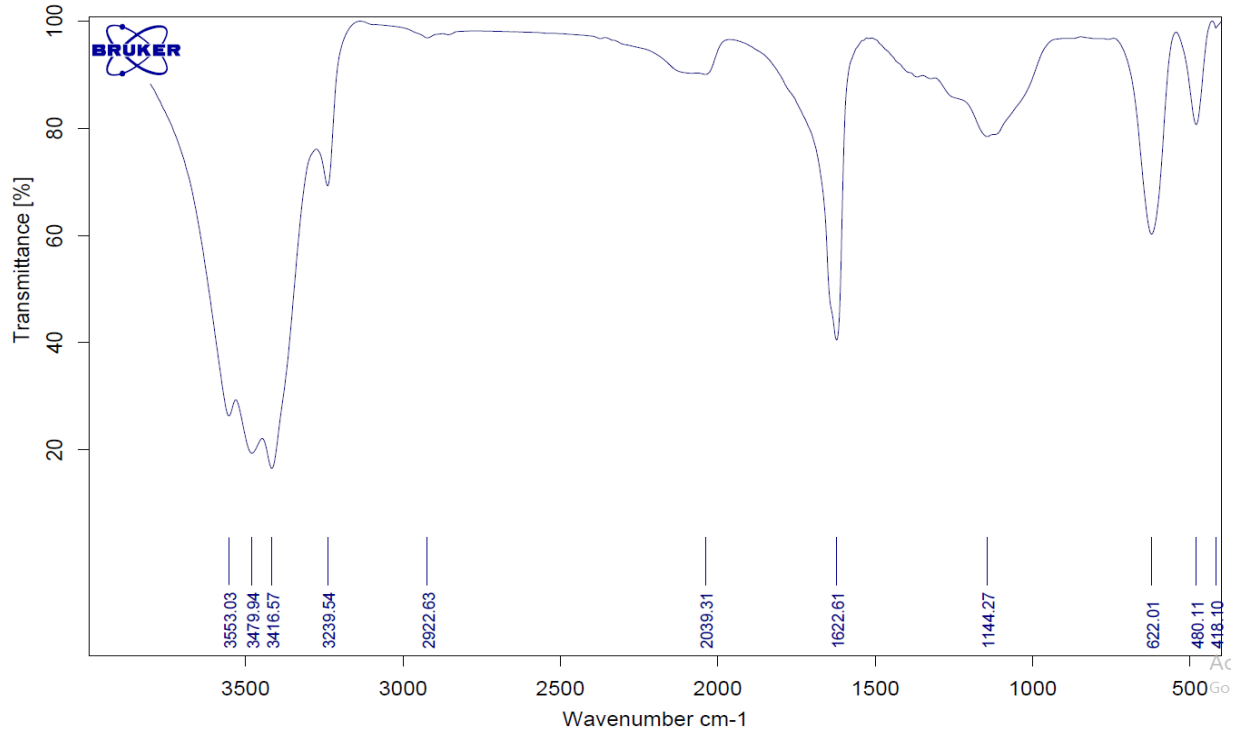

Figure 41. FT-IR spectrum of iron nanoparticles (Fe NPs)

3.2.6. X-Ray Diffraction (XRD) Analysis

XRD is a useful and valuable characterization technique in obtaining information about the atomic structure of materials and indicating formation of NPs. An advantage of the XRD technique is that it results in statistically representative and volume-averaged values. The chemical composition of the nanoparticles could be determined by comparing the obtained peak patterns with reference patterns which are available from International Centre for Diffraction Data (ICDD) database. However, it is not suitable for amorphous materials and for particles with a size below 3 nm, as XRD peaks are too broad in such cases [2].

Synthesized NPs were subjected to X-Ray diffraction studies, confirm the presence of the NPs, obtain the crystallinity or amorphic nature and to detect possible impurities. XRD also used to calculate the average crystal size of NPs by Scherrer's equation, by the use of the most intense peak's broadening of an XRD measurement for each sample [2,91].

C-ZnO. Figure 42 shows XRD pattern of calcinated zinc oxide NPs. Number of Bragg reflections for biosynthesized calcinated ZnO NPs appears at $2\theta = 31.77°$ (100), 34.44° (002), 36.26° (101), 47.55° (102), 56.61° (110), 62.89° (103), 66.39° (200), 67.97° (112), 69.10° (201).72.61° (004), 76.99° (202), 81.43° (104) and 88.65° (203).

The planes show a good agreement with the COD file (COD database code: 96-900-4181) [92], which elucidates the hexagonal structure and corresponds to pure zinc oxide nanocrystals with no impurity patterns.

Using Scherrer's equation [67], average particle size of biosynthesized NPs calculated to be 25.3 nm for C-ZnO NPs, which matches the average diameter of particles determined by FESEM. This finding suggests that the NPs are mainly

single crystals rather than polycrystalline [67]. Diffraction peaks of other impurities were not detected. These outcomes are similar to previous works [77,83,78].

NC-ZnO. According to the Figure 43, peaks for biosynthesized non-calcinated ZnO NPs appears at 2θ = 31.73° (100), 34.38° (002), 36.21° (101), 47.48° (102), 56.53° (110), 62.77° (103), 66.30° (200), 67.86° (112), 69.00° (201), 72.46° (004), 76.86° (202), 81.27° (104) and 89.49° (203) respectively. The planes show a good agreement with the COD file (COD database code: 01-076-0704, calculated from ICSD using POWD-12++, 1997) [93], which shows the hexagonal structure, corresponded to pure zinc oxide NPs without any impurity patterns.

For the NC-ZnO NPs, the calculated average particle size using Scherrer's equation was 27.46 nm. These findings are very close to the particle sizes attained from FESEM analysis. Previous studies have reported similar results [38,90].

Zn. XRD pattern of biosynthesized Zn NPs is provided in Figure 44. The pattern shows no distinctive diffraction peaks, suggesting that the synthesized Zn NPs are largely amorphous in nature rather than crystalline, or the size of the individual NPs are smaller than detection limit of the XRD. Also, it could be suggested that the amount of the crystals was lower than the XRD detection level. As there is no diffraction peak, the particle size cannot be calculated using Scherrer's equation.

MgO. Figure 45 shows XRD patterns of biosynthesized MgO NPs. The wide angle XRD pattern indicates presence of cubic structure of MgO NPs determined with diffraction peaks at 2θ values are 37.04° (111), 43.04° (200), 62.49° (220), 47.93° (311) and 78.89° (222). No subsequent peaks of $Mg(OH)_2$, Mg or other impurities were detected in the XRD pattern of MgO NPs, showing high purity of biosynthesized nanocrystals. The obtained data was matched with reported COD data card no: 01-087-0653, calculated from ICSD using POWD-12++, (1997) [94].

The average grain size 69.6 nm was calculated using Scherrer's equation which is in close agreement with the size of 65 nm obtained from FESEM. The broad peaks indicate the decreasing in crystallinity, which inwardly suggests the formation of smaller particle sizes. Obtained results are also consistent with previous studies [45].

Ag. The XRD pattern of biosynthesized Ag NPs is in Figure 46. The XRD of the Ag NPs between 2θ values of 20^{o} and 90^{o} exhibits crystalline nature and is in agreement with earlier published data showing peaks of silver NPs [48]. Bragg's diffraction peaks for biosynthesized Ag NPs are observed at 2θ= 38.11° (111), 44.30° (200), 64.45° (220), 77.40° (311), and 81.55° (222). The sharp diffraction peaks confirm the crystal nature of sample. According to the COD data card (no: 01-087-0717), the standard diffraction peaks represent the face centered cubic (fcc) structure of Ag NPs, calculated from ICSD using POWD-12++, (1997) [95]. Diffraction peaks of other impurities were not observed, depicting that the peaks belonged to the pure Ag NPs.

The mean grain size of the Ag NPs calculated using Scherer's formula was 40.9 nm, which is close to the obtained size of 50 nm resulted from FESEM analysis.

Cu. Figure 47 shows the XRD pattern of Cu NPs, which showed no peaks assign to crystalline structure. According to the results, biosynthesized Cu NPs are amorphous and/or the particle size is too small. Moreover, it could be suggested that the amount of the nanocrystals was lower than the XRD detection level.

It can be seen that the XRD patterns consist of small shape peak between diffraction angles 20° and 30°, which may indicate some crystalline phase mixed with the primary amorphous structures. The XRD pattern is in agreement with previous reports, but with little differences [26].

Fe. XRD pattern of biosynthesized Fe NPs is shown in Figure 48. The pattern exhibits no discernible diffraction peak corresponding to the crystalline nature of Fe NPs. Results assigned to amorphous particles and show no crystalline phases formed. It also may be related to the fact that the percentage of amorphous particles dominated the number of crystalline particles. Another probability is that the size of NPs is small and cannot be detected by XRD.

Formation of amorphous Fe NPs using the leaf extract of different plants was also reported in other published works [63].

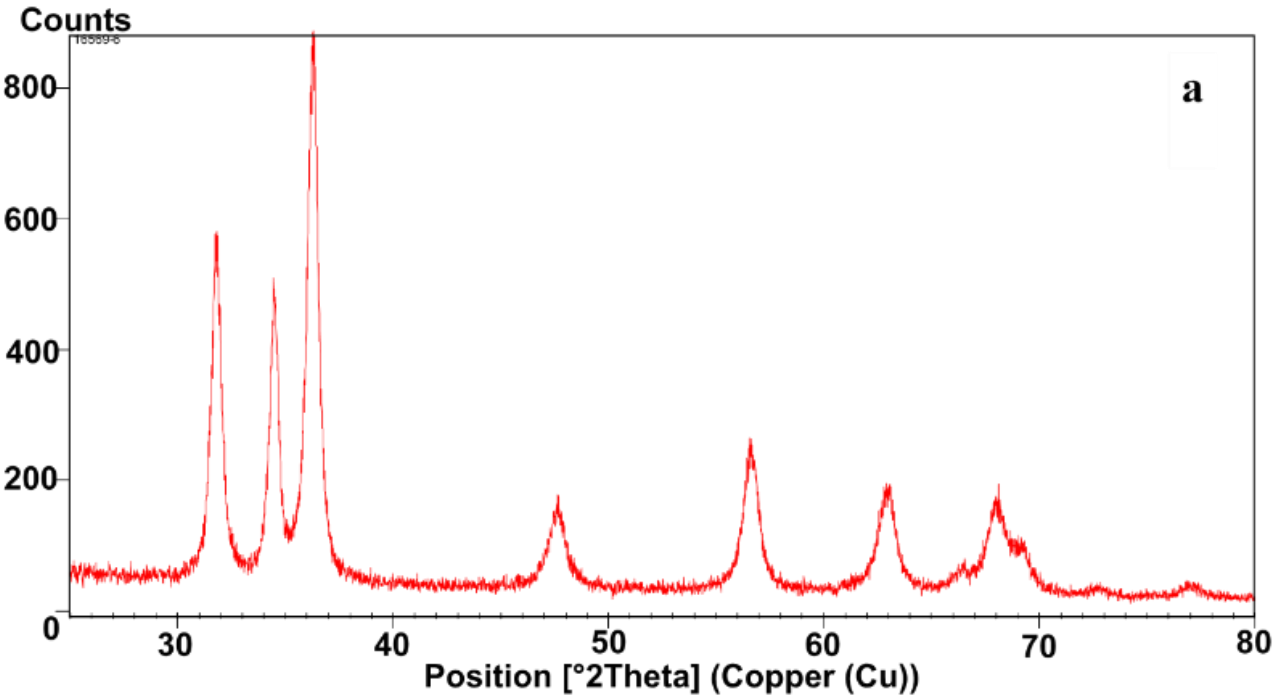

Figure 42. XRD pattern of biosynthesized calcinated zinc oxide nanoparticles (C-ZnO NPs)

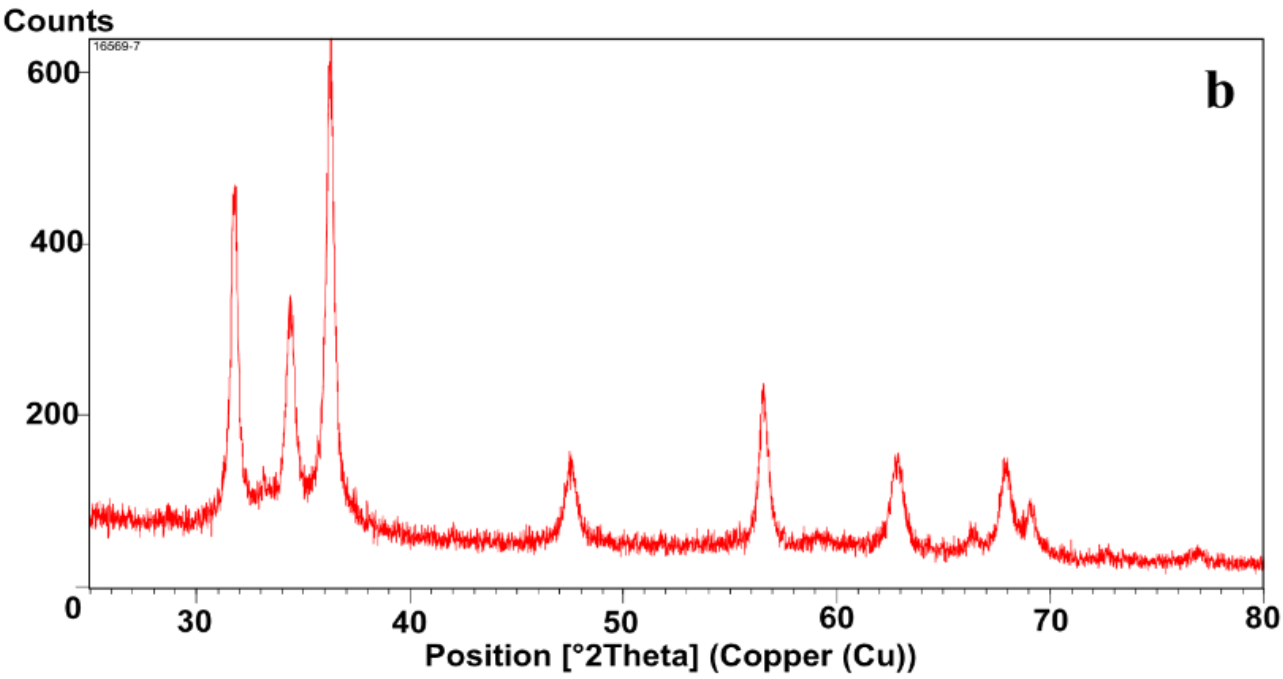

Figure 43. XRD pattern of biosynthesized non-calcinated zinc oxide nanoparticles (NC-ZnO NPs)

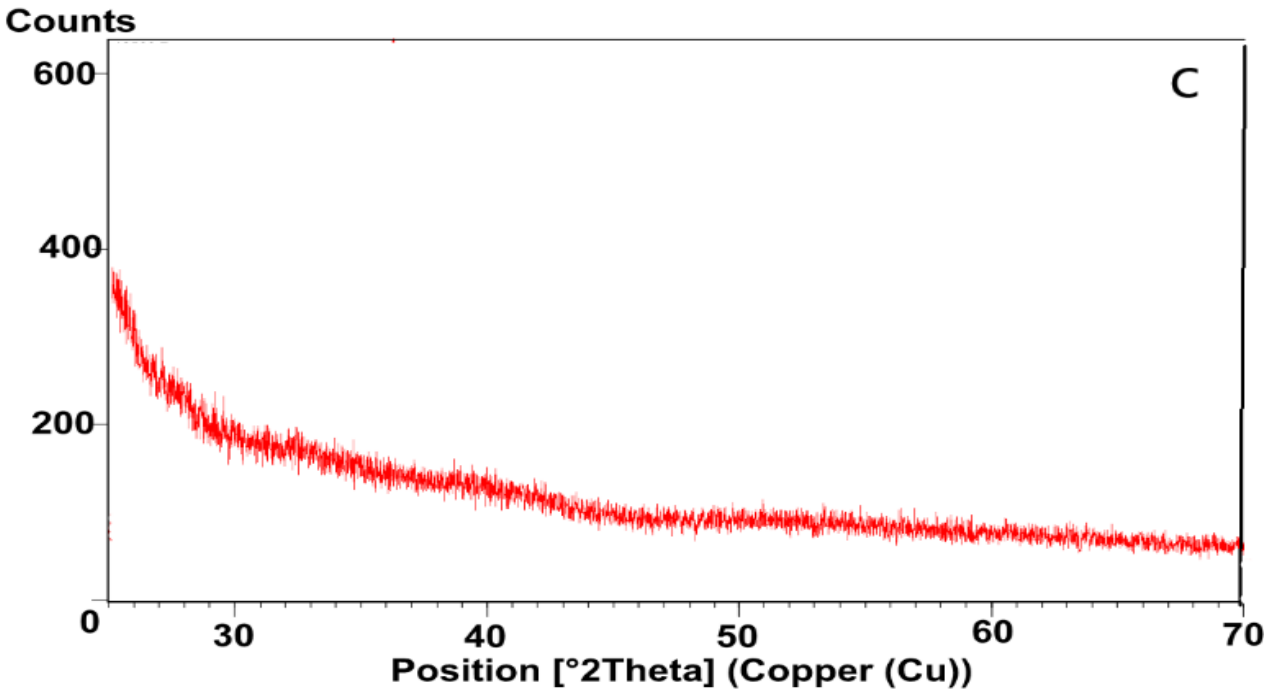

Figure 44. XRD pattern of biosynthesized zinc nanoparticles (Zn NPs)

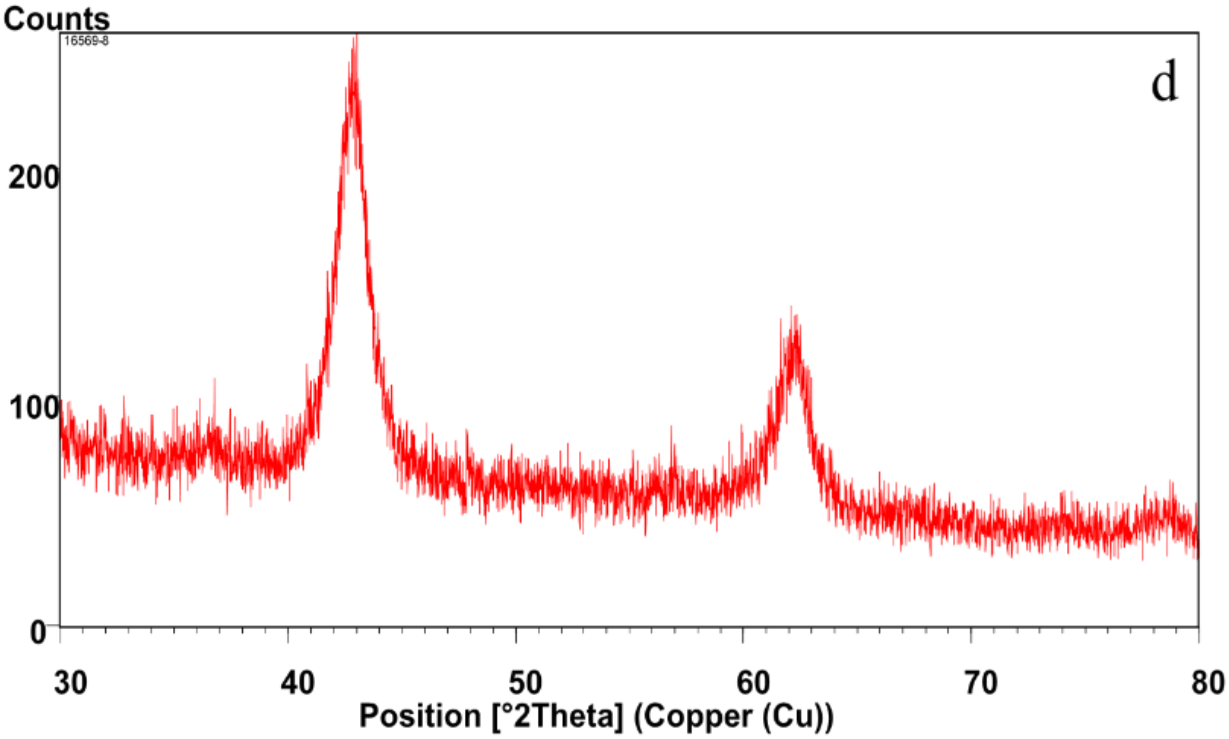

Figure 45. XRD pattern of biosynthesized magnesium oxide nanoparticles (MgO NPs)

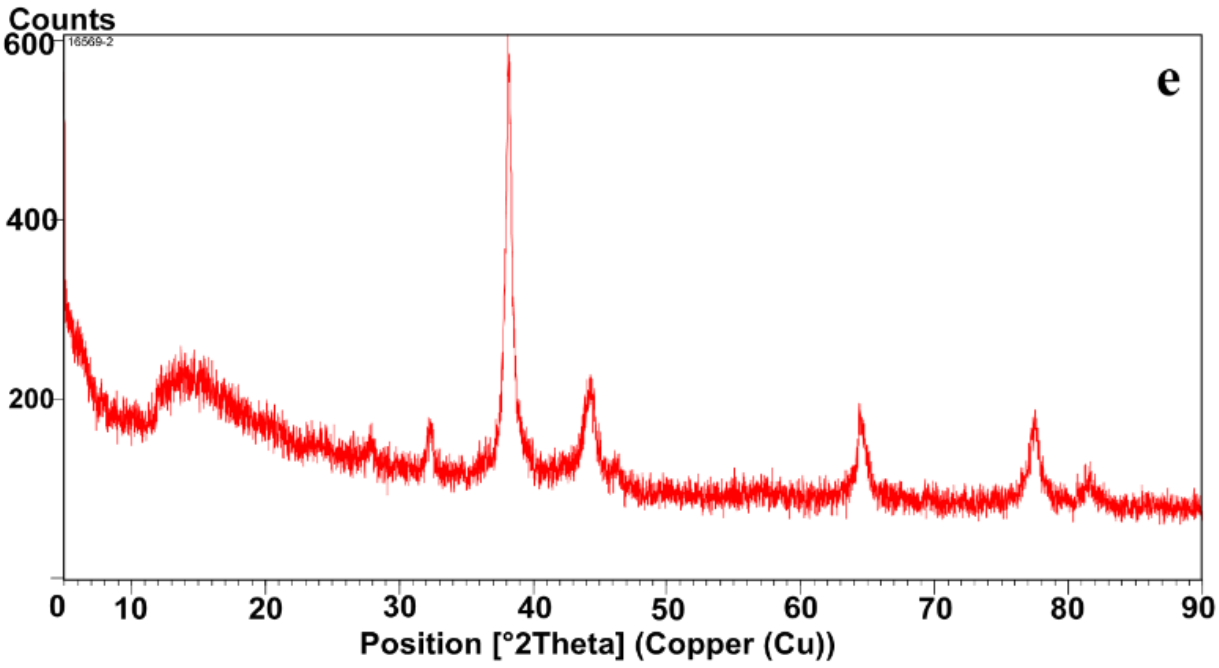

Figure 46. XRD pattern of biosynthesized silver nanoparticles (Ag NPs)

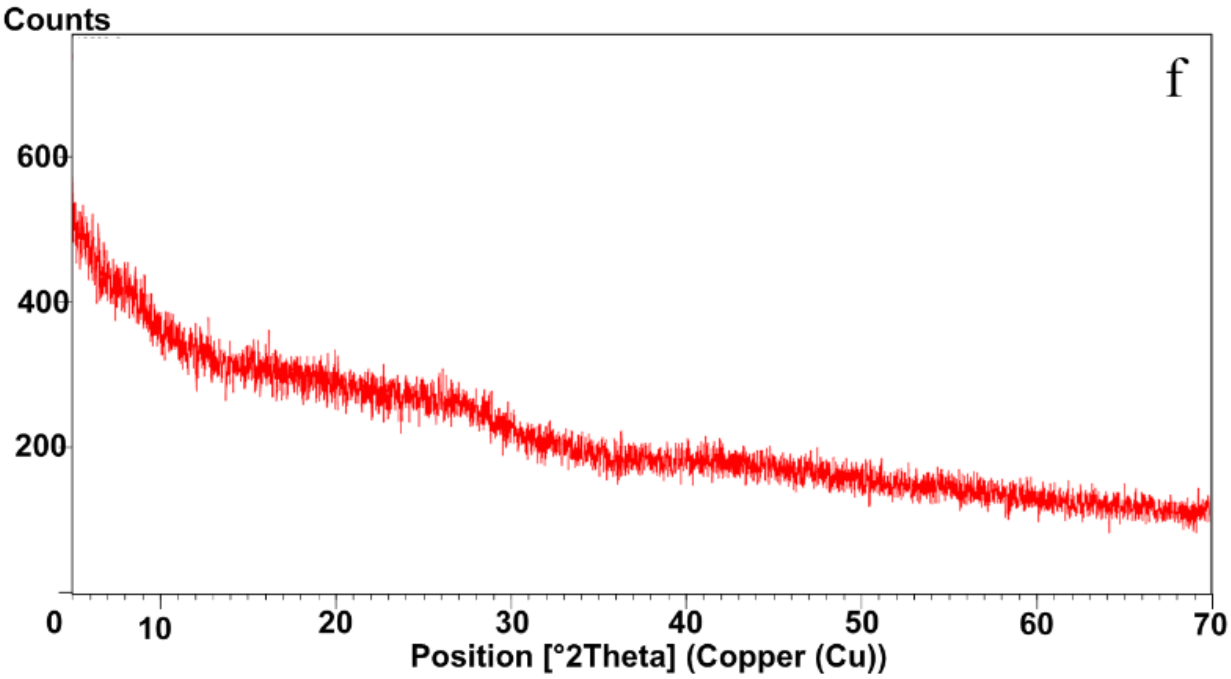

Figure 47. XRD pattern of biosynthesized cupper nanoparticles (Cu NPs)

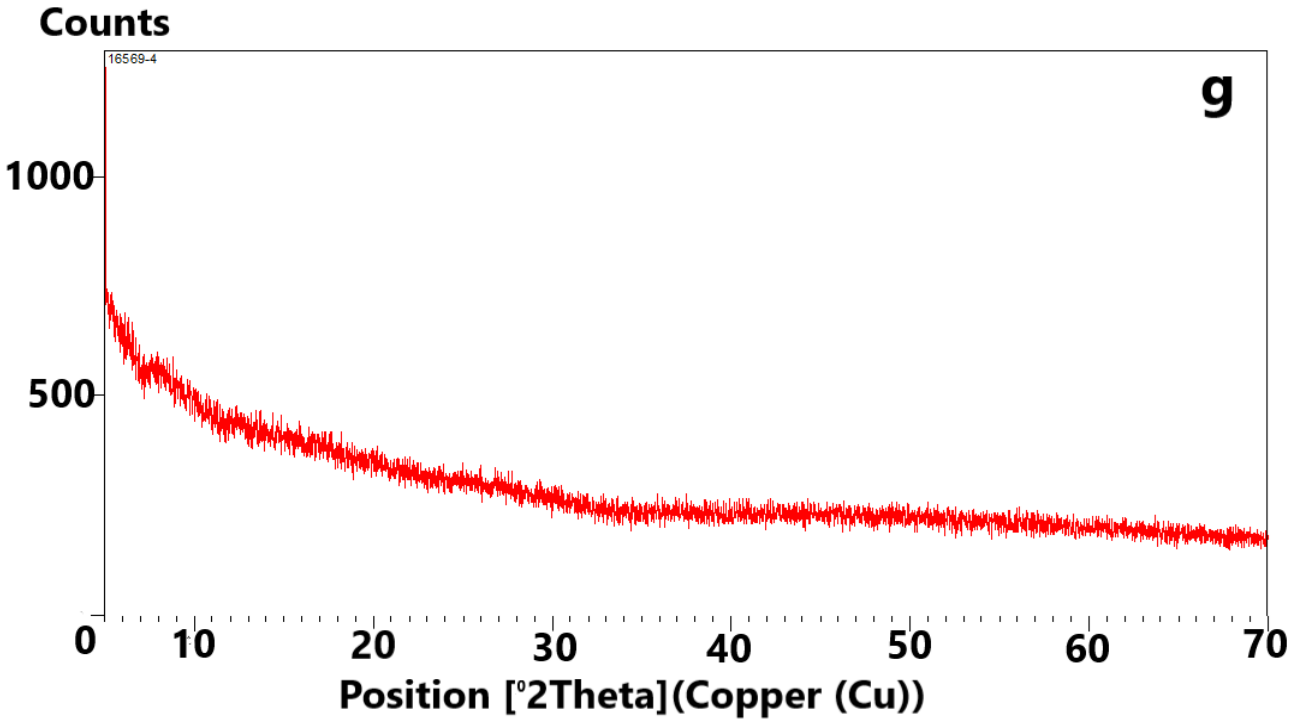

Figure 48. XRD pattern of biosynthesized iron nanoparticles (Fe NPs**)**

3.3. Biological applications of synthesized nanoparticles

Recently, food and drug administration all around the world approval an increasing number of nanotechnology products. Thus, understanding biological responses to nanoparticles is an important area in which to address the safety of nanoscale materials. The potential biotechnological application of biosynthesized NPs could be investigated to develop new green methods in production of nanomaterials. So, the antibacterial and also antifungal activities of biogenic Ag and Cu NPs are evaluated. Bacterium *Pseudomonas aeruginosa* was used for evaluation of antibacterial activity. For evaluation of antifungal activity three pathogenic fungi were selected: *Botrytis cinerea*, as an unspecialized necrotrophic fungal pathogen that attacks over 200 different plant species [96], *Pilidium concavum*, which is an opportunistic pathogen that causes leaf spots and stem necrosis in a wide range of hosts, mainly on strawberry plant [97] and *Pestalotia sp.* which is reported to be infectious for azalea (*Rhododendron L.*) leaves [98]. There are just a few reports carried out on the tow last fungi and there is no report on antifungal effect of NPs on these fungi. To the best of our knowledge, it is for the first time that the antifungal impact of a nanoparticle is tested on *Pilidium concavum* and *Pestalotia sp.*.

3.3.1. *In vitro* evaluation of antibacterial activity of biogenic Ag and Cu nanoparticles

In vitro experiments performed to evaluate the antimicrobial susceptibility of microorganisms and antimicrobial activity of biosynthesized NPs on *P. aeruginosa* bacteria. Dilution methods [99] with slight modifications served as reference methods for these experiments.

According to the results, the inhibitory effect of Ag NPs increased with the enhancement in concentration of nanoparticles. Effective concentration (EC_{50}) was 4ppm and minimum bactericidal concentration (MBC) was obtained 10 ppm. The

use of biosynthesized Ag NPs as antimicrobial agents has been reported previously. For example, Punjabi et al. [36] reported that biosynthesized silver nanoparticles with size of 40 nm were found to show antimicrobial activity against applied strains and also the drug resistant clinical isolates of *P. aeruginosa* with minimum inhibition concentration (MIC) in the range of 1.25–5 mg/ml during a broth dilution method [36]. In comparison of our outcomes with the findings of Punjabi et al. our biosynthesized Ag NPs are more effective antibacterial agents against *P. aeruginosa*. However, there is no significant difference in the average size of the Ag NPs reported by Punjabi et al. [36] with our biosynthesized Ag NPs, this great difference in antibacterial activity may arise from non-spherical shape and polydispersity of their Ag NPs.

Okafor et al. [100] biosynthesized Ag NPs using several plant extracts such as aloe, geranium, magnolia and black cohosh extracts and reported that at concentration of 4 ppm all had a bacteriostatic effect on *Pseudomonas* compared to the untreated species, based on the OD (optical density) readings compared to the control [100].

Patra and Baek [101] tested biologically synthesized Ag NPs against various gram positive and gram negative foodborne pathogenic bacteria including *B. cereus, L. monocytogenes, S. aureus, E. coli,* and *S. typhimurium* and reported the moderate antibacterial activity of Ag NPs (9.26–11.57 mm inhibition zone). MBC values are 50ppmfor gram positive *B. cereus* and *L. monocytogenes,* 25 ppm for gram negative *S. aureus,* 100ppmfor gram negative *E. coli,* and *S. typhimurium* [101].

According to the literature, possible mechanism of antibacterial effect of Ag NPs could be illustrated as interaction of Ag^+ ions (released from Ag NPs) with cell membrane of bacteria. It results in many damages such as cell membrane damage by accumulating in the interperinial spaces, exhaustion of the intracellular adenosine

triphosphate, disrupt transport systems including ion efflux, interrupt cellular processes such as metabolism and respiration by reacting with molecules and so on [16,36,102].

Silver-based antimicrobials can be effective in the treatment of infections on account non-toxicity of active Ag^+ to human cells. Interestingly, silver nitrate imparts different functions to bacteria depending upon its concentration. At higher concentrations, it kills bacteria, whereas, at lower concentrations it induces them to synthesize Ag NPs where *Bacillus licheniformis* is used for analysis. The biosynthesis of Ag NPs occurred at a concentration of 1 mM of silver nitrate. At higher concentrations it induced cell death as the MIC was 5 mM, and it induced catalase production, apoptotic body formation and DNA fragmentation [103]. In the study conducted by Hidalgo et al. antimicrobial activity of $AgNO_3$ against *P. aeruginosa* exerting antimicrobial effects $\geq 270 \times 10^{-5}$% (27 ppm) [104].

Ag NPs also disrupt transport systems, including ion efflux, and interrupt cellular processes such as metabolism and respiration by reacting with molecules. Similarly, silver ions react with oxygen and produce reactive oxygen species (ROS), which, in turn, causes detrimental effects and damages the protein synthesis. Ag NPs also cause loss of DNA replication followed by ribosomal subunit inactivation, thereby hampering protein synthesis. However, Ag NPs are known to primarily affect the function of membrane-bound enzymes such as those in the respiratory chain (Figure 49) [16,100].

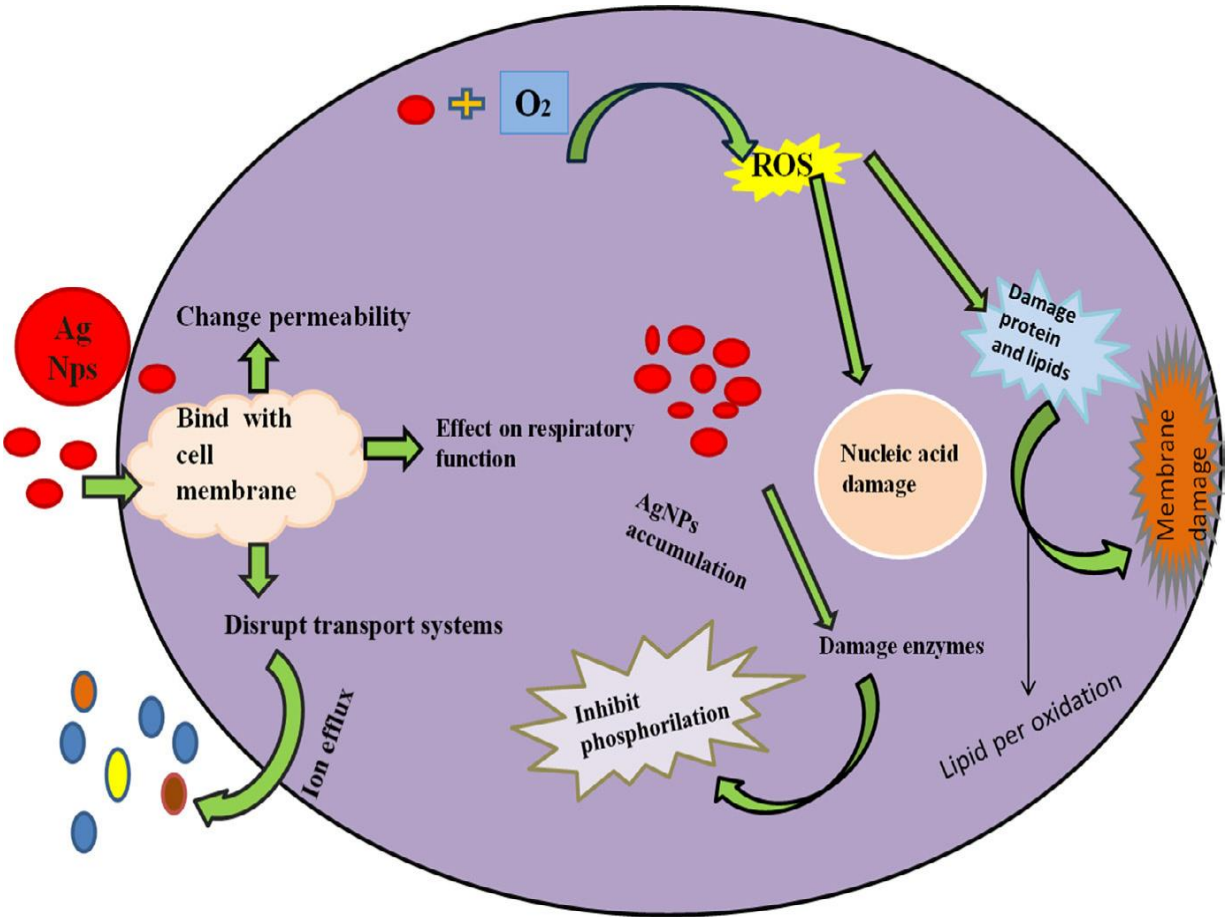

Figure 49. Mechanism of action of silver nanoparticles in plant disease management [16].

It has proven that Ag NPs' surface charge is a significant factor affecting bactericidal activity-positively charged NPs showed a high level of effectiveness against five species of pathogenic bacteria. Those authors explain that the membrane of the bacterial cells possesses a negative charge because of the presence of carboxyl, phosphate, and amino groups. The repulsion between the bacteria and negatively charged NPs could result in formation of an electrostatic barrier by limiting the interactions between NPs and bacteria. The cell membrane consists of an anionic hydrophilic outer surface. In contrast to neutral or anionic NPs, cationic particles

attach more readily to the cell surface, from where they may also be taken up more avidly if size permits [102].

Cu NPs. Green synthesized copper nanoparticles also demonstrated antibacterial activity against Gram-negative *P. aeruginosa* bacteria. The inhibitory effect of Cu NPs enhanced with the increase in NPs concentration. Effective concentration (EC_{50}) was 2.2 mg/ml and minimum bactericidal concentration (MBC) was 5 mg/ml, which is in accordance with earlier published results [22,84]. However, the MBC of Cu nanoparticles are greater than MBC of Ag NPs, indicating higher antibacterial activity of Ag NPs than Cu NPs.

Ebrahimi et al. [105] tested green synthesized Cu NPs with particle size of 17-41nm on different bacteria such as *B. cereus, S. aureus, E. coli* and *K. pneumoniae* and reported MBC values of 5, 5, 10 and 10 mg/ml respectively [105]. According to Mandava et al. [26], the minimum inhibitory concentrations (MIC) of green synthesized Cu NPs were determined by macrodilution method. MIC values were found to be 100, 50, 75 and 75 ppm for various tested bacteria *E. coli*, *S. typhi*, *M. luteus* and *S. mutans*, respectively [26].

Like Ag NPs, the antimicrobial activity of Cu NPs may be due to several facts such as permeation of copper ions released form Cu NPs to bacterial cell membrane and destroying morphology of cell membrane by attachment to cell wall, resulting to the cell death. Copper ions also could involve in the cross-linkage of DNA molecule of the bacteria resulting the denaturation of proteins [22,84].

3.3.2 *In vitro* evaluation of antifungal activity of synthesized Ag nanoparticles

Botrytis cinerea is selected for testing antifungal activity of biosynthesized Ag NPs. The next fungus was *Pilidium concavum* (Desm.) Höhn. To the best of our knowledge, there are not any reports on antifungal effect of nanoparticles on this fungus. The other fungal pathogen was *Pestalotia sp.,* on which just a little research

has been carried out and there is no report on antifungal effect of NPs on this fungus. Results from the present study indicated that Ag NPs have antifungal activity against different pathogenic fungi.

Ag NPs. The antifungal activity of the Ag NPs was tested using two different methods: agar dilution method and spore germination method.

(a) Agar dilution method. Pathogenic fungi, *Botrytis cinerea, Pilidium concavum* and *Pestalotia sp.* were used in this experiment. Figure 50 compares the control and the treatments with the 1 ppm, 10 ppm and 100 ppm concentrations of Ag NP suspensions. Figures 51&52 show the properties of *B. cinerea* and *P. concavum* growth at the age of nine days on oatmeal agar-based culture medium. The images represent clearly the effective treatment of Ag NPs on fungal growth inhibition. Morphological changes were observed in area of fungal growth in initial days.

To calculate the growth inhibition percent of *B. cinerea* and *P. concavum* resulted from Ag NP treatment, the control considered as reference and the equation of "Percent (%) inhibition'' was used. The calculated results are shown in Tables 13, and Figure 50. To obtain percent inhibition, the average radius of the fungus colony was measured on assigned successive days. The findings of these research show that the biosynthesized Ag NPs exhibit antifungal activity against *B. cinerea* and *P. concavum* when compared to the control. The antifungal activity on *Pestalotia sp.* was visible but not measurable (Fig. 53). Here, different types of fungi with different structures and morphology, showed different responses to Ag NPs. Since the mechanism of the effect of NPs on fungal growth is not entirely clear, it is difficult to determine the reason of different responses to NPs as one type is more sensitive than the others.

Considering the results represented in Tables 13, the inhibition percentage decreased over time to end of experiment and also the inhibition percentage increased in a dose dependent manner. This could be because of the high density of Ag NPs at which the medium was able to saturate and cohere to fungal hyphe and to deactivate pathogenic fungi [106]. For *B. cinerea*, the lowest percentage was 5.7% for the 1ppm concentration on day 9, against 28% obtained with the 100ppm on the same day. For *P. concavum*, the lowest percentage was 6.5% for the 1ppm concentration on 9^{th} day, against 65.36% attained with the 100ppm on the same day. According to values of the percent inhibition reported in Tables 13, it may be concluded that presence of the Ag NPs in cultures affected the growth of the *P. concavum* more than *B. cinerea*. Both fungi showed a higher inhibition effect at 100 ppm concentration of Ag nanoparticles than other concentrations.

Ag NPs inhibit the growth of various fungi with different levels of intensity. For instance, the growth of *Sclerotinia sclerotiorum* (Lib.) De Bary slows down two times at the concentration of 3.9 ± 0.3 ppm Ag NPs, while the growth of *Alternaria alternata* (Fr.) Keissl slowed down twice only at a concentration of 28 ± 1 ppm [107].

Although the mechanism of fungicidal effect of Ag NPs is still not clear, it is suggested that Ag NPs inhibit the budding process because of the formation of pores on the fungal cell membrane that can lead to cell death. In addition, it is mentioned that antimicrobial activity of Ag NPs might be mediated by formation of free radicals and free radicals can cause severe damages to chemical structure of DNA and proteins [71]. Kim et al. [106] reported the inhibition effect of commercial Ag NPs against *B. cinerea* on PDA. 100% inhibition was achieved in samples treated with Ag NPs at concentration of 100 ppm.

Table 13. Growth of *B. cinerea* and *P. concavum* (colony diameter mm) treated with different concentration of biogenic Ag NPs for 9 days. Data are presented as mean ± SD of three replications

B. cinerea			
Concentration (ppm)	**6th day Colony diameter (mm)**	**9th day Colony diameter (mm)**	**Growth inhibition % (9th day)**
Control	27.5±0.25	70.5±1.0	-
1	27.3±0.25	66.3±2.2	5.7±1.8%
10	11.9±1.6	60.5±3.2	14.25±2.9%
100	5.0±0.1	50.3±4.9	28±4.1%
P. concavum			
Control	3.5±0.25	46.2±6.5	-
1	1.5±0.5	43.2±4.2	6.5±1.7%
10	1.5±0.1	41.6±3.2	10±2.4%
100	0.5±0.1	16±1.0	65.36±2.1%

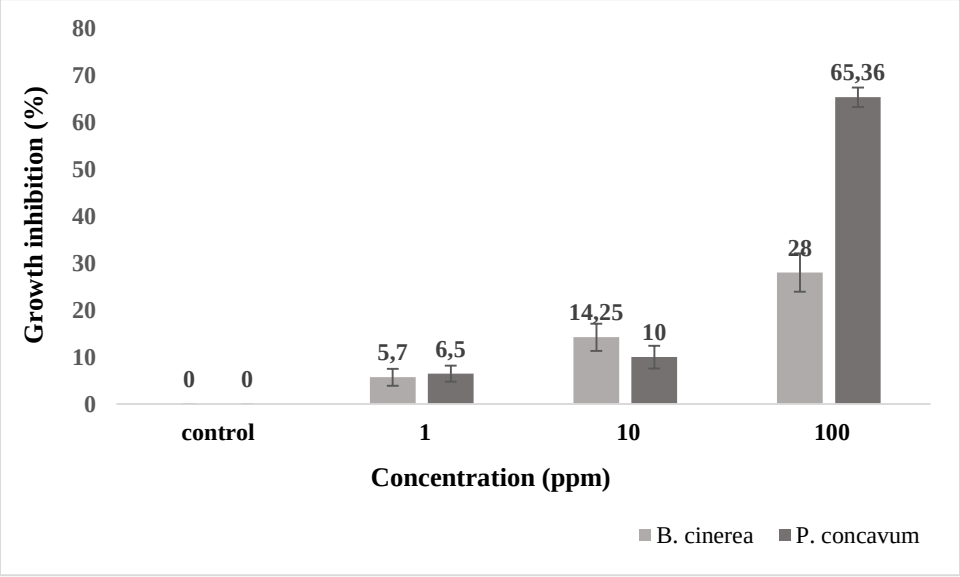

Figure 50. Growth inhibition percentage of *B. cinerea* and *P. concavum* with different concentration of the synthesized Ag NPs for 9 days. Data are presented as mean ± SD of three replications

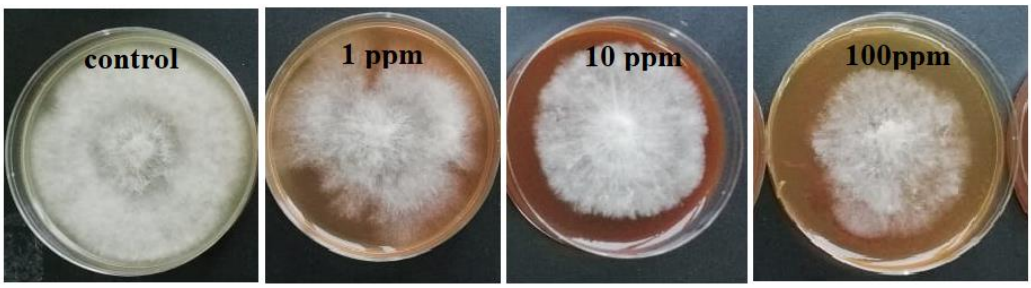

Figure 51. Effect of different concentrations of Ag NP on growth of *B. cinerea* after 9 days: control and treatments with Ag NPs of 0 (as control) 1, 10, and 100 ppm concentrations, agar dilution method.

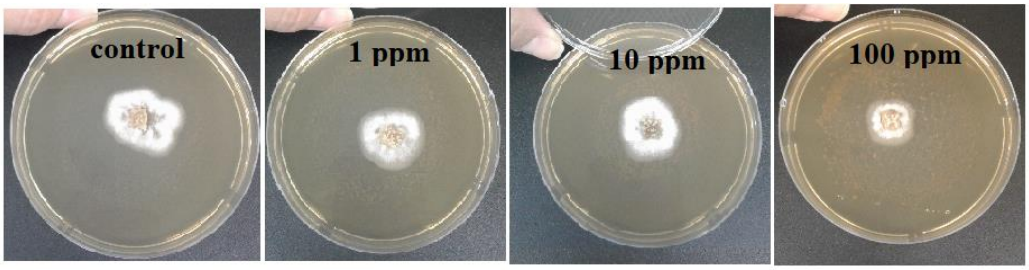

Figure 52. Effect of different concentrations of Ag NP on growth *P. concavum* at 9 days of age: control and treatments with Ag NPs of 0 (as control) 1, 10, and 100 ppm concentrations, agar dilution method.

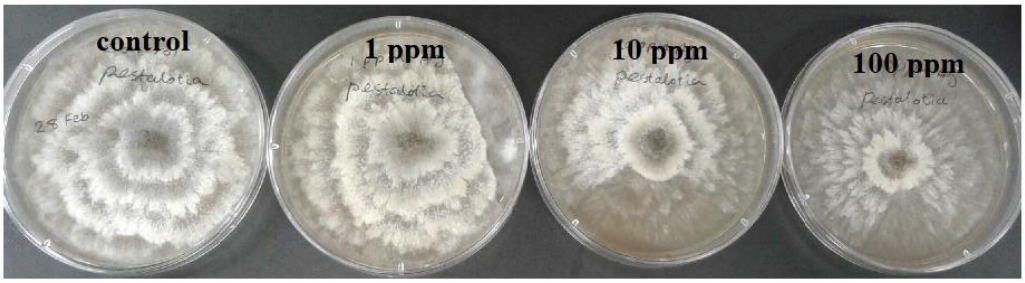

Figure 53. Effect of different concentrations of Ag NP on growth *Pestalotia sp* at 9 days of age: control and treatments with Ag NPs of 0 (as control) 1, 10, and 100 ppm concentrations, agar dilution method.

Spore Germination Inhibition. As the number of germinated spores are crucial for fungi to prominently infect the tissue, it will be very helpful to inhibit

germination of spores [50]. Figure 54 demonstrates that Ag NPs could successfully inhibit spore germination of *B. cinerea*, in a concentration-dependent manner. Under the laboratory conditions, a volume of 20µl of spore suspension placed on agar culture containing different amounts of Ag NPs of 0 (as control) 1, 10, and 100 ppm. The spore germination completely inhibited at 100 ppm Ag NPs which is half of the amount which was reported by Min et al. [108].

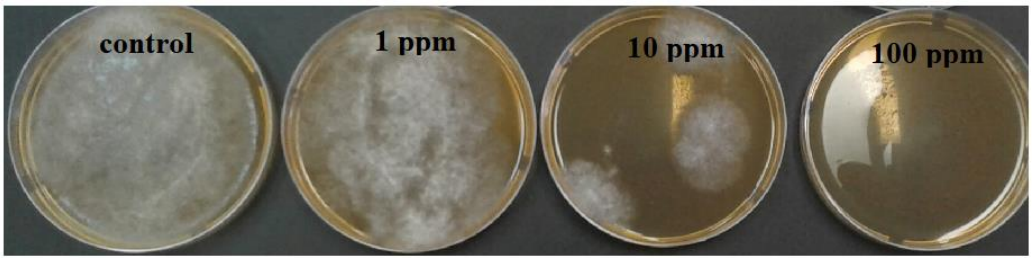

Figure 54. Germination inhibition of *B. cinerea* spores by Ag NPs of 0 (as control) 1, 10, and 100 ppm concentrations dispersed in agar medium.

It was reported that a low concentration of NPs is sufficient for the management of pathogens as it penetrates the cells efficiently. At 100 ppm concentration of Ag NPs, most fungi had a high inhibition effect. It happens because the density of the solution increases, causing coherence/clumping to fungal hyphae [16,108,109].

3.3.3. *In vitro* evaluation of antifungal activity of biogenic Cu nanoparticles

The fungi *B. cinerea* was applied to study the antifungal activity of Cu NPs using agar dilution method. Antifungal effect of Cu NPs on macroscopic growth of *B. cinerea* at 9^{th} day are presented in Figure 55.

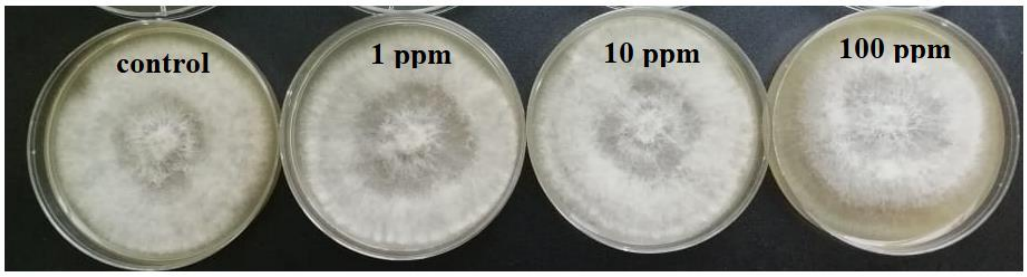

Figure 55. Effect of different Cu NPs concentrations on growth of *B. cinerea* 9 days of age: control and treatments with Cu NPs of 0 (as control) 1, 10, and 100 ppm concentrations, agar dilution method.

Regarding to the obtained results (Table 14), no significant growth inhibitions on *B. cinerea* were observed in the control, 1 ppm, and 10 ppm but there was a 25±0.3% growth inhibition for 100 ppm treated samples. The increase in concentration of the biosynthesized Cu NPs to 100 ppm resulted in a decrease in colony radius and growth inhibition percentage of *B. cinerea*. Few works were reported on the usage of Cu NPs as antifungal materials against *B. cinerea*. According to the Mishra et al. [109], since NPs have larger surface-to-volume ratio, they can strongly adhere to cell surface of fungus, directly penetrate into the cell and damage the cell wall, causing inhibition of cell growth and eventually cell death.

Table 14. Growth of *B. cinerea* (colony diameter mm) with different concentration of the synthesized Cu NPs for 9 days and percentage growth inhibition.

Concentration (ppm)	**Colony diameter (mm) (9^{th} day)**	**Growth inhibition % (9^{th} day)**
Control	80	-
1	72	10%
10	64	20%
100	60	25%

3.3.4. Effect of synthesized nanoparticles on seed germination and seedling growth of crop plants

As seed germination is the first step to start a successful crop improvement, it could be considered as an index to assay the enhancive or inhibitive effect of newly developed agrochemicals such as nanomaterials [6]. In the present research, we carried out some experiments to compare the effect of our synthesized biogenic NPs (C-ZnO, NC-ZnO, Zn, MgO, Ag, Cu and Fe) and their counterpart metallic salts ($Zn(CH_3COO)_2$, $MgSO_4$, $AgNO_3$, $CuSO_4$ and $FeCl_3$) on germination of seeds and seedling growth of wheat and flax by considering their effect on different parameters including germination percentage, shoot length, root length, seedlings length, root/shoot ratio, seedling vigor index (SVI), shoot length stress tolerance index (SLSI) and root length stress tolerance index (RLSI). Three different concentrations of 50, 100 and 150 ppm were used for seed priming. These concentrations were selected according to the literature [102,110]. Wheat and flax plantlets were grown In vitro and all the observations were recorded up to 7 days. Results are tabulated in Tables 15 to 22. We observed that plant growth parameters of wheat and flax, varied considerably among the plants and also different priming solutions with various concentrations. Moreover, both effects of "stimulation" and "phytotoxicity" and in some cases no significant effect of NPs and their counterpart salts was observed on germination and seedling growth. The p-values less than 0.05 indicate there is a significant difference within the results.

3.3.4.1. Effect of biogenic NPs and their counterpart salts on physiological characteristics of wheat seedling

As the seeds were exposed to the NPs or salts only for 12 hours and the effect is observed up to several days, it could be suggested that the NPs or metal ions are

absorbed on surface of seeds and gradually release to show their effect during a period of seven days.

Tables 15-18 summarize the effect of priming with biogenic NPs and their counterpart metal salts (precursors) on seed germination parameters of wheat on 2nd and 7th day.

Germination percentage: The data showed that exposure to different concentrations of biogenic NPs resulted in increase in germination percentage (G%) of all the treatments over the control at 2nd day (Table 15). The maximum G% is related to the seeds primed with Zn NP at concentration of 150 and then 100ppm i.e., 98 and 96% respectively. Vise a versa, a decrease in G% occurred in samples treated with metal salts, comparing to the control, except the sample primed with 50ppm of zinc acetate in which the G% was similar to control (Table 17).

The reason of difference between response of nano-primed seeds with salt-primed ones may be illustrated as the result of gradually release of ions from NPs by sub-toxic levels rather than the exposure to a large number of ions in case of priming with metal salts which may cause stress in the germination process [111].

At 7th day, an increase was observed in most of the samples and the highest G% was related to the concentrations of 50 and 150ppm of Zn NPs and also 50ppm of Cu NPs treated seeds (Table 16). Interestingly, for the samples treated with metal salts, the G% values are similar or close to the control except to the seeds primed with iron chloride, which shows a concentration dependent increase (Table 18). Among all of the applied NPs, Zn NPs are more effective for developing the seed germination of wheat seeds. Previous findings have reported that the zinc nanoparticulate priming were more effective than zinc salt in enhancing the seedling growth. For instance, it is found that Zn NP treated wheat seeds surpassed elemental Zn values over $ZnSO_4$, indicating that NPs are more efficient at delivering Zn to plant tissues than $ZnSO_4$, which suggests it is done during a particle-specific

mechanism [112]. Similar studies have shown that accumulation of Zn from NP treatment was more than predicted values upon dissolved Zn concentration [6]. However, Zn is an essential metal for plant growth, it may be a phytotoxic metal when exceeds the tolerance limit depending on plant species or plant's studied part [31].

Shoot length and SLSI: At 2nd day of the experiment, the best results of shoot elongation were related to the seeds treated with NC-ZnO NPs among all of the used NPs (Table 15) and also the maximum SLSI caused by 50 and 100 ppm of NC-ZnO and 50 ppm of Fe NPs treatments (115 to 120%). In the case of priming with salts (Table 17), the shoot elongations and SLSI values were less than the control, except 100 ppm zinc acetate which was close to the control. Ag NPs induced a significant decrease in shoot length and SLSI, both in 2nd and 7th day. According to the Tables 16 and 18, the maximum shoot lengths and SLSI at 7th day are related to the concentrations of 50 ppm of Zn and Fe, and also 50 and 150 ppm of Cu NPs (108 to 112%). In salt primed samples, just priming with 100 ppm of $FeCl_3$ had a positive effect on SLSI (125%) and no other significant increase was observed. There were also decrease of shoot length in $CuSO_4$ primed samples (Figure 56).

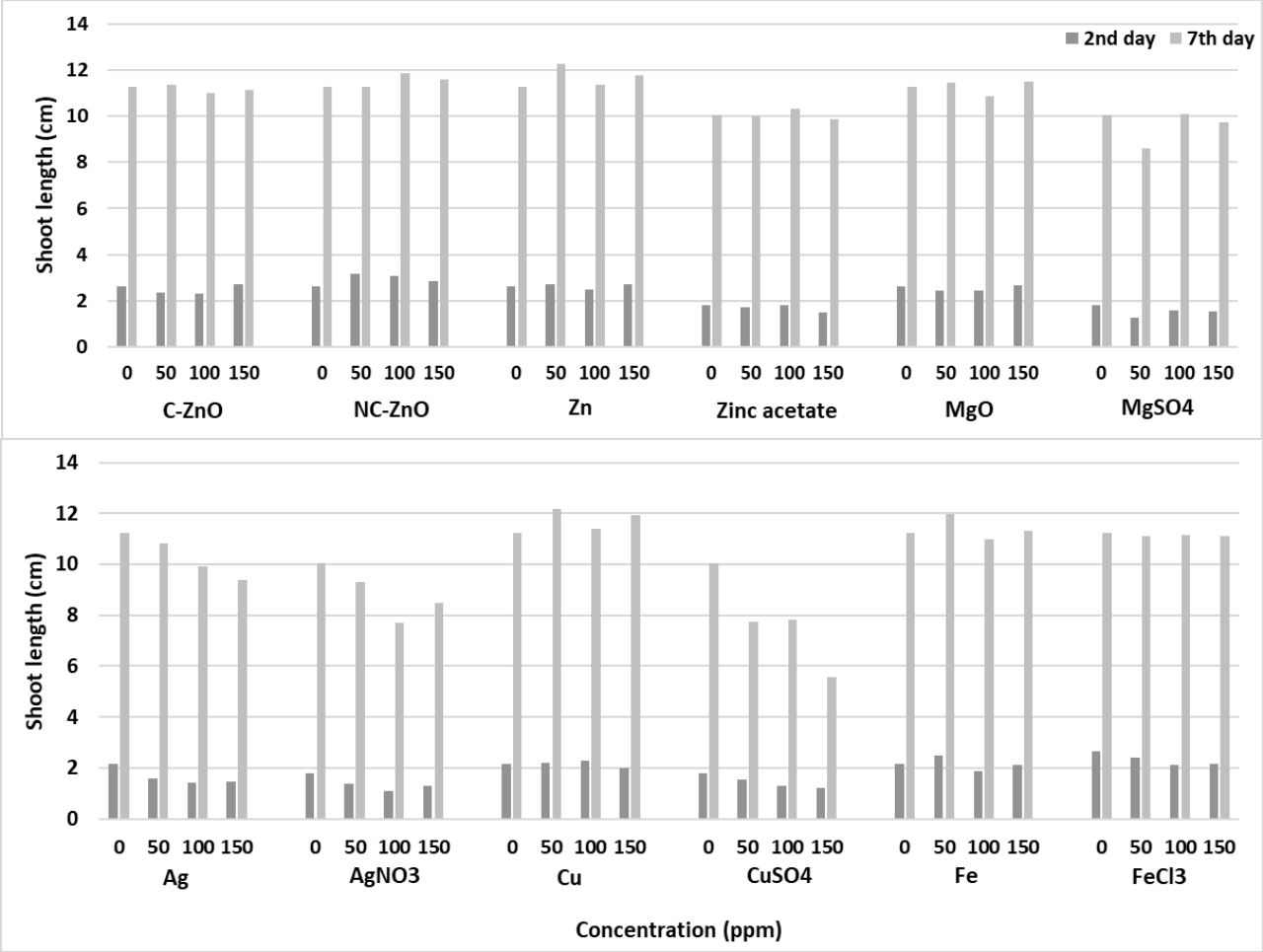

Figure 56: Shoot lengths of primed wheat seeds and control samples at 2nd and 7th days of the experiment.

Root length and RLSI: According to the Tables 15&17, at the 2nd day of the test, the most significant promoting effect on root length and RLSI is related to the soaking with NC-ZnO NPs. Root lengths of the Zn NPs treated seeds were similar to the control and the other NP treatments had an inverse effect on root elongation. Considering the results of the priming with salts, the increase in root lengths and RLSI observed in zinc acetate treated seeds, also in150 ppm $MgSO_4$ and $AgNO_3$ and 50 ppm $CuSO_4$ treatments. For seeds treated with $FeCl_3$, 50 ppm $MgSO_4$ and 100 ppm $CuSO_4$ a significant decline was indicated.

In 7th day (Table 16&18), there were a significant improvement in root length for all of the NP-primed seeds, except Ag NP-primed samples. NC-ZnO had the best effect on root length development and Ag NP showed a dose dependent inhibition effect on root lengths. For metal salt priming cases, the best results in root elongation and RLSI were related to the 100 and 150 ppm of $FeCl_3$ and then 100 and 150 ppm of zinc acetate priming. For the other samples there were a decrease in root length, mainly in $CuSO_4$ primed seeds (Figure 57).

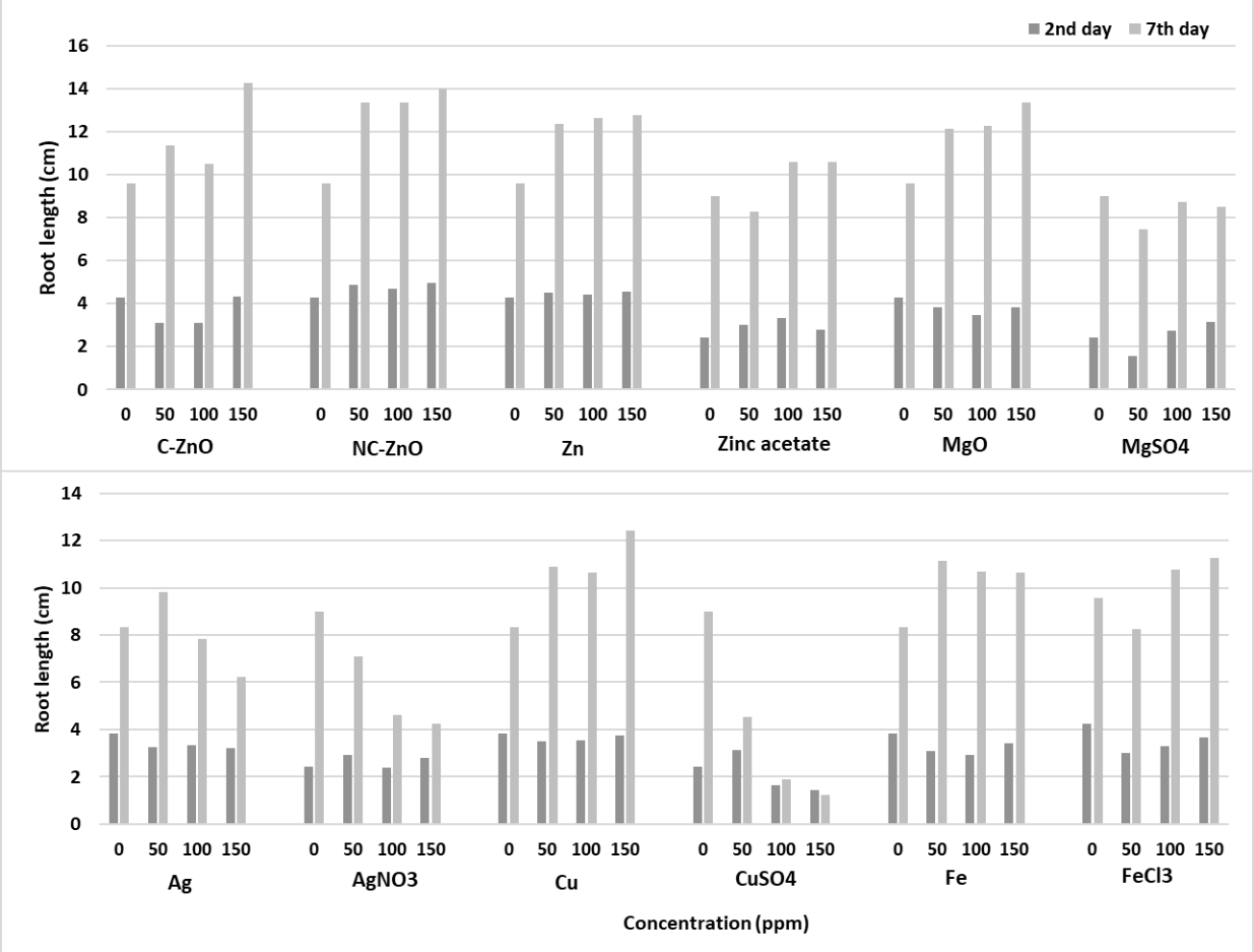

Figure 57: Root lengths of primed wheat seeds and control samples at 2nd and 7th days of the experiment.

Seedling length: In 2nd day (Tables 15&17), for Ag primed seeds, there were a remarkable decrease in seedling length. 100&150 ppm NC-ZnO and 50&150 ppm Zn NPs exhibited an increase in seedling development. Additionally, zinc acetate was the most effective salt in improving seedling length and $CuSO_4$ was the most toxic one. For other samples the results were similar to the control or just a little less than the control.

For all NP treatments in 7th day (Tables 16& 18), seedling length improvement in comparison with control was observed, except Ag NP treated seeds. The maximum effect obtained with 150ppm C-ZnO, 100 ppm NC-ZnO and 150 ppm MgO NPs (about 25% more than the control). Previous studies also reported similar results on seedling growth of ZnO treated wheat seeds [30]. In the study conducted by Ahmed et al., C-ZnO NPs with very high concentrations of 0.05, 0.5, 2, 5 mg/ml were applied on four different seeds such as radish, cucumber, tomato and alfalfa to study the toxicity effect of NPs on seeds. They reported that C-ZnO exhibited no obvious toxic effect on germination of seeds, roots and shoots growth of these seeds [6]. Similarly, in our study C-ZnO and NC-ZnO NP treatment improved the seedling growth.

For metal salt primed seeds, application of $CuSO_4$, $AgNO_3$ and $MgSO_4$ led to a notable inhibition of seedling growth respectively. $FeCl_3$ treatments, had the best improving effect in a dose dependent manner (Figure 58).

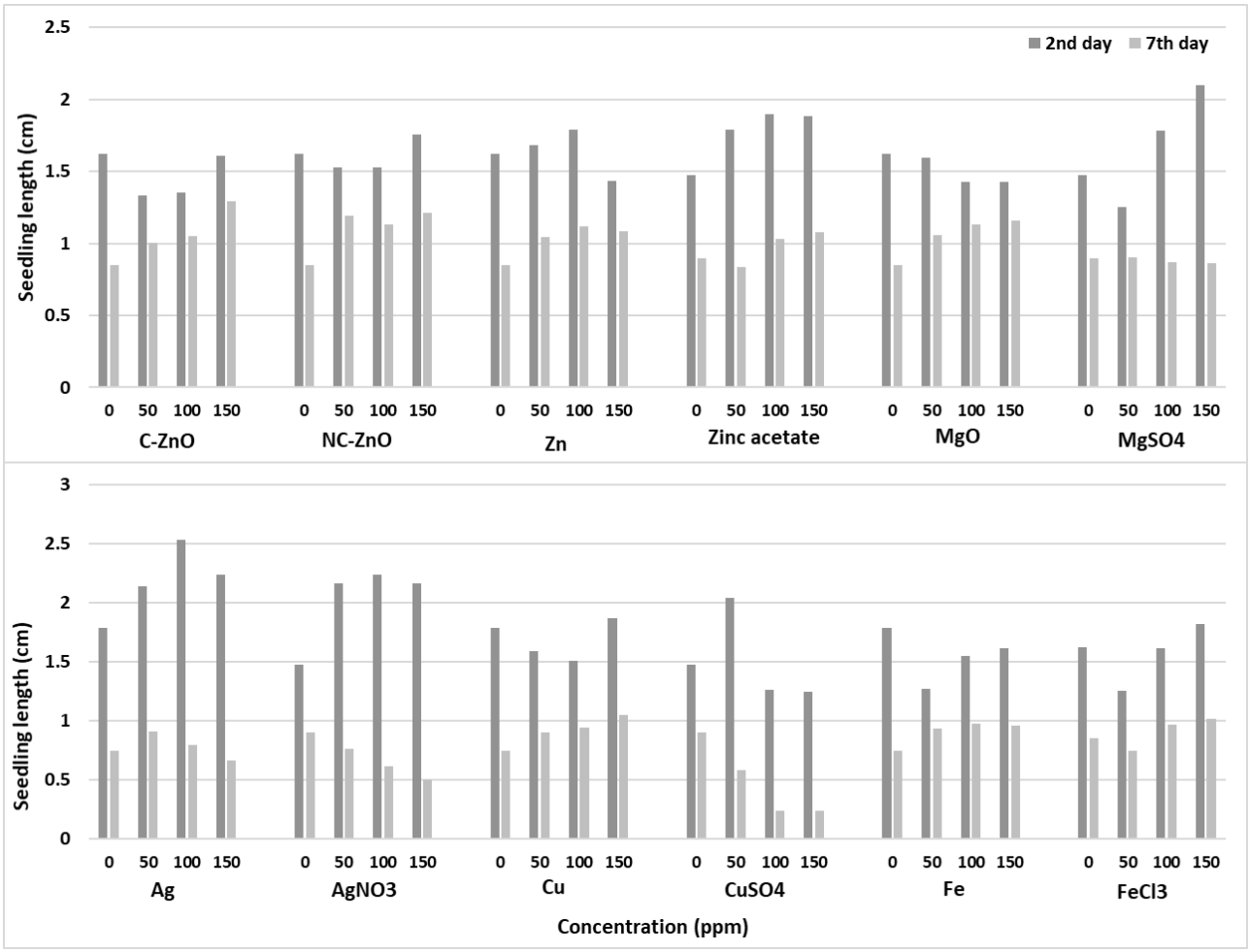

Figure 58: Seedling lengths of primed wheat seeds and control samples at 2nd and 7th days of the experiment.

Root/soot ratio (R/S): Under specific conditions, higher proportion of roots can help plants to compete more efficiently for water uptake and soil resources, while a higher proportion of shoots can help plants to collect more light energy [113].

In 2nd day (Table 15&17), all of the samples had the R/S of more than 1, indicating root lengths longer than shoot lengths and the values were similar to the control or less than that, except the Ag NP treatments. In Ag NP primed seeds, a great improvement in R/S observed mainly at the concentration of 100 ppm which was about 1.5 times more than its respective control and the minimum was related

to the 50 ppm Fe NP which was 0.3 times less than the control. For metal salt treatments, $AgNO_3$ showed the results close to the Ag NP treatments, zinc acetate had the most effect in R/S values and $CuSO_4$ had a dose dependent decrease. Overall, the R/S in salt treated seeds was more than NP treated ones.

In 7th day, R/S ratios of the NP treated seeds are more than the control, except 150 ppm Ag treated one and the maximum was for 150 ppm C-ZnO NP treatments (Table 16). For salt priming, the amounts are less than NP treated seeds and just 100&150 ppm zinc acetate and 110&150 ppm $FeCl_3$ rot to shoot ratios were more than the control (Table 18, Figure 59).

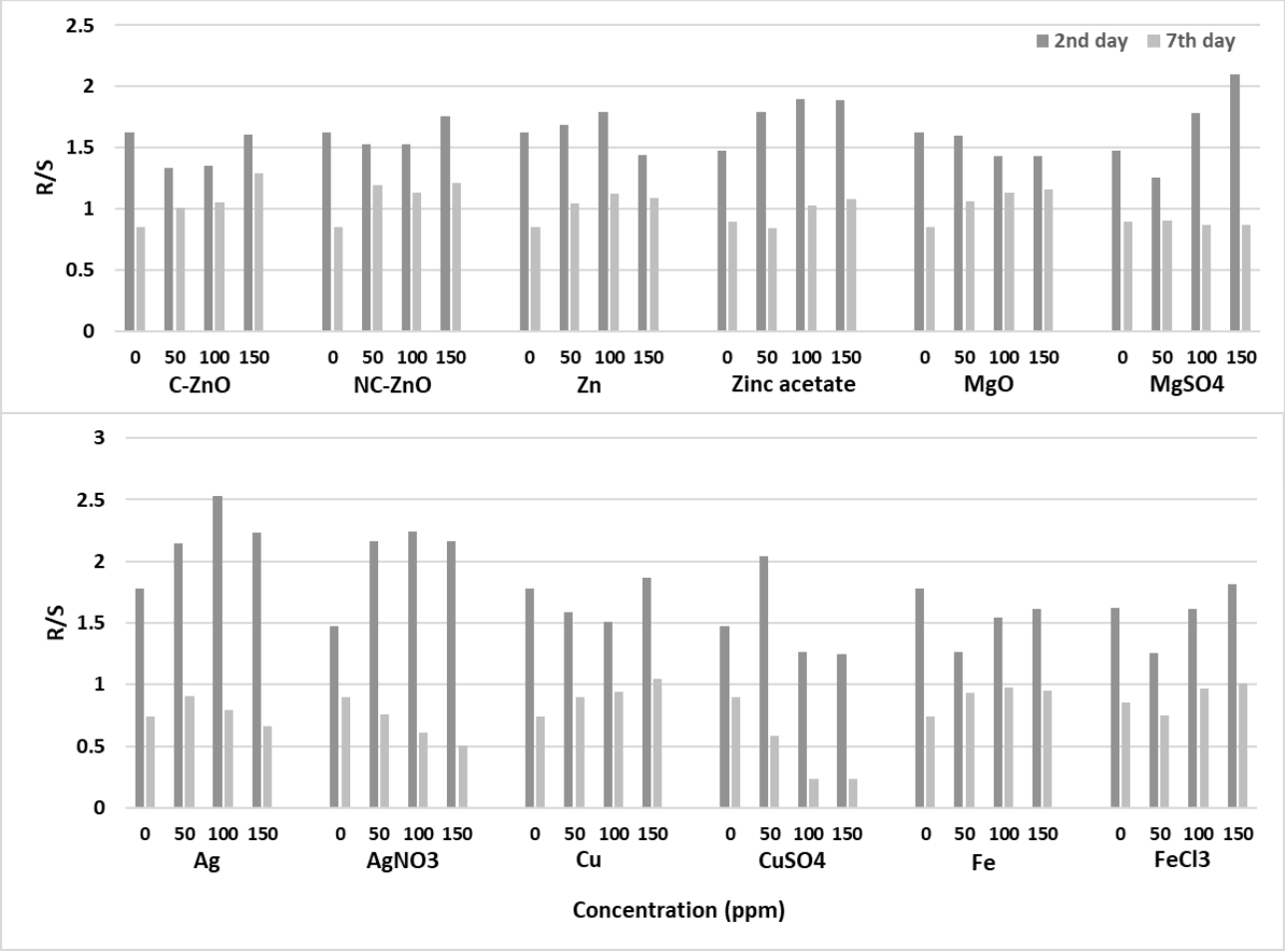

Figure 59: Root to shoot ratio (R/S) of the primed wheat seeds and control samples at 2nd and 7th days of the experiment.

SVI: For evaluating the effect of metal NPs or metal salts on seedling growth, the seedling vigor index (SVI) could be used as a phytotoxicity index [114]. In 2nd day, Ag NP priming resulted in minimum values of SVI. NC-ZnO and Zn NPs had values higher than the control and in salt treated seeds SVIs were less than NP treated seeds. The minimum amounts are due to the $CuSO_4$ and $FeCl_3$ treatments. In 7th day, for NP treatments, all SVI amounts were considerably more than the control. The maximum SVI observed in 150 ppm of C-ZnO, 50&150 ppm of Zn and 150 ppm of MgO NP primed samples. For salt treatments, 100&150ppm of zinc acetate and 150 ppm of $FeCl_3$ solutions had the maximums SVIs. Besides, $CuSO_4$ and $AgNO_3$ showed the most inhibition effect (Figure 60).

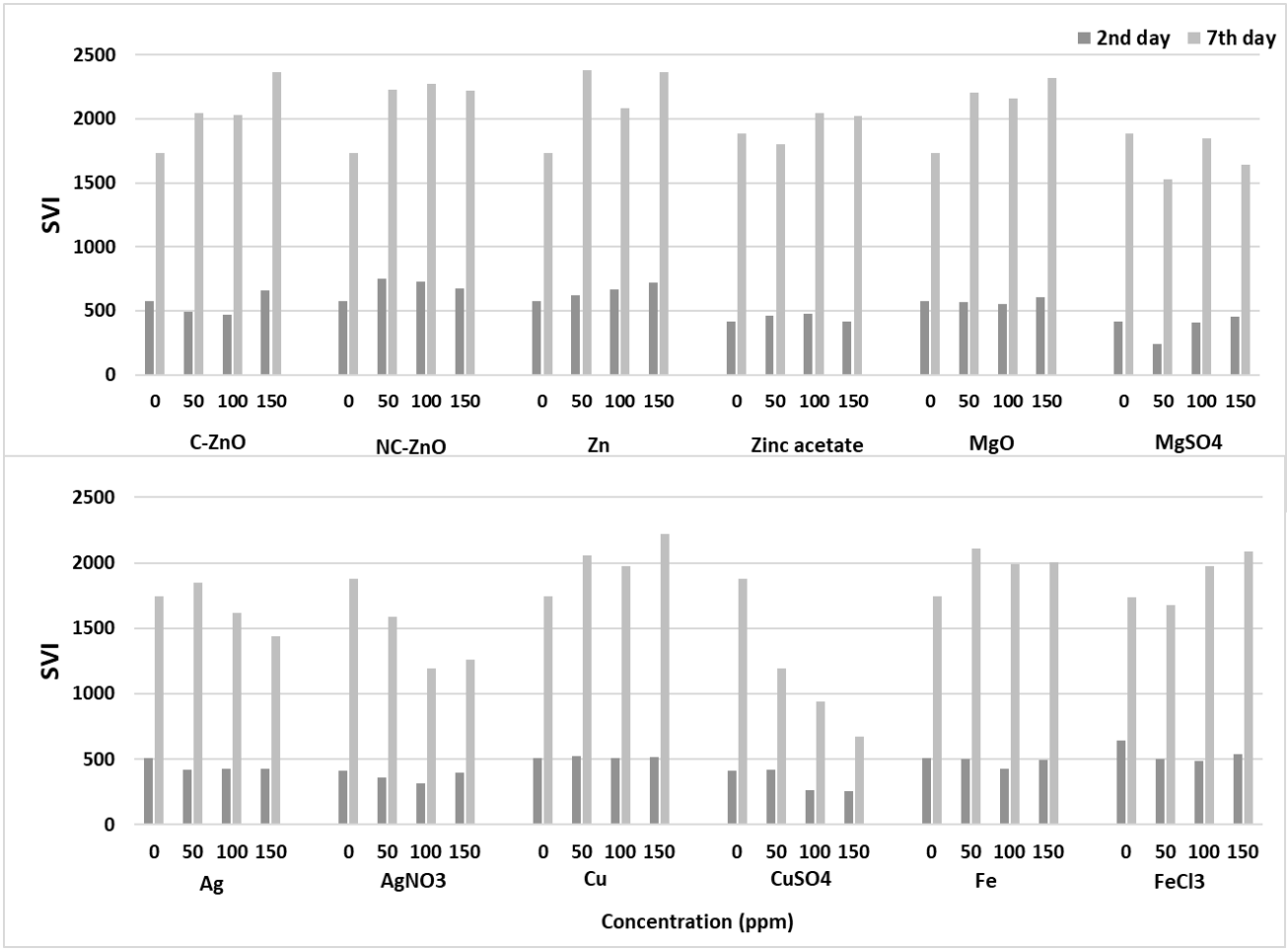

Figure 60: SVI of the primed wheat seeds and control samples at 2nd and 7th days of the experiment.

Several mechanisms are suggested in literature illustrating various effects of NPs on plant parts and cell reactions. For example, the effect of NPs on specific enzymatic reactions and different enzymes such as amylase could elucidate NPs effect on seed germination. It is not clear at this point whether NPs toxicity is stimulated by particles or the dissolved ions [115]. The effect of NPs may be also because of the interaction of NPs with some parts of the plants such as cell wall or membrane components. The size of NPs is consistent with structure of the plant cell wall to enter the cell, at the point that the accumulation of reactive oxygen species (ROS) can be started [31]. ROS can influence the permeability of the cells as it is interfered with the plasma membrane. Consequently, more NPs can result in intense stress after reaching the cells and stimulating the formation of stress-induced secondary metabolites [31].

In another study, Ag NPs toxicity on rockcress seeds was shown to be dependent on size and the concentration [111]. Ag NPs with size of 80 nm were only deteriorative at higher concentrations and those of 20 and 40 nm resulted in severe root growth inhibition. The researchers supposed that Ag NPs apoplastically transported through the root tissues [111]. The inhibitory effect of Ag NPs on the germination index was also seen in the case of cucumber [111]. Similar results are reported by C. Vannini et al. [116] as 10 ppm concentration of Ag NPs influenced the seedling growth of wheat seeds adversely. They also reported induction of morphological modifications in root tip cells by Ag NPs. According to the microscopy of the treated seeds roots, Ag NPs did not enter the cells of root and located in the outer cells of the root cup. It was suggested by TEM analysis, that the toxicity effect of Ag NPs is resulted from release of Ag^+ ions from Ag NPs [116].

Abbasi Khalaki et al. reported an enhancement in seedling growth of *thymus kotschyanus* seeds treated with 20 and 60% concentrations of Ag NPs [117].

The results reported by Zakharova et al. [118] is comparable with our obtained results, in which wheat seeds were soaked in presence of CuO NPs. They also reported that exposure of wheat seeds to 10 ppm CuO NPs showed a 14.5% improvement in germination and a twofold increase in root and shoot length in comparison with control. At higher concentrations of CuO NPs, both stimulation and toxic effects were observed (decline in root length) [118].

The effect of wheat seed treatment with Cu NPs on germination and seedling vigor index has been studied by Yasmeen et al. under laboratory conditions [119]. Germination percentage, root and shoot lengths were calculated and the results indicated exposure of wheat seeds to Cu NPs lead to a decline in germination percentage and severe reduction of root and shoot length. Therefore, Cu NPs adversely affect germination and growth of wheat seeds [119]. This substantial decrease in the plantlet growth is consistent with previous wheat field studies, where the application of excessive NPs resulted in reduced plantlet length and distorted plantlet physiology [120].

Plaksenkova et al. studied on the effect of the stress of Fe_3O_4 NPs on growth and development of rocket seeds. According to the results, 1 ppm, 2 ppm, and 4 ppm concentrations of Fe_3O_4 NPs possess positive effect on growth and development of rocket seedlings [121].

In a similar research, Yi Hao et al. studied the effects nano-priming with different Fe_2O_3 morphologies like Fe_2O_3 nanocubes, Fe_2O_3 short nanorods, Fe_2O_3 long nanorods at the concentrations of 5 to 150ppm on rice seeds during the germination. They found that all NPs considerably stimulated the root growth, and promoted shoot length at most concentrations while Fe_2O_3 long nanorods inhibited the seeds

germination significantly and showed different biological effect from other Fe_2O_3 nanomaterials, due to their different shape [122].

Ngo et al. studied the effects of Fe NPs on germination of soybean seeds, growth, its crop yield and also product quality. In laboratory conditions, the germination rates of soybean seeds soaked with Fe NPs was 80% at the concentration of 0.08 g/ha, while germination of the control sample was 55% [65].

Consequently, various data obtained from such experiments could be really helpful in germination improvement.

Figures 61-69 exhibit selected primed wheat samples and their respective controls at 2nd and 7th day of the experiment.

Table 15: effect of biogenic NPs priming on seed germination parameters of wheat on 2nd day, under different nanoparticle concentrations. Data are presented as mean values ±SD for three independent experiments. The same letters within a column show no significant difference at a 95% probability level at the $p < 0.05$ level.

NP	Concentration (ppm)	Germination percentage (G%)	Shoot length (cm)	Root length (cm)	Seedling length (cm)	Root to shoot ratio	SVI	SLSI (%)	RLSI (%)
C-ZNO	0 (Control)	83.33±3.33e	2.64±0.27b	4.26±0.27ab	6.90±0.45ab	1.62±0.16c	574.97±37c	100.00±0.00b	100.00±0.00b
	50	90.00±1.61bc	2.36±0.28c	3.12±0.41c	5.48±0.56d	1.33±0.20d	493.20±51de	89.85±11.60cd	73.67±12.36e
	100	86.66±2.52cd	2.30±0.30c	3.08±0.29c	5.38±0.51de	1.35±0.19d	466.23±44e	87.10±8.21d	72.40±6.74e
	150	93.33±1.87b	2.70±0.18b	4.34±0.67ab	7.04±0.77ab	1.61±0.23c	657.04±71b	102.76±7.94b	102.06±16.60b
NC-ZnO	0 (Control)	83.33±3.33e	2.64±0.27b	4.26±0.27ab	6.90±0.45ab	1.62±0.16c	574.97±37c	100.00±0.00b	100.00±0.00b
	50	93.33±2.11b	3.18±0.24a	4.86±0.54a	6.82±0.75b	1.53±0.11cd	750.37±70a	120.31±13.3b	115.06±19.59a
	100	93.33±2.37b	3.08±0.21a	4.70±0.56a	7.78±0.72a	1.52±0.14cd	726.11±67a	117.16±8.30a	110.59±14.23a
	150	86.66±1.26cd	2.84±0.26ab	4.96±0.37a	7.80±0.56a	1.75±0.15bc	675.94±48b	107.57±9.87b	116.43±8.87a
Zn	0 (Control)	83.33±3.13e	2.64±0.27b	4.26±0.11ab	6.90±0.45ab	1.62±0.16c	574.97±37c	100.00±0.00b	100.00±0.00b
	50	86.66±3.02cd	2.70±0.34b	4.50±0.79ab	7.20±0.93a	1.68±0.34c	623.95±80b	102.27±12.84b	105.63±18.70b
	100	96.66±1.91ab	2.50±0.24bc	4.42±0.35ab	6.92±0.19ab	1.79±0.32bc	668.88±18b	94.69±9.27c	103.75±8.36b
	150	98.88±2.23a	2.72±0.21b	4.56±0.38ab	7.28±0.46a	1.43±0.19d	719.84±46a	103.03±8.21b	107.04±9.03ab
MgO	0 (Control)	83.23±3.31e	2.64±0.27b	4.26±0.12ab	6.90±0.45ab	1.62±0.16c	574.97±37c	100.00±0.00b	100.00±0.00b
	50	90.00±1.93bc	2.44±0.39bc	3.84±0.35b	6.28±0.71bc	1.59±0.16c	565.20±64cd	92.42±14.81c	90.14±8.23c
	100	93.33±4.05b	2.46±0.30bc	3.46±0.23bc	5.92±0.32c	1.43±0.23d	552.51±30cd	93.18±11.55c	81.22±5.40d
	150	93.31±3.21b	2.66±0.27b	3.82±0.69b	6.48±0.93bc	1.43±0.16d	604.78±87bc	100.75±10.23b	89.67±16.29cd
Ag	0 (Control)	85.00±2.90d	2.16±0.28cd	3.83±0.28b	6.00±0.50c	1.78±0.20bc	510.00±42d	100.00±0.00b	100.00±0.00b

	50	87.00±1.07cd	1.60±0.41e	3.25±0.28bc	4.85±0.46f	2.14±0.61ab	421.95±40e	74.07±18.90e	84.85±7.53d
	100	90.01±1.93bc	1.40±0.36ef	3.33±0.28bc	4.73±0.25f	2.53±0.88a	426.00±22e	64.81±16.69fg	87.03±7.53d
	150	91.00±1.89bc	1.46±0.32ef	3.23±0.46bc	4.70±0.78f	2.23±0.20ab	427.70±71e	67.90±14.88f	84.42±12.05d
Cu	0 (Control)	85.00±2.90d	2.16±0.28cd	3.83±0.28b	6.00±0.50c	1.78±0.20bc	510.00±42d	100.00±0.00b	100.00±0.00b
	50	92.03±1.68b	2.20±0.10c	3.50±0.50bc	5.70±0.60d	1.58±0.15c	524.40±55d	101.85±4.62b	91.38±13.05c
	100	87.06±2.07cd	2.30±0.21c	3.53±0.50bc	5.86±0.71cd	1.51±0.08cd	510.40±61d	108.02±9.63b	92.25±13.14c
	150	90.01±1.93bc	2.00±0.50d	3.73±0.92b	5.73±1.41cd	1.86±0.11bc	516.00±127d	92.59±23.14c	97.47±24.25bc
Fe	0 (Control)	85.00±2.90d	2.16±0.28cd	3.83±0.28b	6.00±0.50c	1.78±0.20bc	510.00±42d	100.00±0.00b	100.00±0.00b
	50	90.00±1.93bc	2.50±0.43bc	3.10±0.17c	5.6±0.40d	1.26±0.23de	504.00±36d	115.74±20.18a	80.93±40.52d
	100	89.00±3.05c	1.87±0.49de	2.92±1.1cd	4.8±1.53f	1.54±0.39cd	427.20±136	86.80±22.79d	76.37±28.86de
	150	90.01±1.93bc	2.10±0.26cd	3.40±0.79bc	5.5±1.01d	1.61±0.27c	495.00±91de	97.22±12.24c	88.77±20.72cd
p value	-	0.0050	0.0011	0.0002	0.0059	0.0010	0.0009	0.0016	0.0007

Table 16: effect of biogenic NPs priming on seed germination parameters of wheat on 7th day, under different nanoparticle concentrations. Data are presented as mean values ±SD for three independent experiments. The same letters within a column show no significant difference at a 95% probability level at the $p < 0.05$ level.

NP	Concentration (ppm)	Germination percentage (G%)	Shoot length (cm)	Root length (cm)	Seedling length (cm)	Root to shoot ratio	SVI	SLSI (%)	RLSI (%)
C-ZNO	0 (Control)	83.33±3.33cd	11.25±0.61bc	9.58±0.49f	20.83±0.9de	0.85±0.03d	1736±86g	100.00±0.00b	100.00±0.00c
	50	90.00±1.26b	11.37±0.47bc	11.37±1.37d	22.75±0.9cd	1.00±0.15c	2047±86d	101.11±4.25b	118.69±14.3bc
	100	90.06±3.03b	11.12±0.81c	10.47±0.95e	22.5±0.5cd	1.05±0.16c	2026±51d	97.77±7.25bc	120.00±10.4bc
	150	93.33±2.54ab	11.25±0.85bc	14.25±0.95a	25.37±0.75a	1.29±0.17a	2368±69a	98.88±7.59bc	144.70±9.99a
NC-ZnO	0 (Control)	83.33±3.33cd	11.25±0.61bc	9.58±0.49f	20.83±0.9de	0.85±0.03d	1736±86g	100.00±0.00b	100.00±0.00c
	50	90.40±2.76b	11.25±1.04bc	13.37±1.10b	24.62±1.7ab	1.19±0.11b	2226±162b	100.00±9.25b	140.78±11.67a
	100	90.03±1.73b	11.87±0.62b	13.37±0.75b	25.25±0.64a	1.13±0.11bc	2273±58b	105.55±5.59ab	139.57±7.82a
	150	86.66±2.98c	11.60±0.41b	14.00±1.83a	24.60±1.7ab	1.20±0.17b	2218±154b	103.11±3.71ab	144.09±19.17a
Zn	0 (Control)	83.33±3.33cd	11.25±0.61bc	9.58±0.49f	20.83±0.9de	0.85±0.03d	1736±86g	100.00±0.00b	100.00±0.00c
	50	96.66±2.69a	12.25±2.72a	12.37±0.47c	24.62±2.6ab	1.04±0.21c	2380±256a	108.88±24.20a	129.13±4.99ab
	100	86.66±3.25c	11.37±1.10bc	12.62±0.47c	24.00±1.22b	1.11±0.12bc	2079±106cd	101.11±9.85b	131.74±4.99ab
	150	96.66±1.59a	11.75±0.64b	12.75±1.0bc	24.50±1.6ab	1.08±0.04c	2368±157a	104.44±5.73ab	133.04±10.8ab
MgO	0 (Control)	83.33±3.33cd	11.25±0.61bc	9.58±0.49f	20.83±0.9de	0.85±0.03d	1736±86g	100.00±0.00b	100.00±0.00c
	50	93.33±1.87ab	11.47±0.05bc	12.12±0.85c	23.60±0.8bc	1.05±0.07c	2202±80b	102.00±0.44b	126.52±8.91b
	100	93.33±3.23ab	10.87±0.47d	12.25±0.50c	23.12±0.47c	1.12±0.08bc	2158±44bc	96.66±4.25bc	127.83±5.21b
	150	93.33±2.36ab	11.5±0.57c	13.37±1.37b	24.87±1.93a	1.16±0.06b	2321±180a	102.22±5.13b	139.57±14.36a
Ag	0 (Control)	89.01±2.56bc	11.24±1.07bc	8.34±2.62g	19.58±3.18e	0.74±0.21e	1743±283g	100.00±0.00b	100.00±0.00c
	50	89.5±2.98bc	10.82±0.91d	9.82±1.57ef	20.65±2.1de	0.90±0.13d	1848±188f	100.07±8.47b	100.00±16.06c
	100	91.06±3.02b	9.92±0.90e	7.84±1.13gh	17.76±1.79f	0.79±0.09d	1617±163h	91.69±8.39c	79.85±11.55d

	150	92.33±3.11ab	9.36±0.84f	6.20±1.03i	15.57±1.61g	0.66±0.10ef	1438±149i	86.56±7.85cd	63.21±10.51e
Cu	0 (Control)	89.01±2.56bc	11.24±1.07bc	8.34±2.62g	19.58±3.18e	0.74±0.21e	1743±283g	100.00±0.00b	100.00±0.00c
	50	95.34±2.44a	12.17±0.78a	10.89±1.1de	23.06±1.30c	0.89±0.11d	2052±115d	112.49±7.23a	110.91±11.5bc
	100	89.66±2.81bc	11.39±1.05bc	10.65±1.54e	22.04±2.04d	0.94±0.14d	1976±183de	105.30±9.74ab	108.44±15.7c
	150	91.1±1.20b	11.93±0.90ab	12.43±1.13b	24.36±1.7ab	1.04±0.09c	2219±157b	110.32±8.37a	126.57±11.53b
Fe	0 (Control)	89.01±2.56	11.24±1.07bc	8.34±2.62g	19.58±3.18e	0.74±0.21e	1743±283g	100.00±0.00b	100.00±0.00c
	50	91.3±1.95b	11.98±0.58ab	11.14±0.78d	23.13±1.15c	0.93±0.06cd	2112±105c	110.78±5.43a	113.49±8.03bc
	100	91.85±3.03b	10.96±0.80cd	10.67±1.1de	21.64±1.58d	0.97±0.10cd	1987±145de	101.33±7.43b	108.73±11.2c
	150	91.23±1.23b	11.32±1.40bc	10.63±1.0de	21.95±1.58d	0.95±0.15cd	2002±144d	104.62±12.9ab	108.27±10.79c
P value		0.0100	0.0008	0.0066	0.0003	0.0040	0.0009	0.0160	0.0038

Table 17: Effect of metal salt (precursors) priming on seed germination parameters of wheat on 2nd day, under different nanoparticle concentrations. Data are presented as mean values ±SD for three independent experiments. The same letters within a column show no significant difference at a 95% probability level at the $p < 0.05$ level.

Metal salt	Concentration (ppm)	Germination percentage (G%)	Shoot length (cm)	Root length (cm)	Seedling length (cm)	Root to shoot ratio	SVI	SLSI (%)	RLSI (%)
$Zn(CH_3CO_2)_2$	0 (Control)	98.88±1.92a	1.78±0.64a	2.41±0.37cd	4.20±0.69bc	1.47±0.40de	415±6ab	100.00±0.00a	100.00±0.00c
	50	98.88±1.92a	1.7±0.20a	3.00±0.33b	4.70±0.36b	1.78±0.30cd	464±35a	95.50±11.23ab	124.48±13.8ab
	100	93.33±2.65c	1.78±0.21a	3.35±0.27a	5.13±0.38a	1.89±0.23c	467±36a	100.18±12.00a	139.00±11.36a
	150	96.66±2.92b	1.48±0.09b	2.81±0.54c	4.26±0.54bc	1.88±0.41c	412±5ab	83.33±5.52c	115.49±22.79b
MgSO4	0 (Control)	98.88±1.92a	1.78±0.64a	2.41±0.37cd	4.20±0.69bc	1.47±0.40de	415±6ab	100.00±0.00a	100.00±0.00c
	50	86.66±3.02e	1.25±0.16d	1.55±0.10e	2.80±0.22ef	1.25±0.14f	242±19d	70.22±9.23d	64.31±4.35f
	100	93.33±2.65c	1.58±0.24ab	2.75±0.30c	4.33±0.18bc	1.78±0.40cd	404±12b	88.95±13.49bc	114.10±12.51b
	150	96.66±1.92b	1.51±0.16b	3.16±0.25ab	4.68±0.38b	2.09±0.17b	452±36a	85.20±9.00bc	131.39±10.71a
AgNO3	0 (Control)	98.88±1.92a	1.78±0.64a	2.41±0.37cd	4.20±0.69bc	1.47±0.40de	415±6ab	100.00±0.00a	100.00±0.00c
	50	83.33±3.25f	1.38±0.20bc	2.91±0.20bc	4.30±0.24bc	2.16±0.45ab	358±20c	77.71±11.49cd	121.02±8.46ab
	100	90.12±2.98d	1.08±0.13d	2.38±0.37cd	3.46±0.34d	2.23±0.51a	312±31cd	60.86±7.46e	98.89±15.61cd
	150	96.66±2.92b	1.31±0.21bc	2.78±0.34c	4.10±0.4cc	2.16±0.41ab	396±40b	73.97±12.00d	115.49±14.47b
CuSO4	0 (Control)	98.88±1.92a	1.78±0.64a	2.41±0.37cd	4.20±0.69bc	1.47±0.40de	415±6ab	100.00±0.00a	100.00±0.00c
	50	90.89±3.12d	1.53±0.08bc	3.11±0.37b	4.65±0.37b	2.03±0.28b	422±3ab	86.14±4.58bc	129.32±15.6ab
	100	90.23±3.65d	1.31±0.29bc	1.63±0.48e	2.95±0.66e	1.26±0.33f	266±60d	73.97±16.44d	67.77±19.92ef
	150	96.66±2.92b	1.20±0.18d	1.45±0.19f	2.65±0.18fg	1.24±0.30f	256±1d	67.41±10.65de	60.16±8.19f
FeCl3	0 (Control)	98.88±1.92a	1.78±0.64a	2.41±0.37cd	4.20±0.69cd	1.47±0.40de	415±6cd	100.00±0.00a	100.00±0.00c
	50	90.62±3.02d	1.61±0.17a	1.69±0.10e	3.29±0.10d	1.25±0.13f	299±9d	90.90±6.56b	70.42±2.34ef
	100	94.83±3.03c	1.41±0.38b	1.58±0.50e	2.98±0.64e	1.61±0.44d	283±57d	79.54±14.42c	76.99±11.90e

	150	98.33±2.65a	1.44±0.46b	2.07±0.49d	3.52±0.52d	1.81±0.67c	346±49c	81.06±17.48c	85.91±11.57d
P value		0.0008	0.0111	0.0101	0.0022	0.0009	0.0100	0.0061	0.0004

Table 18: Effect of metal salt (precursors) priming on seed germination parameters of wheat on 7th day, under different nanoparticle concentrations. Data are presented as mean values ±SD for three independent experiments. The same letters within a column show no significant difference at a 95% probability level at the $p < 0.05$ level.

Metal salt	Concentration (ppm)	Germination percentage (G%)	Shoot length (cm)	Root length (cm)	Seedling length (cm)	Root to shoot ratio	SVI	SLSI (%)	RLSI (%)
$Zn(CH_3CO_2)_2$	0 (Control)	98.88±1.92a	10.03±0.70b	8.99±0.84c	19.00±1.4d	0.89±0.07b	1881±141c	100.00±0.0b	100.00±0.00b
	50	98.66±2.10a	10.00±1.47b	8.26±1.67cd	18.26±2.41e	0.83±0.19c	1802±237c	99.70±14.71b	91.95±18.66c
	100	97.66±2.65a	10.32±0.82b	10.60±1.33b	20.92±1.96b	1.02±0.10a	2043±192a	102.90±8.2ab	114.81±9.15a
	150	98.88±1.92a	9.85±1.18bc	10.58±1.63b	20.43±2.4bc	1.07±0.14a	2020±242a	98.20±11.82b	117.72±18.19a
MgSO4	0 (Control)	98.88±1.92a	10.03±0.70b	8.99±0.84c	19.03±1.43d	0.89±0.09b	1881±112c	100.00±0.0b	100.00±0.00b
	50	95.02±3.02bc	8.62±2.59cd	7.45±1.80d	16.07±4.30f	0.90±0.17b	1526±409e	85.95±25.8cd	82.86±20.07de
	100	98.33±2.25a	10.07±0.56b	8.73±1.45cd	18.80±1.5de	0.86±0.15bc	1843±155c	100.46±5.67b	98.09±16.34b
	150	98.88±1.92a	9.73±1.08c	8.48±1.92cd	18.21±2.86e	0.86±0.13bc	1639±257d	97.01±10.8bc	94.37±21.42bc
AgNO3	0 (Control)	98.88±1.92a	10.03±0.70b	8.99±0.84c	19.01±1.41d	0.89±0.05b	1881±121c	100.00±0.0b	100.00±0.00b
	50	97.06±3.25ab	9.28±0.72c	7.10±1.45d	16.39±2.05f	0.76±0.11d	1591±199de	92.57±7.24c	79.05±16.20de
	100	97.03±2.98ab	7.70±1.07d	4.62±0.90e	12.33±1.45g	0.61±0.15e	1196±140ef	76.85±10.72d	51.44±10.09f
	150	98.88±1.92a	8.47±1.04cd	4.25±1.13e	12.72±1.88g	0.50±0.11f	1258±186e	84.49±10.4cd	47.27±12.66fg
CuSO4	0 (Control)	98.88±1.92a	10.03±0.70b	8.99±0.84c	19.02±1.43d	0.89±0.04b	1881±141c	100.00±0.0b	100.00±0.00b
	50	97.06±3.12ab	7.73±2.77d	4.53±2.17e	12.27±4.7g	0.58±0.17e	1191±457ef	77.15±27.67d	50.48±24.17f
	100	96.66±2.92b	7.83±1.29d	1.87±0.74f	9.70±1.88h	0.23±0.07g	938±182g	78.09±12.87d	20.83±8.32g
	150	98.88±1.92a	5.55±0.82e	1.22±0.65f	6.77±0.87i	0.23±0.14g	670±86h	55.33±8.27e	13.66±7.33h
FeCl3	0 (Control)	98.88±1.92a	10.03±0.70b	8.99±0.84c	19.02±1.43d	0.89±0.04b	1881±141c	100.00±0.0b	100.00±0.00b
	50	86.66±2.96d	11.12±0.25a	8.25±2.17cd	19.37±1.93d	0.74±0.20d	1679±167d	98.88±2.22b	86.11±22.74d
	100	90.00±3.03cd	11.15±0.30a	10.75±1.84b	21.90±1.79b	0.96±0.17ab	1971±161ab	125.43±3.37a	112.21±19.9ab
	150	93.33±2.65c	11.12±0.47a	11.25±0.64a	22.37±0.62a	1.01±0.08a	2088±58a	98.88±4.15b	117.43±6.73a
P value		0.0200	0.0000	0.0055	0.0007	0.0108	0.0077	0.0100	0.0006

Figure 61. Effect of C-ZnO NPs on wheat seedling growth, on 2nd day.

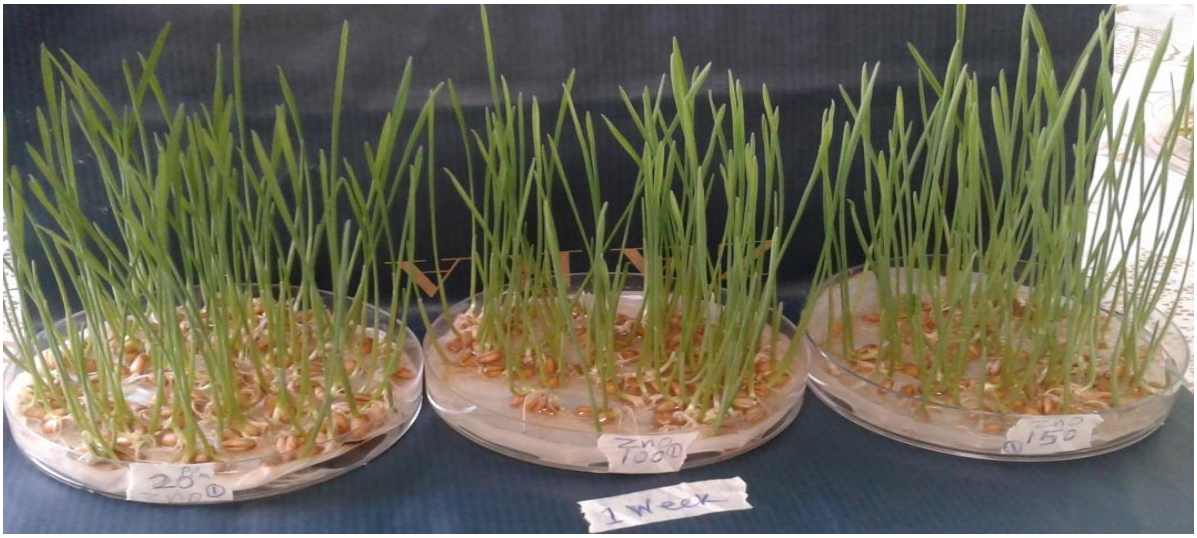

Figure 62. Effect of C-ZnO NPs on wheat seedling growth, on 7th day.

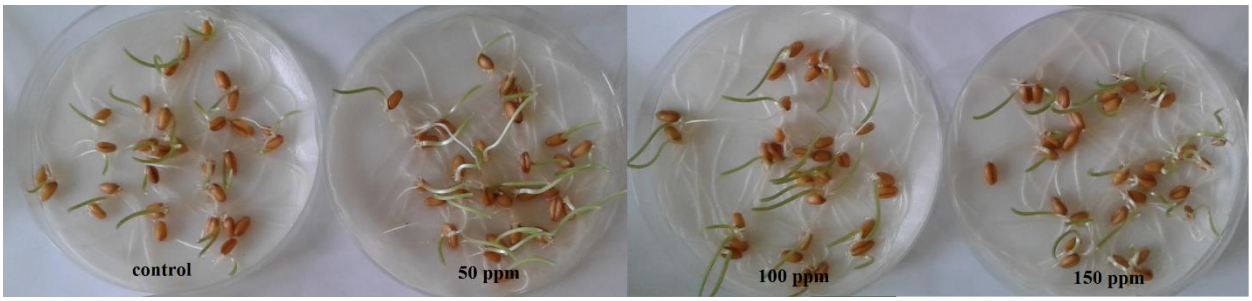

Figure 63. Effect of NC-Zn NPs on wheat seedling growth, on 2nd day.

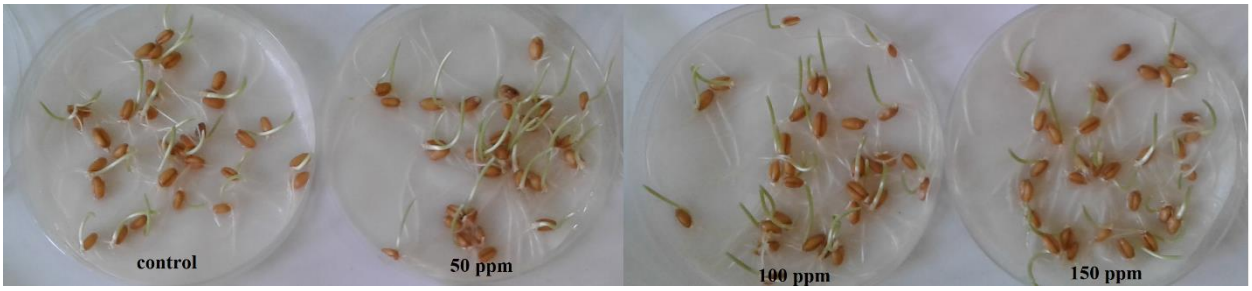

Figure 64. Effect of Zn NPs on wheat seedling growth, on 2nd day.

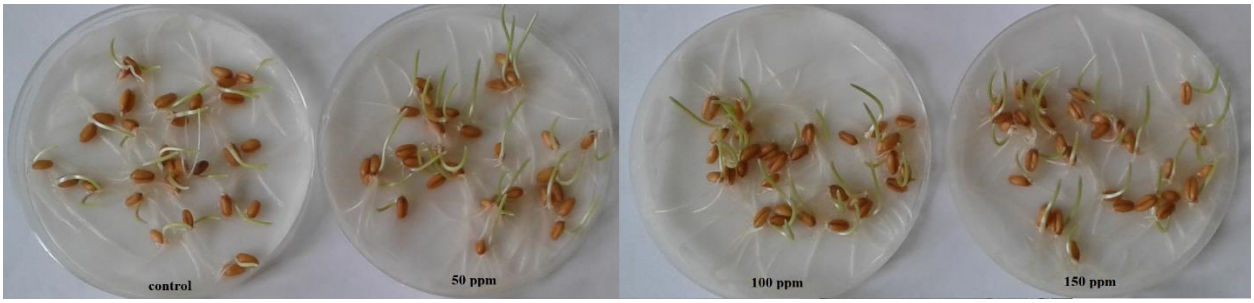

Figure 65. Effect of MgO NPs on wheat seedling growth, on 2nd day.

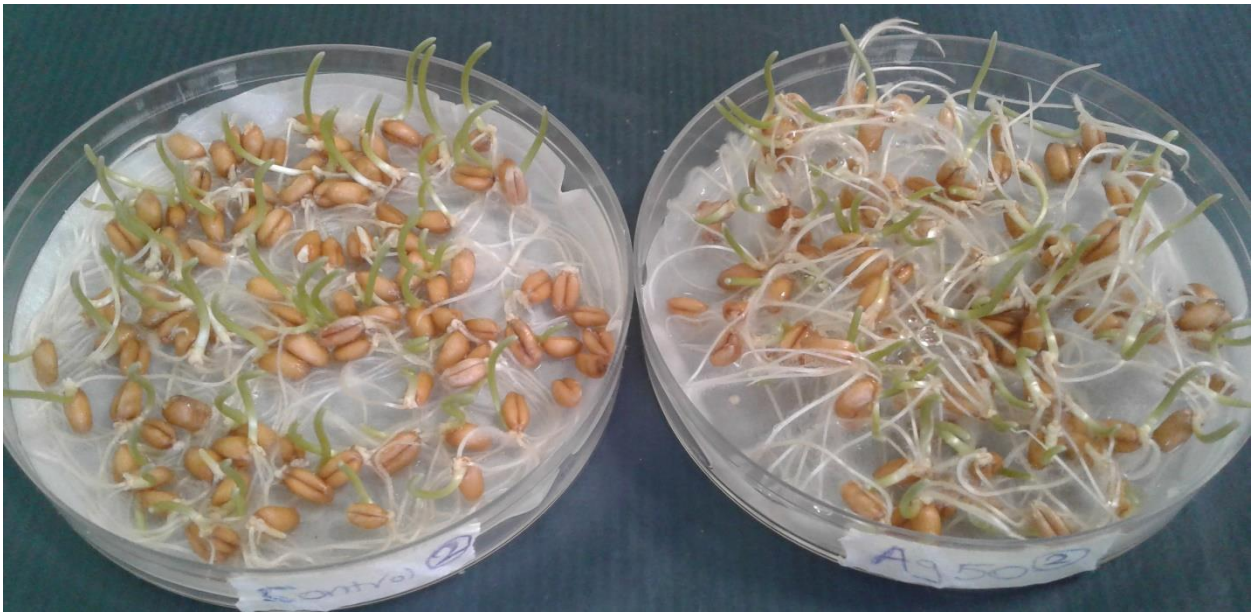

Figure 66. Effect of Ag NPs on wheat seedling growth, on 2nd day.

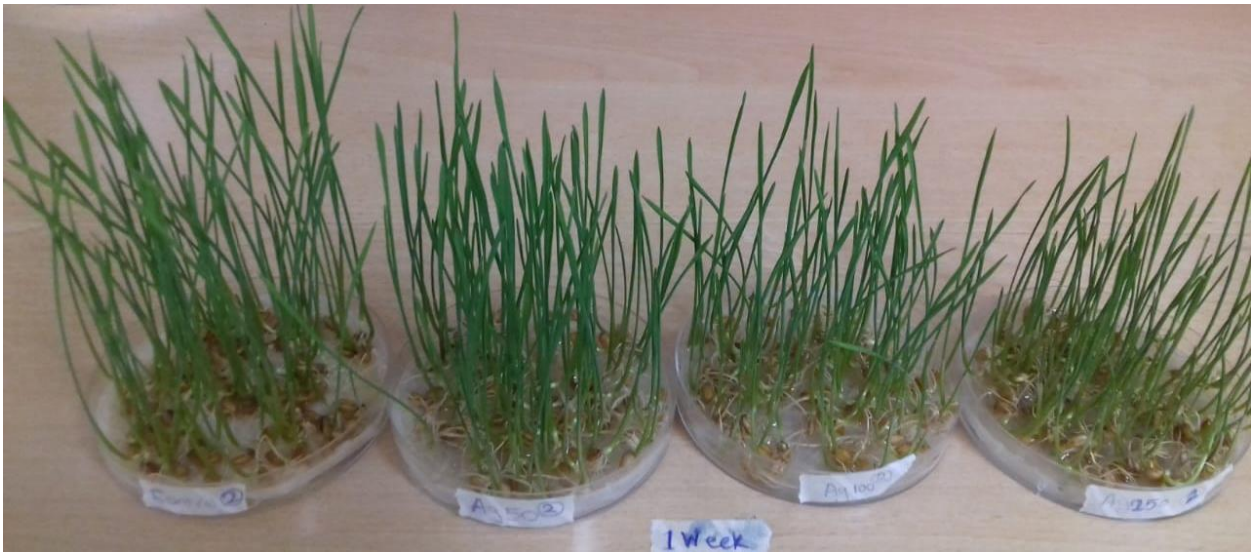

Figure 67. Effect of Ag NPs on wheat seedling growth, on 7th day.

Figure 68. Effect of Cu NPs on wheat seedling growth, on 2nd and 7th day.

Figure 69. Effect of Fe NPs on wheat seedling growth, on 2nd day.

3.3.4.2. Effect of biogenic NPs and their counterpart salts on physiological characteristics of flax seedling

The special structure of flax seed's coat was the reason we chose this plant for our experiments. The envelope or testa of the flax seed contain about 15% of mucilage, that mainly contains distinct types of arabinoxylans and water-soluble hydrocolloid/polysaccharides, which contribute to its gel qualities by forming large aggregates in solution [123]. It is suggested that nano-priming of the flax seeds and also the NPs behavior may be affected by mucilage of the seed coat due to the thick chemical environment in which NPs were trapped. Therefore, according to the following results, it could be considered as one the reasons that we observed different results of flax seeds seedling in comparison with wheat seeds.

Germination percentage: Considering the results of the Tables 19&21, in early stages of seedling, the maximum seed germination percentage (90%) was for flax

seeds soaked with 100ppm C-ZnO NPs and all of the other treatments showed G% similar or less than the control. The minimum G% was related to the seeds soaked with 100 ppm of Cu NPs. Among metal salt, zinc acetate had improving effect on G% and except 100 ppm of $CuSO_4$ and $FeCl_3$ primed seeds, no increase in G% was observed with respect to the control. At 7th day of the experiment (Tables 20&22), just 150 ppm of C-ZnO NPs suspension had improving effect over the control and all of the other NP treatments showed inhibition effect. Among salts, G% of the 150 ppm of $MgSO_4$ treated seeds was close to the control and the others were less than the control. 150 ppm of $AgNO_3$ had such a severe toxic effect so no gemination was observed and there are not any data reported in following for this case.

Shoot length and SLSI: According to the Tables 19&21, at 2nd day of the test, all of the NP treatments showed enhancement in shoot length over the control. The most effective NP was NC-ZnO and the less effective one was Ag. In support of our results, the effect of different metallic and metal oxide NPs are presented. As an example, it was reported that the application of biosynthesized MgO NPs enhanced the seed germination and growth parameters of peanut seeds as compared with control. The authors by using physicochemical methods including UV and SEM analyses, indicated that the MgO NPs penetrates into the seed coat, support water uptake inside the seeds, and then affect seed germination and growth rate mechanism [43].

The most effective salts in improving shoot length were $MgSO_4$ and then zinc acetate. 50 ppm of $AgNO_3$ was also very effective in this regard and 100 ppm concentration of $AgNO_3$ and $CuSO_4$ had the worse effect on shoot elongation. Tables 20&22 record the results of the 7th day of the experiment which show that the most effective NP in shoot length development of flax seeds was Ag. In contrast, Gorczyca et al. noticed that the 100ppm of Ag NP treatments applied to flax seeds

had a limited effect on the germination and early development of the seedlings in comparison with the control. The response of the flax seeds to the NPs was reported as an increase of chlorophyll content [102].

$MgSO_4$ and $FeCl_3$ were the most effective in shoot length development and 100 ppm $AgNO_3$ was the most toxic one, completely inhibiting the germination of seeds (Figure 70).

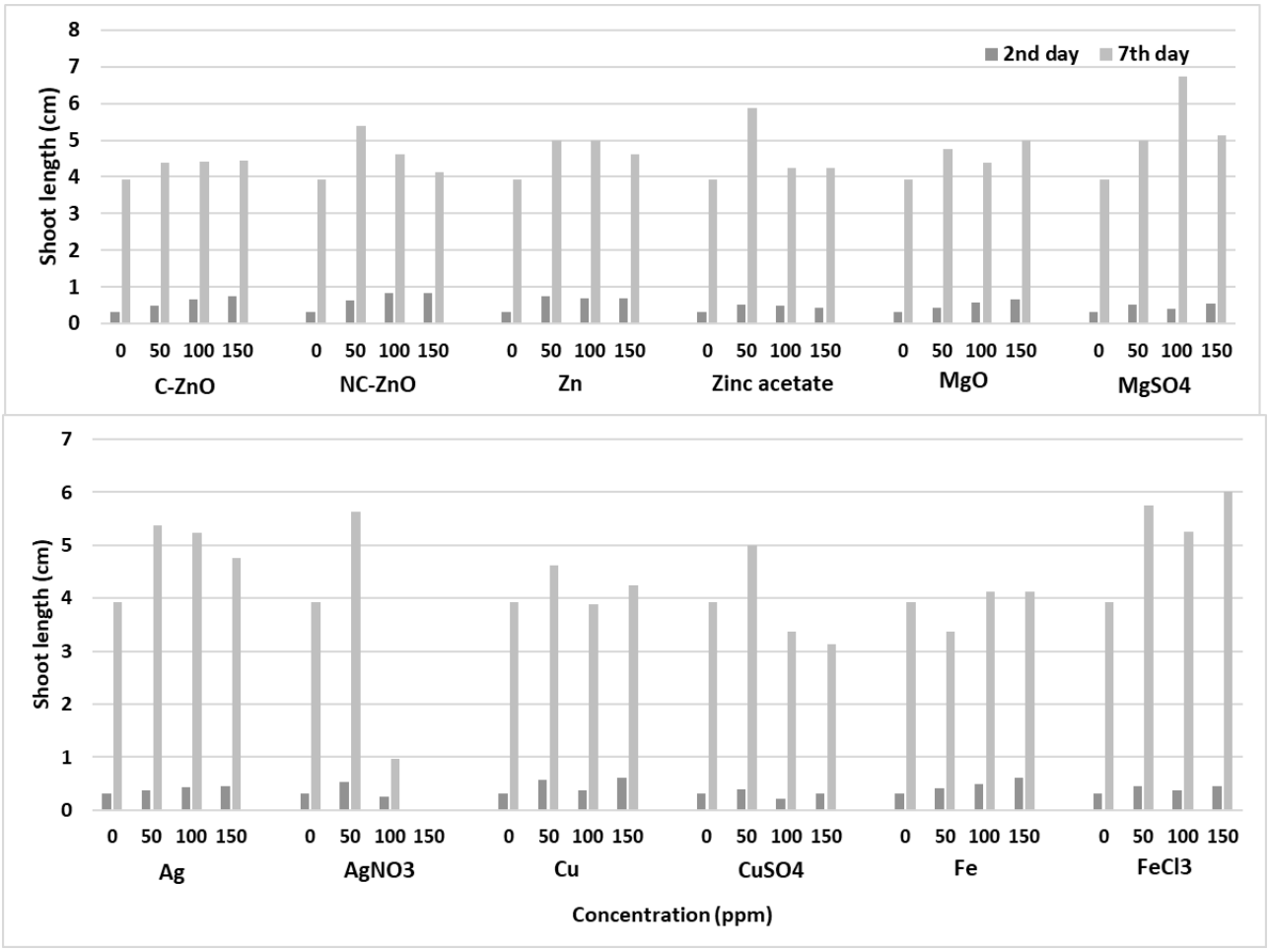

Figure 70: Shoot lengths of the primed flax seeds and control samples at 2nd and 7th days of the experiment.

Root length and RLSI: Flax seeds responded differently toward the treatment at various concentrations of NPs. At 2nd day (Table 19&21), Zn NPs had the best

effect on root growth. Ag and Fe NPs had the most inhibition effect. $MgSO_4$ was the most effective salt in root length development and $CuSO_4$ was the most toxic one. At 7^{th} day of the experiment, a significant increase in root length observed in most of the treatments, especially in Zn NPs treated samples and the root lengths were about 2 to 3 times more than the control which is considered as a great positive effect. Cu 100 ppm besides 50 and 150 ppm concentrations of Fe NPs showed a notable toxic effect on root length. Zinc acetate and $MgSO_4$ solutions induced a significant root length increase of about twofold over the control. 100 and 150 ppm of $CuSO_4$ priming inhibited the root growth to the lengths about 27% of the control (Figure 71). There are a few works studying the influence of NPs on seedling parameters of flax seeds. Zaeem et al. [31] investigated the effect of biosynthesized C-ZnO NPs at the concentrations of 0, 1, 10, 100, 500 and 1000 ppm on growth of flax seeds. All the treated flax seeds had root development of different lengths, ranging from 2.62 cm (for 1000 ppm ZnO NPs) to 7.08 cm (for 10 ppm ZnO NPs) with 3.85 cm for the control. These results indicate efficiency of different concentrations of the ZnO NPs in seed germination. At ZnO NPs concentration of above 10ppm, the higher concentration of the NPs, the lower the root length. The increased sensitivity of radicle to NPs is attributed to the larger surface area of the NPs. They suggested that the observed inhibitory effect on seed germination may be because of the very small size of NPs and the dissolution power of ZnO to Zn^{2+} ions [31].

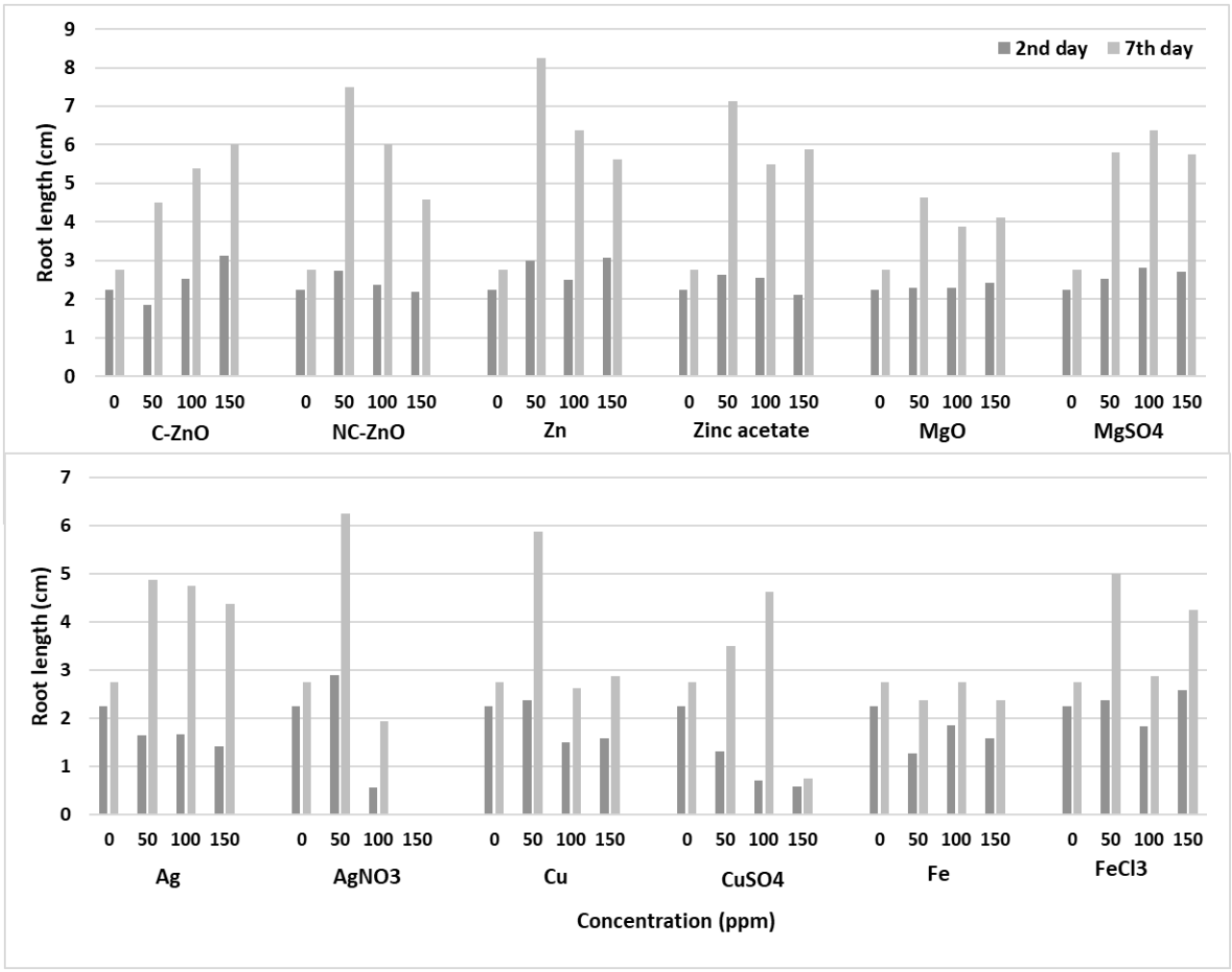

Figure 71: Root lengths of the primed flax seeds and control samples at 2nd and 7th days of the experiment.

Seedling length: Like root and shoot length, the best results of seedling length is related to Zn NPs treated samples. After 48 h (Tables 19&21), Ag and Fe had seedling lengths less than the control. For $AgNO_3$ primed samples, 50ppm concentration resulted in maximum seedling length and 100ppm resulted in no seedling. Moreover, $MgSO_4$ showed the best increasing effect in seedling length. After the first week (Tables 20&22), in the case of nano-primed seeds, except Cu and Fe primed samples which had seedling lengths less than the control, the other

treatments had seedling lengths more than the control. Zinc acetate and $MgSO_4$ were most effective in increase of seedling length and the minimum was related to the 100 ppm $AgNO_3$ treatments (Figure 72).

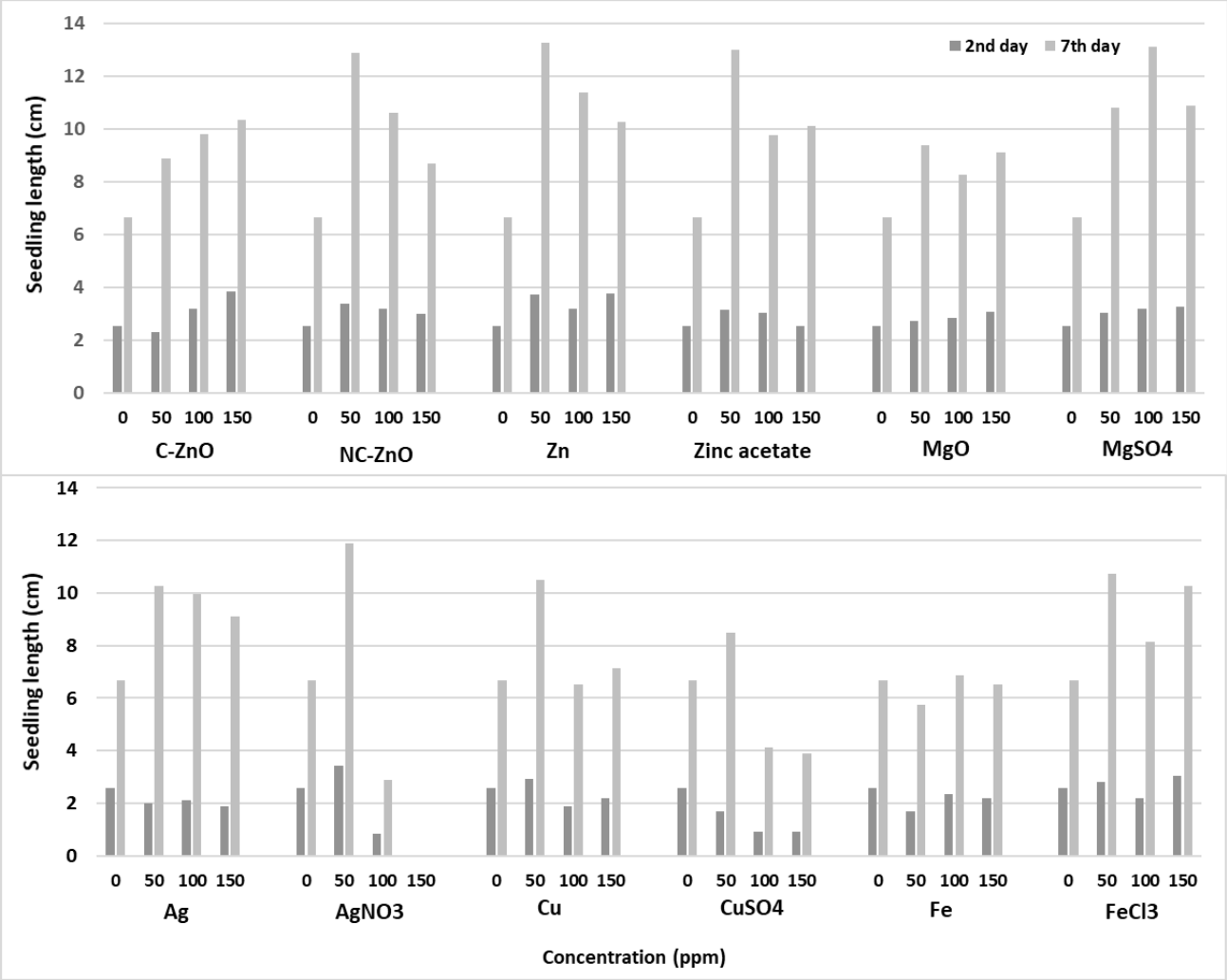

Figure 72: Seedling lengths of the primed flax seeds and control samples at 2nd and 7th days of the experiment.

Root/Shoot ratio: In early stages of flax seedling, the shoot grew with a higher speed in comparison with root. Considering the results of the Tables 19&21, at 2nd day, all of the R/S values were less than the control in NP and salt primed samples.

At 7th day, except Fe NPs and 100-150 ppm Cu NPs primed seeds, the other samples had R/S more than the control. 100 and 150 ppm of $CuSO_4$ (like Cu NP) and 100 ppm of $FeCl_3$ treated seeds had R/S less than the control (Figure 73). To the best of our knowledge, there was not any report on positive or negative effect of Cu NPs on flax seedling to be compare with our findings.

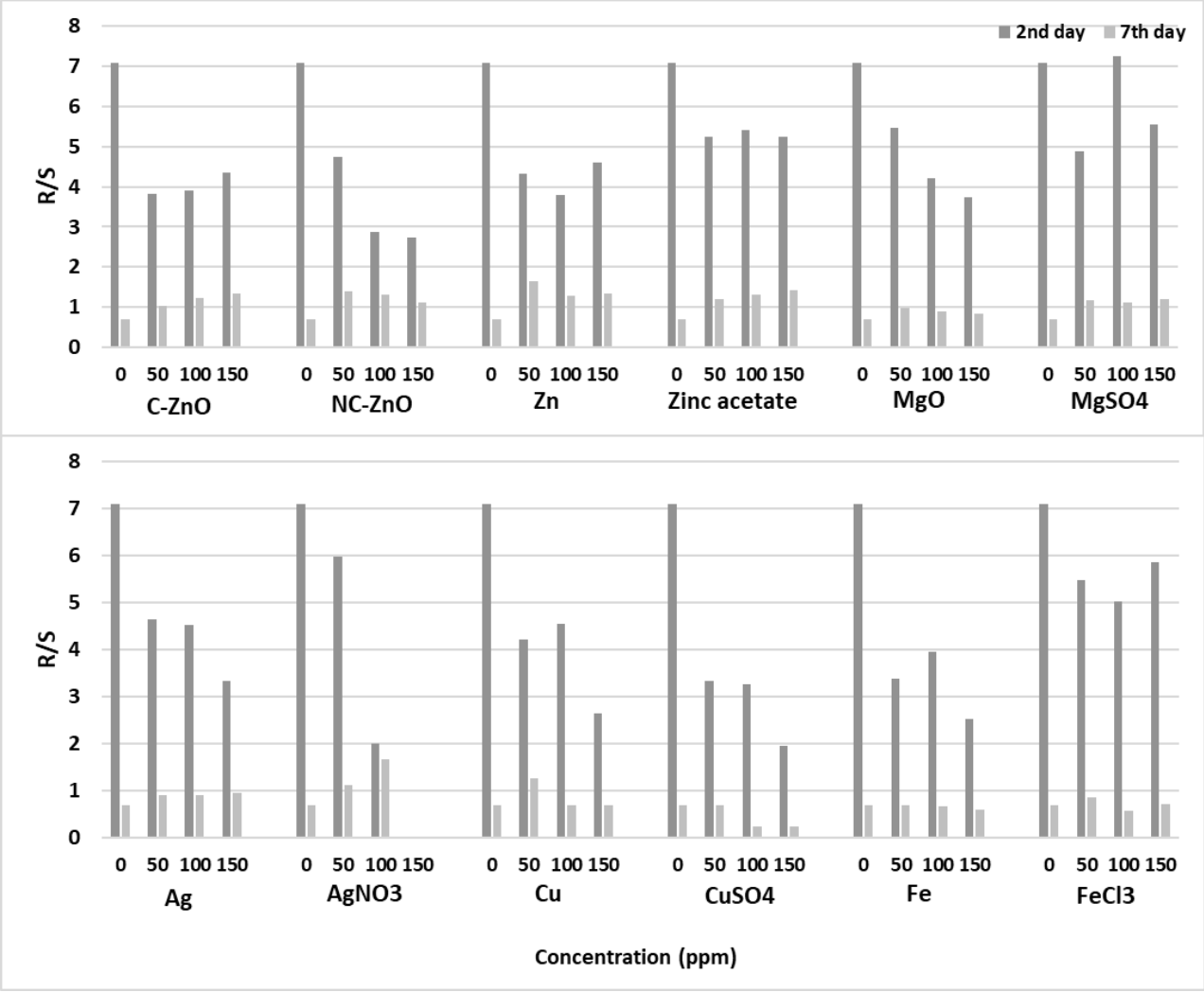

Figure 73: Root to shoot ratios of the primed flax seeds and control samples at 2nd and 7th days of the experiment.

SVI: At 2nd day of the experiment, maximum SVI was related to the 150 ppm C-ZnO and 50 ppm of Zn NPs due to their high seedling length values and the minimum was related to the 100 ppm of Cu NPs primed samples. At 7th day, Fe NPs primed samples had the minimum SVIs due to their minimum seedling lengths. In contrast, in previously reported research, stimulating effects of Fe NPs on seedling of different species have been described, for example in rocket [115], rice [122] and soybean [65]. $MgSO_4$ primed samples had the maximum SVIs and 50 ppm zinc acetate and 100 ppm $AgNO_3$ had the minimum SVIs (Figure 74).

Clearly, different results obtained from flax seed priming in comparison to the wheat seeds in germination and seedling growth parameters. Figures 75-81 represents the primed and non-primed flax seed samples at 2nd and 7th days of the experiments.

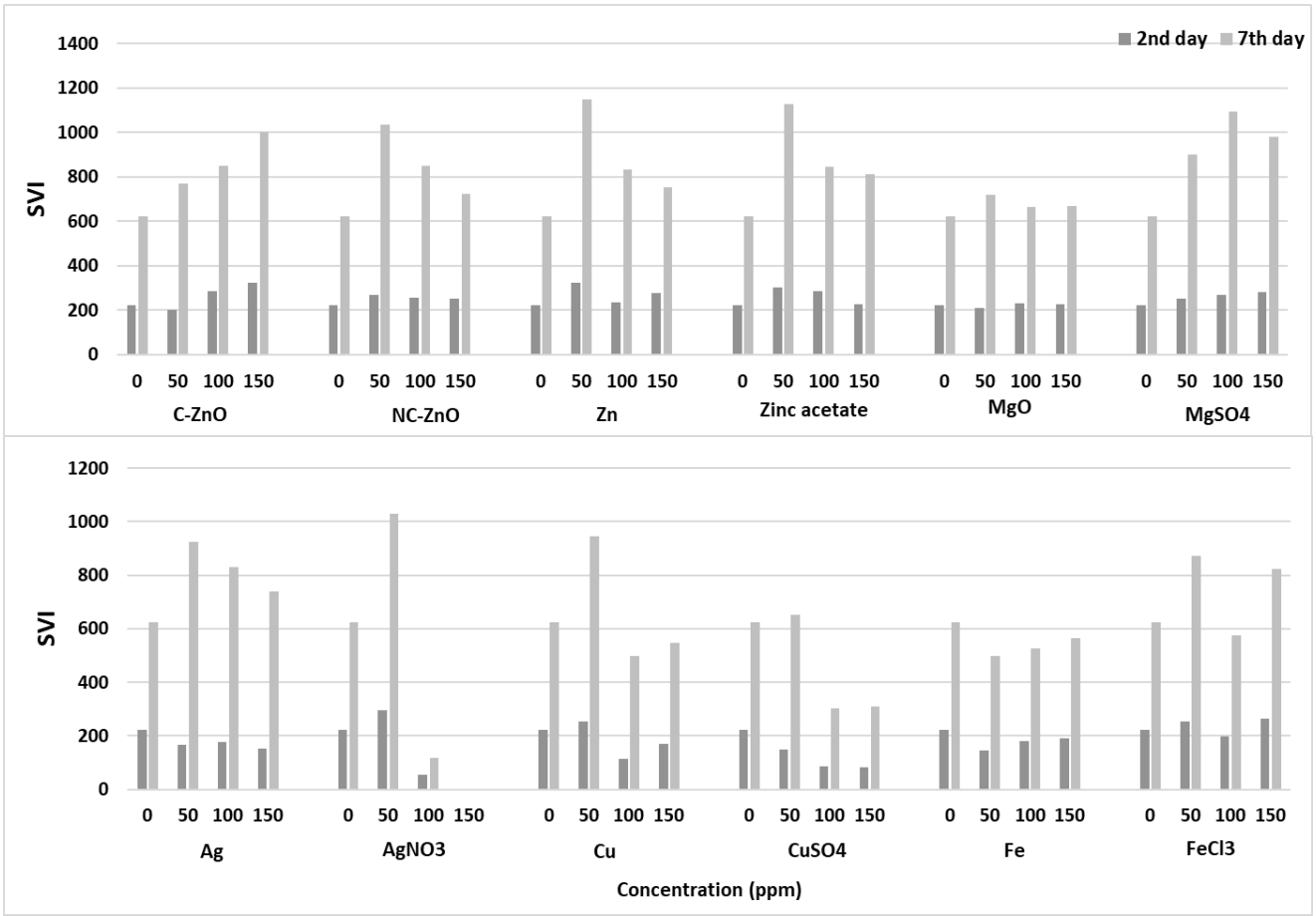

Figure 74: SVI values of the primed flax seeds and control samples at 2nd and 7th days of the experiment.

Table 19: Effect of biogenic NPs priming on seed germination parameters of flax on 2nd day, under different nanoparticle concentrations. Data are presented as mean values ±SD for three independent experiments. The same letters within a column show no significant difference at a 95% probability level at the $p < 0.05$ level.

NP	Concentration (ppm)	Germination percentage (G%)	Shoot length (cm)	Root length (cm)	Seedling length (cm)	Root to shoot ratio	SVI	SLSI (%)	RLSI (%)
Non(Control)	0	86.61±2.12b	0.32±0.04ef	2.24±0.28cd	2.56±0.28c	7.10±1.31a	221.84±24.96c	100.00±0.00f	100.00±0.00bc
C-ZnO	50	86.56±2.23b	0.47±0.04de	1.84±0.47e	2.32±0.49cd	3.83±0.87d	201.05±43.06cd	150.00±13.97e	82.14±21.31e
	100	90.00±1.93a	0.66±0.11bc	2.52±0.20c	3.18±0.25b	3.90±0.72d	286.20±23.29b	206.25±35.63b	112.50±9.14b
	150	83.33±3.3bc	0.74±0.16b	3.12±0.41a	3.86±0.49a	4.35±1.02cd	321.65±41.07a	231.25±52.29ab	139.28±18.51a
NC-ZnO	50	80.03±3.33c	0.64±0.18c	2.74±0.37bc	3.38±0.25b	4.73±1.99c	270.50±20.71b	200.00±56.78b	122.32±16.58ab
	100	80.11±2.98	0.84±0.15a	2.32±0.15cd	3.20±0.22b	2.87±0.50e	256.35±17.91bc	262.5±47.39a	105.35±6.77b
	150	83.43±3.33c	0.82±0.10a	2.20±0.23cd	3.02±0.19b	2.73±0.55e	251.65±16.02bc	256.25±34.23a	98.21±10.46bc
Zn	50	86.66±2.12b	0.74±0.25b	3.00±0.50ab	3.74±0.68a	4.33±1.22bc	324.10±58.96a	231.25±78.43ab	133.92±22.32a
	100	73.43±4.01d	0.70±0.12b	2.50±0.60c	3.20±0.51b	3.78±1.54d	234.65±38.10c	218.75±38.27b	111.60±27.15b
	150	73.33±4.04d	0.70±0.21b	3.08±0.40ab	3.78±0.59a	4.61±0.99c	277.18±43.50b	218.75±66.29b	137.50±18.24a
MgO	50	76.82±3.15d	0.44±0.13de	2.30±0.62cd	2.74±0.71c	5.46±1.74b	210.04±54.63cd	137.50±41.92de	102.67±28.05bc
	100	80.00±2.45c	0.56±0.08d	2.30±0.27cd	2.86±0.25bc	4.20±0.88c	228.80±20.07c	175.00±27.5c-e	102.67±12.22bc
	150	73.33±3.25d	0.66±0.08bc	2.42±0.37c	3.08±0.37b	3.74±0.87d	225.85±27.14c	206.25±27.95b	108.03±16.52b
Ag	50	83.43±3.20c	0.36±0.15ef	1.63±0.65ef	2.00±0.75de	4.65±1.31c	166.66±62.91e	114.58±47.73f	72.91±29.04f
	100	83.83±3.35c	0.44±0.13de	1.66±0.20ef	2.10±0.1d	4.52±3.06c	174.99±8.33de	137.50±41.92ef	74.10±9.25f
	150	80.24±2.86c	0.46±0.6c-e	1.42±0.35fg	1.88±0.44f	3.33±1.36de	150.85±31.85ef	143.75±52.29e	63.39±15.90f
Cu	50	86.66±2.52b	0.58±0.16cd	2.33±0.47cd	2.94±0.61bc	4.20±0.73c	254.78±52.92bc	181.25±51.34cd	105.35±21.08bc
	100	61.00±3.70e	0.38±0.16e	1.50±0.38f	1.88±0.46f	4.55±2.37c	114.68±28.41g	118.75±51.34f	66.96±16.99f
	150	76.55±4.31d	0.62±0.13c	1.58±0.40f	2.20±0.43cd	2.64±0.90ef	166.65±32.97e	193.75±40.16bc	70.53±17.96f
Fe	50	86.55±2.42b	0.42±0.17e	1.26±0.27h	1.86±0.29f	3.39±1.28d	145.58±25.56ef	131.25±55.90de	56.25±12.06g
	100	76.66±4.26d	0.50±0.14d	1.84±0.29e	2.34±0.28cd	3.95±1.40cd	179.38±22.08de	156.25±44.19e	82.14±13.97e
	150	86.66±2.52b	0.62±0.13c	1.58±0.50f	2.20±0.1cd	2.53±0.55ef	190.65±53.06d	193.75±40.74bc	70.53±22.63f
P value		0.0011	0.0001	0.0300	0.0005	0.0066	0.0110	0.0009	0.0043

Table 20: Effect of biogenic NPs priming on seed germination parameters of flax on 7th day, under different nanoparticle concentrations. Data are presented as mean

values ±SD for three independent experiments. The same letters within a column show no significant difference at a 95% probability level at the $p < 0.05$ level.

NP	Concentration (ppm)	Germination percentage (G%)	Shoot length (cm)	Root length (cm)	Seedling length (cm)	Root to shoot ratio	SVI	SLSI (%)	RLSI (%)
Non(Control)	0	93.33±1.87a	3.91±0.20d	2.75±0.68h	6.66±0.75h	0.70±0.16f	622.20±70.25g	100.00±0.00c	100.00±0.00h
C-ZnO	50	86.61±2.42b	4.37±0.62c	4.50±0.57e	8.87±1.10ef	1.03±0.11c	769.10±96.07e	112.17±16.13bc	163.63±20.99ef
	100	86.66±2.52b	4.42±0.29c	5.47±0.75d	9.80±0.62de	1.22±0.23b	849.26±54.34d	115.46±7.65bc	195.45±27.7cd
	150	96.66±1.91a	4.44±0.37c	6.00±0.11cd	10.34±0.65d	1.33±0.12b	999.46±63.23b	114.84±9.69bc	214.54±15.21c
NC-ZnO	50	80.23±2.86bc	5.37±0.25a	7.50±1.58b	12.87±1.37b	1.40±0.36b	1032.96±110.46ab	137.82±6.41b	272.72±57.49b
	100	80.00±2.45bc	4.62±0.47bc	6.00±0.40cd	10.62±0.75d	1.32±0.13b	850.00±60.00d	118.58±12.27bc	218.18±14.84c
	150	83.33±3.33bc	4.12±0.25cd	4.575±0.65e	8.70±0.62f	1.11±0.18bc	724.97±52.26ef	105.76±6.41c	166.36±23.63ef
Zn	50	86.66±2.12b	5.00±0.22ab	8.25±0.86a	13.25±1.25a	1.64±0.06a	1148.24±109.04a	128.20±10.46ab	300.00±31.49a
	100	73.35±3.15d	5.00±0.00ab	6.37±1.25c	11.37±1.10c	1.28±0.33b	834.12±81.29d	128.20±10.46ab	231.81±45.45bc
	150	73.33±3.35d	4.62±1.18bc	5.62±0.62d	10.22±0.64d	1.32±0.57b	751.63±47.33e	118.58±30.29bc	204.54±22.87cd
MgO	50	76.66±4.26d	4.79±0.50b	4.62±0.62e	9.37±0.75e	0.98±0.17c	718.68±57.49ef	121.79±12.82b	168.18±22.87ef
	100	80.30±2.86bc	4.37±0.47bc	3.87±1.10fg	8.45±1.50f	0.87±0.17e	662.47±120.45fg	114.17±12.27bc	140.90±40.31fg
	150	73.33±3.25d	5.00±0.40ab	4.12±0.75ef	9.12±0.75e	0.83±0.19e	669.13±54.99f	128.20±10.46b	150.00±27.27f
Ag	50	90.05±1.98ab	5.37±0.62a	4.87±0.25e	10.25±0.50d	0.91±0.14d	923.01±45.02c	137.39±16.13a	177.27±9.09de
	100	83.33±3.33bc	5.22±0.63a	4.75±1.32e	9.97±1.51d	0.91±0.26d	831.21±126.62d	133.97±16.40a	172.72±48.10e
	150	81.00±2.33bc	4.85±1.25b	4.37±0.75e	9.12±1.84e	0.96±0.25cd	739.12±149.26e	121.79±32.26bc	159.09±27.27f
Cu	50	90.00±1.93ab	4.62±0.47bc	5.87±0.62c	10.50±0.91d	1.27±0.16b	945.00±82.15bc	118.58±12.27bc	213.63±22.87c
	100	76.26±4.25d	3.87±0.47d	2.65±0.47h	6.50±0.40h	0.69±0.17f	498.29±31.29i	99.35±12.27cd	95.45±17.40hi
	150	76.66±4.25d	4.25±0.28c	2.77±0.85h	7.12±0.62g	0.68±0.24f	546.20±48.23h	108.97±7.40c	104.54±31.05h
Fe	50	86.56±2.52b	3.37±0.47e	2.37±0.62i	5.75±1.04i	0.69±0.14f	498.29±90.19i	86.53±12.27e	86.36±22.87i
	100	76.36±4.26d	4.12±0.62cd	2.75±0.61h	6.87±0.75gh	0.68±0.21f	537.03±57.49h	105.76±16.13c	100.00±23.47h
	150	86.64±2.42b	4.12±0.47cd	2.37±0.77i	6.50±0.00h	0.59±0.19g	553.29±0.00h	105.76±12.27c	86.36±17.40i
P value		0.0000	0.0100	0.0007	0.0001	0.0033	0.0082	0.0004	0.0201

Table 21: Effect of metal salt (precursors) priming on seed germination parameters of flax on 2nd day, under different nanoparticle concentrations. Data are presented as mean values ±SD for three independent experiments. The same letters within a column show no significant difference at a 95% probability level at the $p < 0.05$ level.

Metal salt	Concentration (ppm)	Germination percentage (G%)	Shoot length (cm)	Root length (cm)	Seedling length (cm)	Root to shoot ratio	SVI	SLSI (%)	RLSI (%)
Non(Control)	0	86.66±2.52bc	0.32±0.04d	2.24±0.28b	2.56±0.2cd	7.13±1.31a	221±24bc	100.00±0.00c	100.00±0.00bc

$Zn(CH_3CO_2)_2$	50	96.66±1.91a	0.52±0.10a	2.62±0.35ab	3.10±0.3b	5.28±1.52c	303±31a	164.50±34.23a	116.96±15.90b
	100	93.03±1.87ab	0.48±0.08b	2.56±0.28ab	3.04±0.1b	5.40±0.81c	283±30ab	147.00±26.14b	114.28±12.86b
	150	91.00±1.93ab	0.42±0.08bc	2.12±0.88b	2.54±0.7cd	5.27±2.15c	228±79bc	131.25±26.4bc	94.64±39.47c
MgSO4	50	83.33±3.33bc	0.52±0.04a	2.52±0.25ab	3.04±0.2b	4.89±0.78d	255±19b	164.50±13.97a	112.50±11.55b
	100	83.33±2.22bc	0.40±0.12bc	2.80±0.57a	3.2±0.9ab	7.25±1.49a	266±53b	125.00±38.2bc	125.00±25.45a
	150	86.66±2.11bc	0.54±0.16a	2.72±0.31ab	3.26±0.35a	5.58±2.28bc	282±30ab	168.75±52.29a	121.42±13.9ab
AgNO3	50	86.66±2.52bc	0.54±0.15a	2.88±0.61a	3.42±0.54a	5.98±2.96b	297±46a	167.75±47.39a	128.57±27.41a
	100	66.66±2.54d	0.26±0.31e	0.56±0.32ef	0.82±0.6fg	2.00±0.88f	54±41f	81.25±97.82d	25.00±14.32fg
	150	0e	0f	0g	0h	0g	0g	0f	0h
CuSO4	50	86.66±2.52bc	0.40±0.07bc	1.30±0.29d	1.70±0.29e	3.34±0.92e	147±25d	125.00±22.9bc	58.03±13.01e
	100	93.66±2.71ab	0.22±0.16e	0.70±0.12e	0.92±0.2f	3.27±1.88e	86±24e	68.75±51.34e	31.25±5.46f
	150	90.33±3.25b	0.32±0.08d	0.58±0.16ef	0.90±0.1f	1.97±0.76f	82±14e	100.00±26.14c	25.89±7.33fg
FeCl3	50	89.66±1.77b	0.46±0.08b	2.36±0.35b	2.82±0.29c	5.46±2.21c	255±26b	143.75±27.95b	105.35±15.6bc
	100	91.33±3.25ab	0.38±0.08c	1.82±0.20c	2.20±0.5d	5.03±1.41cd	198±14c	120.75±6.14bc	81.25±9.14d
	150	87.00±2.12bc	0.46±0.13b	2.58±0.29ab	3.04±0.4b	5.86±1.12b	264±36b	143.85±41.92b	115.17±13.16b
P value		0.0111	0.0001	0.0008	0.0039	0.0007	0.0004	0.0100	0.0006

Table 22: Effect of metal salt (precursors) priming on seed germination parameters of flax on 7th day, under different nanoparticle concentrations. Data are presented as mean values ±SD for three independent experiments. The same letters within a column show no significant difference at a 95% probability level at the $p < 0.05$ level.

Metal salt	Concentration (ppm)	Germination percentage (G%)	Shoot length (cm)	Root length (cm)	Seedling length (cm)	Root to shoot ratio	SVI	SLSI (%)	RLSI (%)
Non(Control)	0	93.33±1.87a	3.91±0.20de	2.75±0.68h	6.66±0.75g	0.70±0.16e	622±70f	100.00±0.00d	100.00±0.00f
$Zn(CH_3CO_2)_2$	50	86.66±2.52b	5.87±0.7a-c	7.12±1.43a	13.00±1.77a	1.20±0.19bc	112±154i	150.64±12.27b	259.09±52.22a
	100	86.66±2.52b	4.25±0.50d	5.50±0.70cd	9.75±0.64d	1.35±0.26b	844±55de	108.97±12.82d	200.54±18.18c
	150	80.00±2.45bc	4.25±0.86d	5.87±1.10c	10.12±1.43cd	1.43±0.38b	810±114de	108.97±22.20d	213.63±40.31bc
MgSO4	50	83.33±3.33bc	5.00±0.31c	5.81±1.21c	10.81±1.06c	1.17±0.31c	901±88c	128.20±10.46c	211.36±44.14bc
	100	83.33±3.33bc	6.75±3.27a	6.37±2.46b	13.12±3.77a	1.11±0.65c	1093±314a	173.07±84.06a	231.81±89.53b
	150	90.00±1.93a	5.12±1.25c	5.75±0.50c	10.87±0.94c	1.20±0.39bc	978±85bc	131.41±32.05bc	209.09±18.18bc
AgNO3	50	86.66±2.52b	5.62±0.47bc	6.25±0.64b	11.87±0.62b	1.12±0.19c	1029±54b	144.23±12.27b	227.27±23.47b
	100	40.00±4.65e	0.97±0.75g	1.92±1.86i	2.90±2.57i	1.67±1.03a	116±103i	25.00±19.45g	70.00±67.92g
	150	0f	0h	0k	0j	0h	0j	0h	0i
CuSO4	50	76.66±4.26c	5.00±0.40c	3.50±0.70g	8.50±0.70e	0.70±0.17e	651±54f	128.20±10.46c	127.27±25.71ef
	100	73.33±3.25cd	3.37±0.85e	4.62±0.28e	4.00±0.62h	0.24±0.14g	302±46h	86.53±21.89e	27.26±10.49h
	150	80.03±2.86bc	3.12±0.25ef	0.75±0.28j	3.97±0.47h	0.23±0.08g	310±38h	80.12±6.41ef	27.27±10.21h
FeCl3	50	81.00±2.33bc	5.75±0.50bc	5.00±0.70d	10.75±1.19c	0.86±0.05d	870±96d	147.43±12.82b	181.81±25.71d

	100	70.66±1.33cd	5.25±0.50c	2.87±1.10h	8.10±0.47ef	0.58±0.30ef	574±33g	134.61±22.20bc	104.54±40.31f
	150	80.30±2.86bc	6.00±0.57ab	4.25±0.86ef	10.25±0.86cd	0.71±0.17e	823±69de	153.84±14.80b	154.54±31.49de
P value		0.0044	0.0400	0.0006	0.0007	0.0055	0.0050	0.0001	0.0001

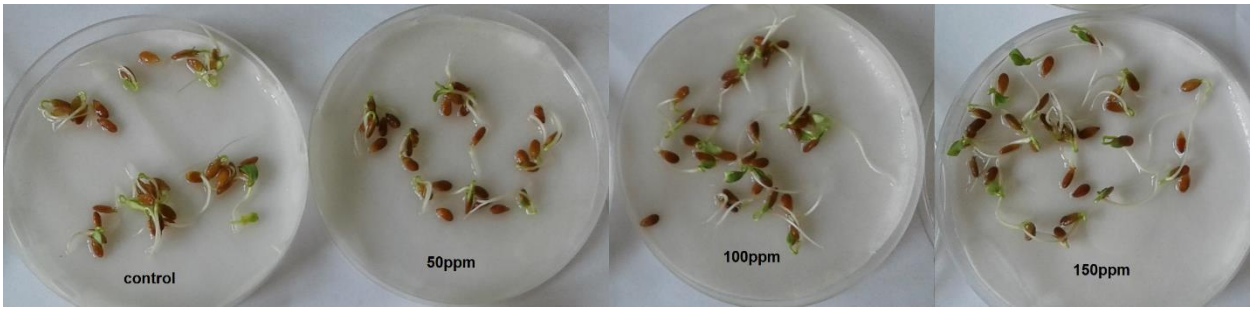

Figure 75. Effect of the C-ZnO NPs on flax seedling growth, on 7th day.

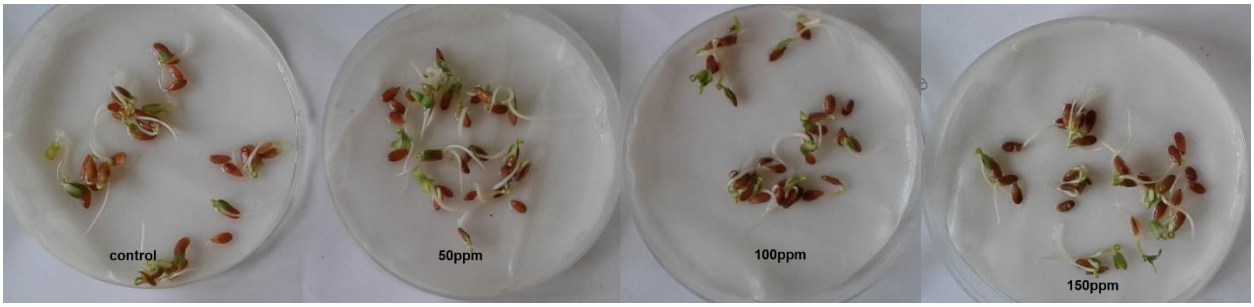

Figure 76. Effect of the NC-ZnO NPs on flax seedling growth, on 7th day.

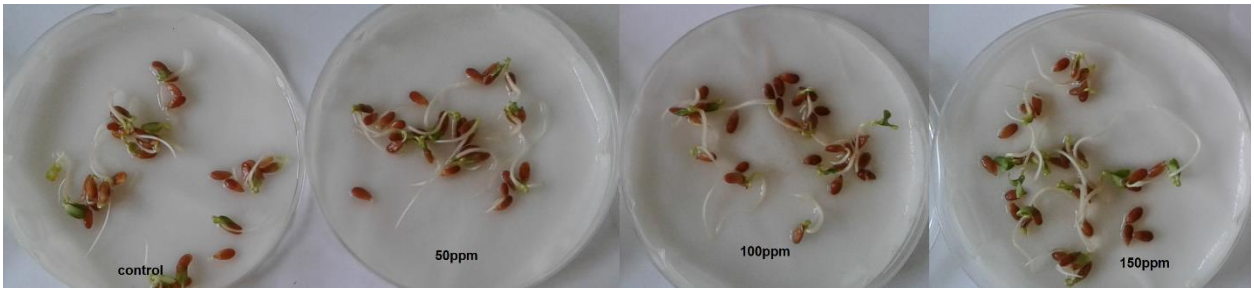

Figure 77. Effect of the Zn NPs on flax seedling growth, on 7th day.

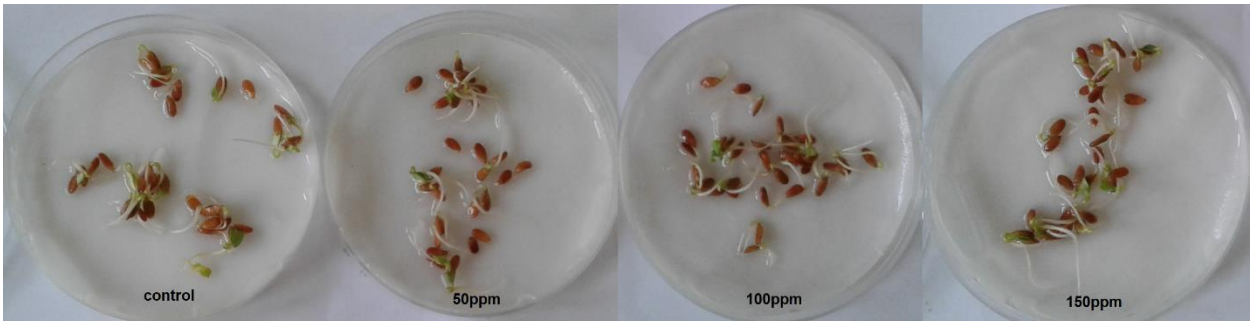

Figure 78. Effect of MgO NPs on flax seedling growth, on 7th day.

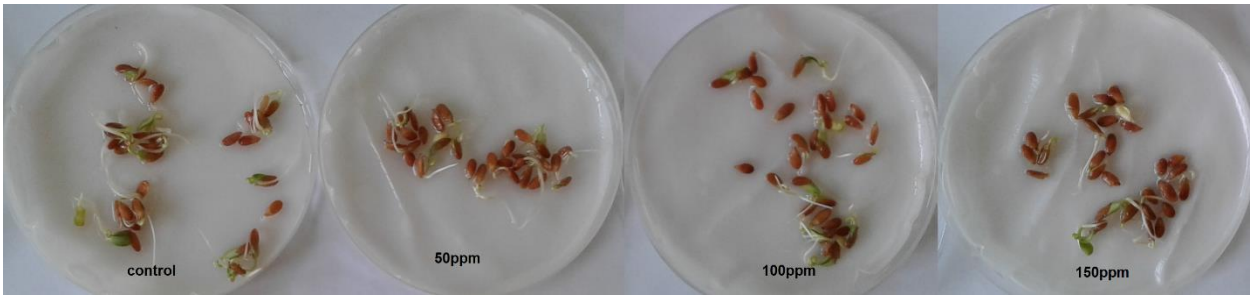

Figure 79. Effect of Ag NPs on flax seedling growth, on 7th day.

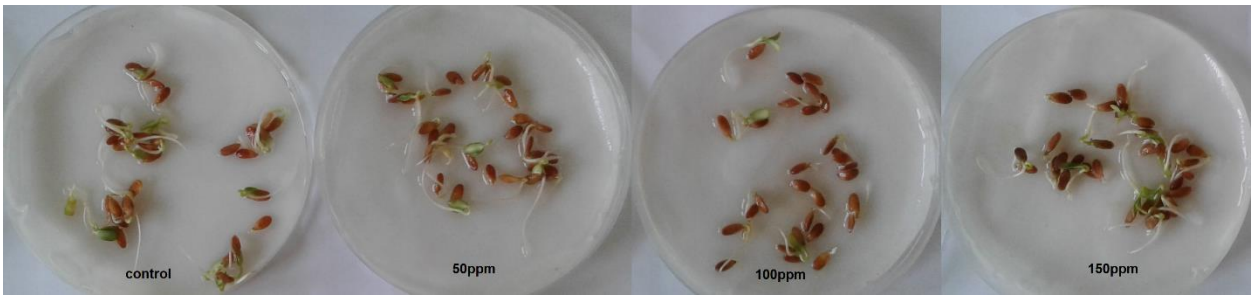

Figure 80. Effect of Cu NPs on flax seedling growth, on 7th day.

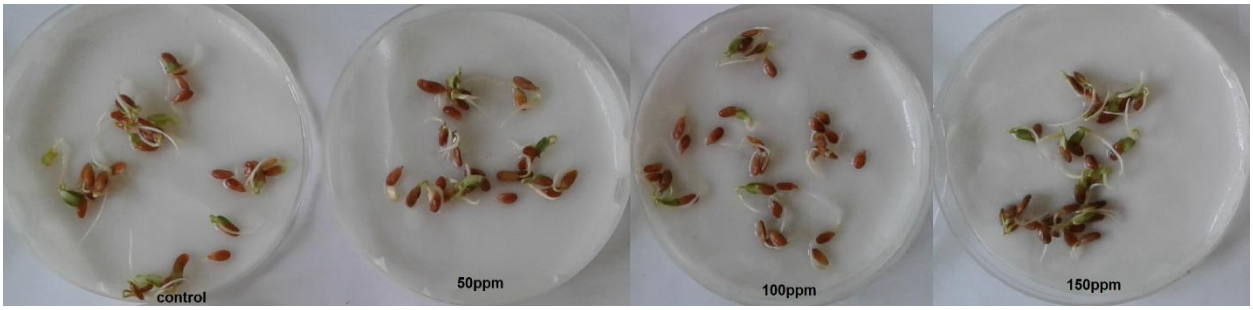

Figure 81. Effect of Fe NPs on flax seedling growth, on 7th day.

3.3.4.3. A comparison between the effect of biogenic NPs and their counterpart salts on physiological characteristics of wheat and flax seedlings

At 7th day of the experiment, in a comparison between the effect of studied NPs in applied concentrations, the most effective one in shoot and root development was Zn NP and the less effective NPs were Ag for wheat and Fe for flax seeds (Figure 82). It shows Zn NPs are not toxic at the applied concentrations and even show stimulating effect on both wheat and flax seeds. Vice versa the applied concentrations of Ag NPs are toxic for wheat but stimulating for flax. As all of the experiment conditions are the same for all of the samples, it could be concluded these differences are related to the seed species. Among the tested metal slats, zinc acetate had the most stimulating effect and $CuSO_4$ was the most toxic one for both flax, and wheat. Nano forms of the metals and also metal oxides, have been reported to significantly improve root or shoot elongation and seed germination of wheat in comparison with bulk materials [124]. This kind of growth development mainly depends on the concentration of NP, duration of nano-priming, growth medium and species of plant [6].

Among measured parameters, root length is more sensitive than shoot length. Between wheat and flax roots, the flax root length was more sensitive against NP and salt treatments and wheat shoot length was the less sensitive parameter. All over,

flax seeds were more sensitive to the treatments compared to the wheat seeds. Although the factors which impact the root and shoot elongation following NP exposure are not clear yet, it could be suggested that the polymeric network of flax seeds mucilage trap NPs or metal ions and then the accessibility of them for flax seeds differs from wheat seeds in the period of our experiment [6].

Figure 83 provides an image for better comparison between germination percentage variations with changes in concentrations of used NPs and salts. In majority of the cases wheat seeds had more G% than flax seeds. 150 ppm of $AgNO_3$ solution had such a toxic effect on flax seeds that no germination was observed in this treatment. Similarly, metal-based NPs are reported to show dual impacts on plants growth, such as seed germination. Positive effects of metal-based NPs treatments were displayed in different plants [111]. Seed germination of soybean seeds enhanced by nano-priming with Co, Fe and Cu NPs [123], also similar findings were reported in the case of some Solanaceae crops after treatment with ZnO and TiO_2 NPs [110].

The obtained results were comparable with those reported by Feizi et al. [124], in which seed treatment with TiO_2 NPs at low concentrations (1-2 ppm) resulted in an improve in germination of wheat seeds and also seedling elongation compared to untreated wheat, but no significant effect at concentration of 100 ppm was observed [124].

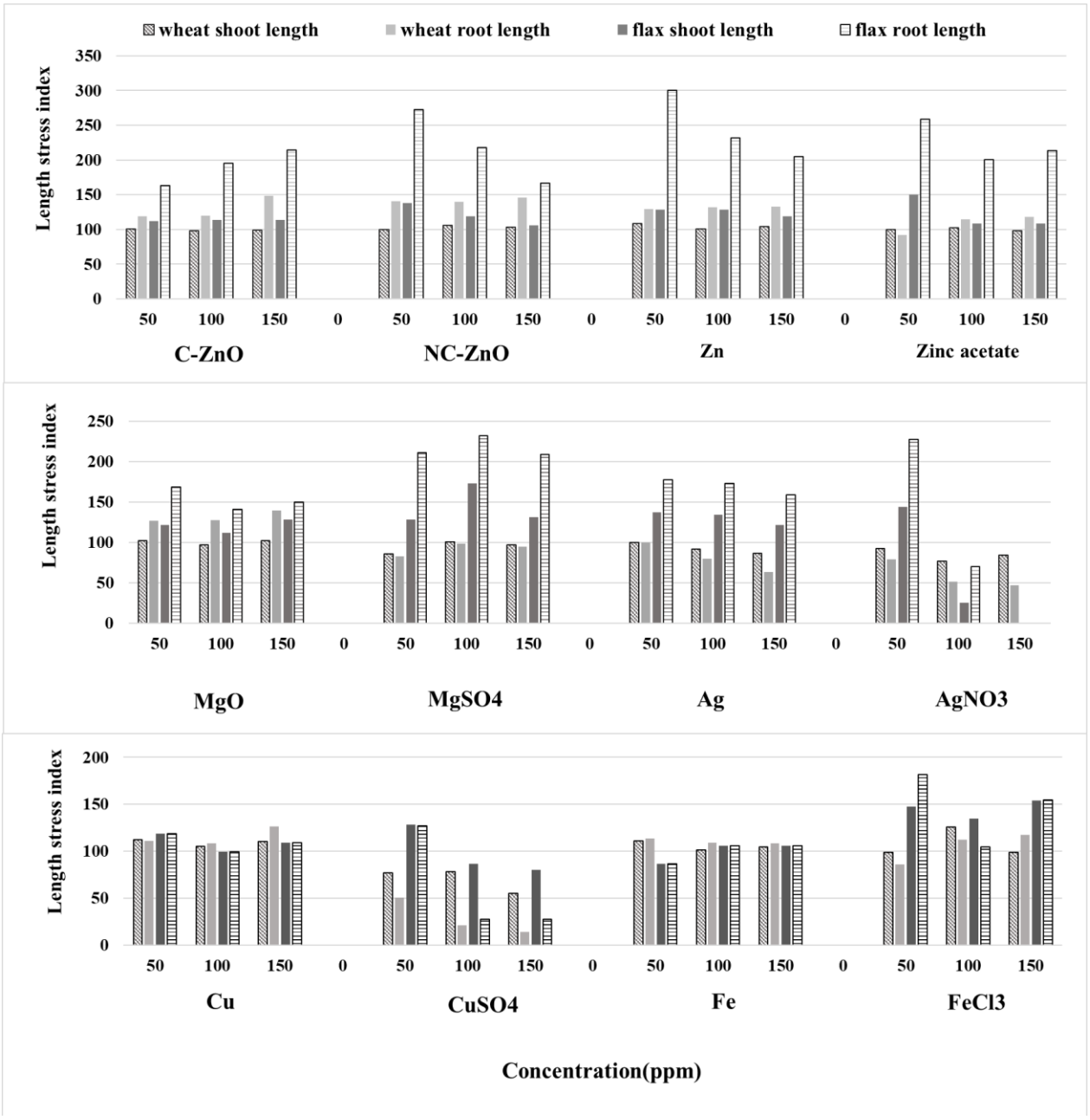

Figure 82: Dose response effect of NPs and their correspondent metal salts on shoot and root stress tolerance index (SLSI and RLSI, respectively) of wheat and flax seeds at 7th day of the experiment.

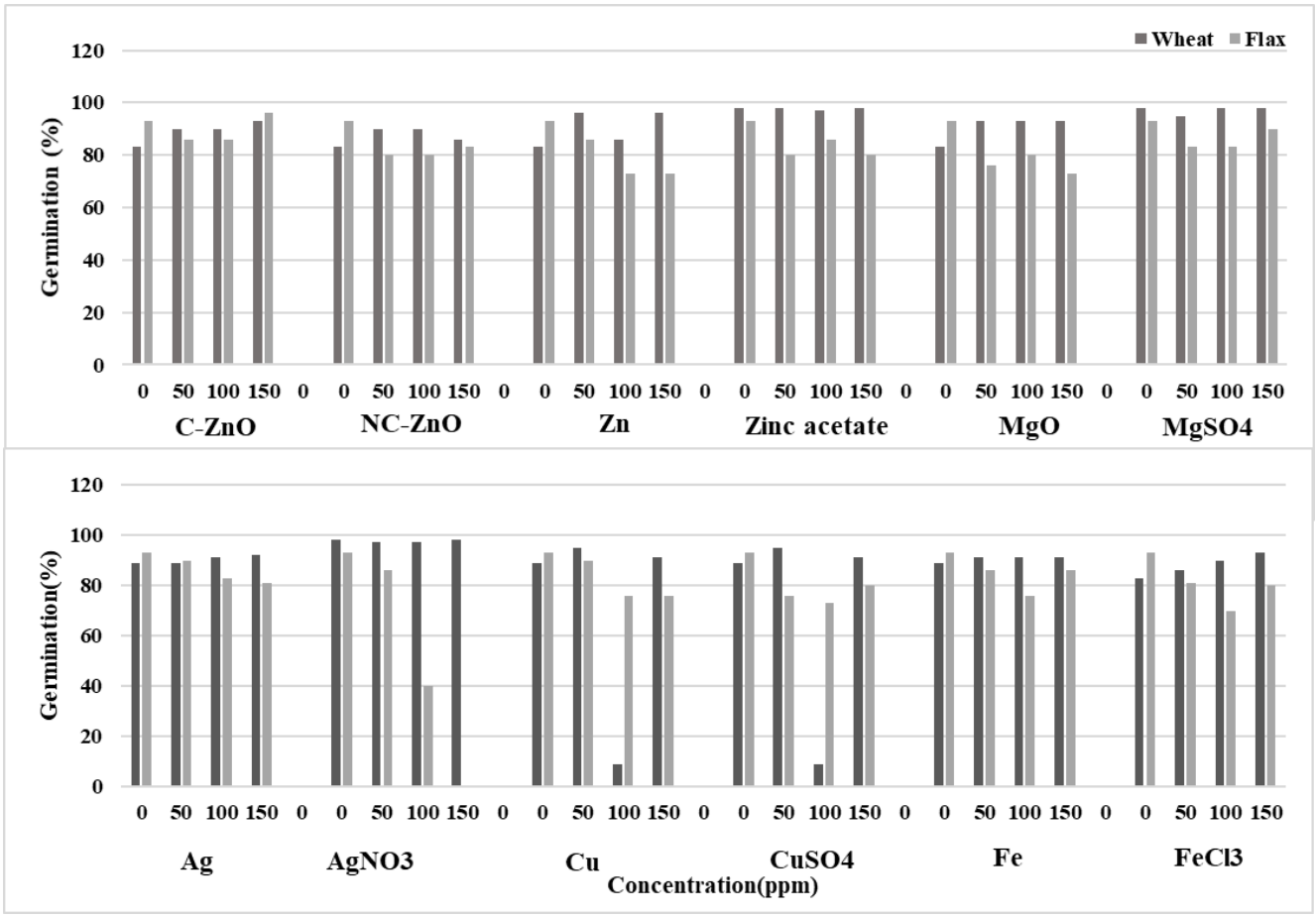

Figure 83: Dose response effect of NPs and their correspondent metal salts on germination percentage of wheat and flax seeds at 7th day of the experiment.

CONCLUSION

Currently, the industrial synthesis of high-quality metal nanoparticles is a major concern. Laser pyrolysis, ultrasonication, UV irradiation, photochemical, etc., are some of the most popular physical and chemical methods used for nanoparticle synthesis. But keeping in mind the biosafety risks associated with the hazardous and toxic chemicals used in order to biosynthesize nanoparticles is a growing concern. Alternative ecofriendly, biological methods for biosynthesis of nanoparticles is a rapidly gaining trend.

Many metal nanoparticles successfully biosynthesized through biological methods. In the agricultural sector, biologically synthesized nanoparticles have given very effective results regarding plant growth promotion and disease management. However, it is worth highlighting that the long-term environmental impact of nanoparticles and their effects on human health are major concerns, even for biosynthesized nanoparticles. There is a lack of consensus on the issue and more studies on the biotoxicity and environmental risks associated with the same must be the focus of future research.

- The water extract of an agro-waste materials, strawberry leaf, prepared and applied instead of chemicals to develop a safe, cost-effective and ecofriendly method.
- During a completely green method, strawberry leaf extract, as a reducing/capping agent, successfully applied in green production of metallic NPs (C-ZnO, NC-ZnO, Zn, MgO, Ag, Cu, Fe)
- Synthesized NPs characterized using several analytical instruments, the nano-size structure of them proved and their characteristics identified. UV-Vis spectroscopy, X-ray Diffraction (XRD) spectroscopy, Field Emission Scanning Electron Microscopy (FESEM) coupled with Energy Dispersive X-

ray Spectroscopy (EDS), Photon Cross-Correlation Spectroscopy (PCCS) and Fourier Transformed Infrared Spectroscopy (FT-IR) were used for that reason.

- Synthesized NPs effect on seedling of wheat and flax studied and compared with effect of metallic salts ($Zn(CH_3COO)_2$, $MgSO_4$, $AgNO_3$, $CuSO_4$, $FeCl_3$), and both effects of improving and toxicity on seedling growth observed
- Synthesized NPs including C-ZnO, NC-ZnO, Ag and Cu, tested against bacteria *Pseudomonas* to evaluate their antibacterial activity and experiments showed satisfactory results
- Synthesized NPs antifungal activity tested on Pathogenic fungi, *Botrytis cinerea, Pilidium concavum* and *Pestalotia sp.* and satisfactory results obtained.

REFERENCES

1. Al-Hakkani M., Biogenic copper nanoparticles and their applications: A review, SN Applied Sciences (2020) 2:505-525, https://doi.org/10.1007/s42452-020-2279-1

2. Mourdikoudis S., Pallares R.M., Thanh N.T.K., Characterization techniques for nanoparticles: Comparison and complementarity upon studying nanoparticle properties. Nanoscale (2018) 10: 12871–12934, doi:10.1039/c8nr02278j.

3. Heera, P., Shanmugam S., Nanoparticle Characterization and Application: An Overview. Int. J. Curr. Microbiol. App. Sci. (2015) 4: 379–386. https://www.ijcmas.com/vol-48/P.%20Heera%20and%20S.%20Shanmugam.pdf.

4. Gondwal M., Pant G. J., Synthesis and Catalytic and Biological Activities of Silver and Copper Nanoparticles Using *Cassia occidentalis*, International Journal of Biomaterials, Volume (2018) 10 pages, https://doi.org/10.1155/2018/6735426

5. Nasrollahzadeh M., Sajadi S. M., Khalaj M., Green synthesis of copper nanoparticles using aqueous extract of the leaves of *Euphorbia esula L* and their catalytic activity for ligand-free Ullmann coupling reaction and reduction of 4-nitrophenol, RSC Adv. (2014) 4: 47313, DOI: 10.1039/c4ra08863h

6. Ahmed B., Rizvi A., Zaidi A., Khan M. S., Musarrat J., Understanding the phyto-interaction of heavy metal oxide bulk and nanoparticles: evaluation of seed germination, growth, bioaccumulation, and metallothionein production, RSC Adv. (2019) 9, 4210, DOI: 10.1039/c8ra09305a

7. Auld D. S., Zinc coordination sphere in biochemical zinc sites, BioMetals (2001) 14: 271–313

8. Wani A. H., Shah M. A., A unique and profound effect of MgO and ZnO nanoparticles on some plant pathogenic fungi, Journal of Applied Pharmaceutical Science (2012) 02 (03): 40-44

9. Vijayaraghavan K., Kamala Nalini S. P., Biotemplates in the green synthesis of silver nanoparticles, Biotechnol. J. (2010) 5: 1098–1110, DOI 10.1002/biot.201000167

10. Gultekin D. D., Gungor A. A., Onem H., Babagil A., Nadaroğlu H., Synthesis of Copper Nanoparticles Using a Different Method: Determination of Their Antioxidant and Antimicrobial Activity, JOTCSA. (2016) 3(3): 623-636

11. Saif S., Tahir A., Chen Y., Green Synthesis of Iron Nanoparticles and Their Environmental Applications and Implications, Nanomaterials (2016) 6, 209, doi:10.3390/nano6110209

12. Agarwal H., Kumar S. V., Rajeshkumar S., A review on green synthesis of zinc oxide nanoparticles – An eco-friendly approach, Resource-Efficient Technologies (2017) 3(4):406-413

13. Roy A., Bulut O., Some S., Mandal A. K., Yilmaz M. D., Green synthesis of silver nanoparticles: biomolecule-nanoparticle organizations targeting, antimicrobial activity, RSC Adv. (2019) 9: 2673, DOI: 10.1039/c8ra08982e

14. Divya N.T., Gautam Y.K., Facile green synthesis and applications of silver nanoparticles: a state-of-the-art review, RSC Adv (2019) 9: 34926, doi: 10.1039/c9ra04164h.

15. Iravani S., Green synthesis of metal nanoparticles using plants, Green Chem. (2011) 13: 2638, DOI: 10.1039/c1gc15386b

16. Narware J., Yadav R., Keswani S., Singh S.P., Sing, H.B., Silver nanoparticle-based biopesticides for phytopathogens: Scope and potential in agriculture, Chapter 13, Nano-Biopesticides Today and Future Perspectives, Elsevier Inc. (2019), doi.org/10.1016/B978-0-12-815829-6.00013-9 303, 2019

17. Mourdikoudis S., Pallares R. M., Thanh N. T. K., Characterization techniques for nanoparticles: comparison and complementarity upon studying nanoparticle properties, Nanoscale (2018,) 10: 12871

18. Heera P., Shanmugam S., Nanoparticle Characterization and Application: An Overview, *Int.J. Curr. Microbiol. App. Sci* (2015) 4(8): 379-386

19. Baer D.R., Engelhard M. H., Johnson G. E., Laskin J., Lai J., Mueller K., Munusamy P., Thevuthasan S., Wang H., Washton N., Surface characterization of nanomaterials and nanoparticles: Important needs and challenging opportunities, Journal of Vacuum Science & Technology A (2013) 31, 050820

20. Lamichhane J. R., Osdaghi E., Behlau F., Köhl J., Jones J. B., Aubertot J. N., Thirteen decades of antimicrobial copper compounds applied in agriculture. A review, Agronomy for Sustainable Development (2018) 38: 28, https://doi.org/10.1007/s13593-018-0503-9

21. Koul O., Nano-Biopesticides Today and Future Perspectives, chapter 13, 2019, Elsevier Inc.. https://doi.org/10.1016/B978-0-12-815829-6.00013-9

22. Khashan K. S., G. M. Sulaiman, Abdulameer F. A., Synthesis and Antibacterial Activity of CuO Nanoparticles Suspension Induced by Laser Ablation in Liquid, Arab J Sci Eng (2016) 41:301–310, DOI 10.1007/s13369-015-1733-7

23. Chung I. M., Rahuman A. A., Marimuthu S., Kirthi A. V., Anbarasan K., Padmini P., Rajakumar G., Green synthesis of copper nanoparticles using *Eclipta prostrata* leaves extract and their antioxidant and cytotoxic activities, Experimental And Therapeutic Medicine (2017) 14: 18-24

24. Nagar N., Devra V., Green synthesis and characterization of copper nanoparticles using Azadirachta indica leaves, Materials Chemistry and Physics (2018) 213: 44e51

25. Siddiqi K. S., Rahman A., Tajuddin, Husen A., Properties of Zinc Oxide Nanoparticles and Their Activity Against Microbes, Nanoscale Research Letters (2018) 13:141, https://doi.org/10.1186/s11671-018-2532-3

26. Mandava K., Kadimcharla K., Keesara N. R., Fatima S. N., Bommena P., Batchu U. R., Green Synthesis of Stable Copper Nanoparticles and Synergistic Activity with Antibiotics, Indian J Pharm Sci (2017) 79(5):695-700

27. Shobha G., Moses V., Ananda S., Biological Synthesis of Copper Nanoparticles and its impact - a Review, International Journal of Pharmaceutical Science Invention (2014) 3 (8): PP.06-28-38

28. Sabir S., Arshad M., Saboon, Satti S. H., Batool T., Farghaulit F., Chaudhari S. K., Effect of green synthesized copper nanoparticle on seed germination and seedling growth in wheat, international journal of bioscience (2018) 13(2): 28-35

29. Almutairi Z.M., Alharbi A., Effect of Silver Nanoparticles on Seed Germination of Crop Plants, Journal of advances in agriculture (2015) 4(1):280-285, DOI:10.24297/jaa.v4i1.4295

30. Pankaj Singh Rawat, Rajeew Kumar, Pradeep Ram, Priyanka Pandey, Effect of Nanoparticles on Wheat Seed Germination and Seedling Growth, International Journal of Agricultural and Biosystems Engineering, Vol:12, No:1, 2018

31. Zaeem A., Drouet S., Anjum S., Khurshid R., Younas M., Blondeau J. P., Tungmunnithum D., Giglioli-Guivarc'h N., Hano C., Abbasi B. H., Effects of Biogenic Zinc Oxide Nanoparticles on Growth and Oxidative Stress Response in Flax Seedlings vs. In Vitro Cultures: A Comparative Analysis, Biomolecules (2020) 10, 918, doi:10.3390/biom10060918

32. Ingale A. G., Chaudhari A. N., Biogenic Synthesis of Nanoparticles and Potential Applications: An Eco-Friendly Approach, Ingale and Chaudhari, J Nanomed Nanotechol (2013) 4:2, http://dx.doi.org/10.4172/2157-7439.1000165

33. Nikolaos Pantidos and Louise E Horsfall, Biological Synthesis of Metallic Nanoparticles by Bacteria, Fungi and Plants, J Nanomed Nanotechnol (2014) 5:5, http://dx.doi.org/10.4172/2157-7439.1000233

34. Singh A., Singh N. B., Afzal S., Singh T., Hussain I., Zinc oxide nanoparticles: a review of their biological synthesis, antimicrobial activity, uptake, translocation and biotransformation in plants, Journal of Material Science (2018) 53:185–201

35. Upadhyaya H., Roy H., Shome S., Tewari S., Bhattacharya M. K., Physiological impact of Zinc nanoparticle on germination of rice (*Oryza sativa* L) seed. J Plant Sci Phytopathol. (2017) 1: 062-070, https://doi.org/10.29328/journal.jpsp.1001008

36. Punjabi K., Mehta S., Chavan R., Chitalia V., Deogharkar D., Deshpande S., Efficiency of Biosynthesized Silver and Zinc Nanoparticles Against Multi-Drug Resistant Pathogens, Front. Microbiol (2018) 9:2207, doi: 10.3389/fmicb.2018.02207

37. Ogunyemi S. O., Abdallah Y., Zhang M., Fouad H., Hong X., Ibrahim E., Masum M. M. I., Hossain A., Mo J., Li B., Green synthesis of zinc oxide nanoparticles using different plant extracts and their antibacterial activity against *Xanthomonas oryzae* pv. oryzae, Artificial Cells, Nanomedicine, and Biotechnology (2019) 47(1): 341-352, DOI: 10.1080/21691401.2018.1557671

38. Dobrucka R., Dugaszewska J., Biosynthesis and antibacterial activity of ZnO nanoparticles using Trifolium pratense flower extract, Saudi Journal of Biological Sciences (2016) 23, 517–523

39. Bhumi G., Savithramma N., Biological synthesis of zinc oxide NPs from Catharanthus roseus (L.) G. Don. Leaf extract and validation for antibacterial activity. Int J Drug Dev Res (2014) 6(1):208–214

40. Ates M., Daniels J., Arslan Z., Farah I.O., Rivera H.F. Comparative evaluation of impact of Zn and ZnO nanoparticles on brine shrimp (Artemia salina) larvae: effects of particle size and solubility on toxicity. Environ sci Processes Impacts (2013) 1(10), doi:10.1039/c2em30540b

41. Yuvakkumar R., Suresh J., Nathanael A. J., Sundrarajan M., Hong S.I., Novel green synthetic strategy to prepare ZnO nanocrystals using rambutan (*Nephelium lappaceum* L.) peel extract and its antibacterial applications, Materials Science and Engineering C (2014) 41:17–27

42. Jeevanandam J., Chan Y. S., Danquah M. K., Biosynthesis and characterization of MgO nanoparticles from plant extracts via induced molecular nucleation, *New Journal of Chemistry* (2017) 41: 2800

43. Jhansi K., Jayarambabu N., Reddy K. P., Reddy N. M., Suvarna R. P., Rao K. V., Kumar V. R., Rajendar V., Biosynthesis of MgO nanoparticles using mushroom extract: effect on peanut (Arachis hypogaea L.) seed germination, 3 Biotech (2017) 7:263, DOI 10.1007/s13205-017-0894-3

44. S Moorthy K., Ashok C. H., Rao K. V., Viswanathan C., synthesis and characterization of MgO nanoparticles by neem leaves through Green method, Materials Today: Proceedings 2 (2015) 4360 – 4368

45. Sushma N. J., Prathyusha D., Swathi G., Madhavi T., Raju B. D. P, Mallikarjuna K., Kim H. S., Facile approach to synthesize magnesium oxide nanoparticles by using Clitoria ternatea—characterization and in vitro antioxidant studies, Applied Nanoscience (2016) 6:437–444, DOI 10.1007/s13204-015-0455-1

46. Abdallah Y., Ogunyemi S. O., Abdelazez A., Zhang M., Hong X., Ibrahim E., Hossain A., Fouad H., Li B., Chen J., The Green Synthesis of MgO Nano-Flowers Using Rosmarinus officinalis L. (Rosemary) and the Antibacterial Activities against Xanthomonas oryzae pv. Oryzae, BioMed Research International, Volume 2019, 8 pages, https://doi.org/10.1155/2019/5620989

47. Krishnaraj C., Jagan E.G., Rajasekar S., Selvakumar P., Kalaichelvan P.T., Synthesis of silver nanoparticles using Acalypha indica leaf extracts and its antibacterial activity against water borne pathogens. Colloids Surf B Biointerfaces (2010) 76: 50-56

48. Behravan M., Panahi A. H., Naghizadeh A., Ziaee M., Mahdavi R., Mirzapour A., Facile green synthesis of silver nanoparticles using Berberis vulgaris leaf and root aqueous extract and its antibacterial activity, International Journal of Biological Macromolecules (2019) 124:148–154

49. Lukman A.I., Gong B., Marjo C.E., Roessner U., Harris A.T. Facile synthesis, stabilization, and anti-bacterial performance of discrete Ag nanoparticles using Medicago sativa seed exudates. J Colloid Interface Sci (2011) 353: 433-444

50. Huang W., Yan M., Duan H., Bi Y., Cheng X., Yu H., Synergistic Antifungal Activity of Green Synthesized Silver Nanoparticles and Epoxiconazole against Setosphaeria turcica, Journal of Nanomaterials, Volume 2020, 7 pages, https://doi.org/10.1155/2020/9535432

51. Kasthuri J., Kathiravan K., Rajendiran N. Phyllanthin-assisted biosynthesis of silver and gold nanoparticles: a novel biological approach. Journal of Nanoparticle Research (2008) 11: 1075-1085

52. Song J.Y., Kim B.S. Rapid biological synthesis of silver nanoparticles using plant leaf extracts. Bioprocess Biosyst Eng (2009) 32: 79-84

53. Mahakham W., Sarmah A. K., Maensiri S., Theerakulpisut P., Nanopriming technology for enhancing germination and starch metabolism of aged rice seeds using phytosynthesized silver nanoparticles, Scientific Reports (2017) 7: 8263, DOI:10.1038/s41598-017-08669-5

54. Zhang D., Ma X. L., Gu Y., Huang H., Zhang G. W., Green Synthesis of Metallic Nanoparticles and Their Potential Applications to Treat Cancer, *Front. Chem. (2020) 8:799,* doi:10.3389/fchem.2020.00799

55. Murthy A., Abebe B., Desalegn T., Prakash C. H., Shantaveerayya K., A Review on Green Synthesis and Applications of Cu and CuO Nanoparticles *Mat. Sci. Res. India* (2018) 15(3): 279-295

56. Murthy H. C. A., Desalegn T., Kassa M., Abebe B., Assefa T., Synthesis of Green Copper Nanoparticles Using Medicinal Plant Hagenia abyssinica (Brace) JF. Gmel. Leaf Extract: Antimicrobial Properties, Journal of Nanomaterials, Volume 2020, 12 pages, https://doi.org/10.1155/2020/3924081

57. Padma P. N., Banu S. T., Kumari S.C., Studies on Green Synthesis of Copper Nanoparticles Using *Punica granatum*, *Annual Research & Review in Biology* (2018) 23(1): 1-10, DOI: 10.9734/ARRB/2018/38894

58. Herlekar M., Barve S., Kumar R., Plant-Mediated Green Synthesis of Iron Nanoparticles, Journal of Nanoparticles, Volume 2014, 9 pages, http://dx.doi.org/10.1155/2014/140614

59. Gautam A., Rawat S., Verma L., Singh J., Sikarwar S., Yadav B.C., Kalamdhad A. S., Green synthesis of iron nanoparticle from extract of waste tea: An application for phenol red removal from aqueous solution, Environmental Nanotechnology, Monitoring & Management (2018) 10: 377–387

60. Murgueitio E., Cumbal L., Abril M., Izquierdo A., Debut A., Tinoco O., Green Synthesis of Iron Nanoparticles: Application on the Removal of Petroleum Oil from Contaminated Water and Soils, Journal of Nanotechnology, Volume 2018, 8 pages, https://doi.org/10.1155/2018/4184769

61. Saranya S., Vijayarani K., Pavithra S., Green Synthesis of Iron Nanoparticles using Aqueous Extract of *Musa ornata* Flower Sheath against Pathogenic Bacteria, Indian Journal of Pharmaceutical Sciences (2017) 79(5):688-694

62. Gottimukkala K. S. V., Green Synthesis of Iron Nanoparticles Using Green Tea leaves Extract, Gottimukkala, J Nanomedine Biotherapeutic Discov (2017) 7:1, DOI: 10.4172/2155-983X.1000151

63. Ebrahiminezhad A., Zare-Hoseinabadi A., Berenjian A., Ghasemi Y., Green synthesis and characterization of zerovalent iron nanoparticles using stinging nettle

(*Urtica dioica*) leaf extract, Green Process Synth (2017) 6(5): 469-475, DOI 10.1515/gps-2016-0133

64. Mushinskiy A. A., Aminova E. V., Effect of iron, copper and molybdenum nanoparticles on morphometric parameters of Solanum tuberosum L. plants, IOP Conf. Series: Earth and Environmental Science (2019) 341:012195, doi:10.1088/1755-1315/341/1/012195

65. Ngo Q. B., Dao T. H., Nguyen H. C., Tran X. T., Nguyen T. V., Khuu T. D., Huynh T. H., Effects of nanocrystalline powders (Fe, Co and Cu) on the germination, growth, crop yield and product quality of soybean (Vietnamese species DT-51), Advances in Natural Sciences: Nanoscience and Nanotechnology, (2014) 5: 015016 (7pp), doi:10.1088/2043-6262/5/1/015016

66. Alam M. D. J., Sultana F., Iqbal M. D. T., Potential of Iron Nanoparticles to Increase Germination and Growth of Wheat Seedling, J Nanosci Adv Tech (2015) 1(3): 14-20, doi: https://doi.org/10.24218/jnat.2015.12

67. Holder C. F., Schaak R. E., Tutorial on Powder X-ray Diffraction for Characterizing Nanoscale Materials, ACS Nano. (2019) 13: 7359−7365. DOI: 10.1021/acsnano.9b05157

68. Aaron S.E., Tosheska-Trajkovska K., Cekovska S., Aaron J.J., Establishment of an EC50 database of pesticides using a Vibrio fischeri bioluminescence method. *Luminescence* (2019) 1–4, doi: 10.1002/bio.3628.

69. Balouiri M., Sadiki M., Ibnsouda S.K., Methods for in vitro evaluating antimicrobial activity: A review. *Journal of Pharmaceutical Analysis* (2016) *6*: 71–79, doi.org/10.1016/j.jpha.2015.11.005.

70. Koneman E.W., Allen S.D., Janda W.M., Schreckenberger P.C., Winn J.R., Color atlas and textbook of diagnostic microbiology, 5th ed. Lippincott-Raven Publishers, Philadelphia, Pa (1997).

71. Ghojavand S., Madani M., Karimi J., Green Synthesis, Characterization and Antifungal Activity of Silver Nanoparticles Using Stems and Flowers of Felty Germander. Journal of Inorganic and Organometallic Polymers and Materials (2020) 1(3): 14-20, https://doi.org/10.1007/s10904-020-01449-1.

72. Arciniegas-Grijalba P.A., Patin˜o-Portela M.C., Mosquera-Sa´nchez L.P., Guerrero-Vargas J.A., Rodrı´guez-Pa´ez J.E., ZnO nanoparticles (ZnO-NPs) and their antifungal activity against coffee fungus Erythricium salmonicolor, Appl Nanosci. (2017) 7: 225–241. DOI 10.1007/s13204-017-0561-3.

73. United States Environmental Protection Agency– USEPA. Ecological effects test guidelines terrestrial plant toxicity, *tier I (seedling emergence)*, 1996.

74. Raskar S., Laware S. L., Effect of titanium dioxide nano particles on seed germination and germination indices in onion. Plant Sciences Feed (2013) 3 (9): 103-107.

75. Ushahra J., Malik C.P., Putrescine and Ascorbic Acid Mediated Enhancement In Growth And Antioxidant Status Of Eruca Sativa Varieties, Tech Journal of Biotechnology (2013) 2 (4): 53-64

76. Herlekar M., Barve S., Kumar R., Plant-Mediated Green Synthesis of Iron Nanoparticles, Journal of Nanoparticles, Volume 2014, 9 pages, http://dx.doi.org/10.1155/2014/140614

77. Chikkanna M. M., Neelagund S. E., Rajashekarappa K. K., Green synthesis of Zinc oxide nanoparticles (ZnO NPs) and their biological activity, SN Applied Sciences (2019) 1:117, https://doi.org/10.1007/s42452-018-0095-7

78. Gupta M., Tomar R. S., Kaushik S., Mishra R. K., Sharma D., Effective Antimicrobial Activity of Green ZnO Nano Particles of Catharanthus roseus, Front. Microbiol. (2018) 9:2030. doi: 10.3389/fmicb.2018.02030

79. Mubayi A., Chatterji S., Rai P. M., Geeta Watal, Evidence based green synthesis of nanoparticles, Adv. Mat. Lett. (2012) 3(6), 519-525

80. Devi H. S., Boda M. A., Shah M. A., Parveen S., Wani A. H., Green synthesis of iron oxide nanoparticles using *Platanus orientalis* leaf extract for antifungal activity, Green Process Synth (2019) 8: 38–45, doi.org/10.1515/gps-2017-0145

81. Baláž M., Balážová Ľ., Daneu, N. Dutková E., Balážová M., Bujňáková Z., Shpotyuk Y., Plant-Mediated Synthesis of Silver Nanoparticles and Their Stabilization by Wet Stirred Media Milling,. *Nanoscale Res. Lett.* (2017) *12*, 83, doi:10.1186/s11671-017-1860-z.

82. Dobrucka R., Synthesis of MgO Nanoparticles Using *Artemisia abrotanum* Herba Extract and Their Antioxidant and Photo-catalytic Properties. *Iran J. Sci. Technol. Trans. Sci.* (2018) *42*, 547–555, doi: 10.1007/s40995-016-0076-x.

83. Vergheese M., Vishal S.K., Green synthesis of magnesium oxide nanoparticles using Trigonella foenum-graecum leaf extract and its antibacterial activity. *J. Pharmacogn. Phytochem*. (2018) *7*, 1193–1200, https://www.phytojournal.com/archives/?year=2018&vol=7&issue=3&ArticleId=4326.

84. Ijaz F., Shahid S., Khan S., Ahmad W., Zaman S., Green synthesis of copper oxide nanoparticles using Abutilon indicum leaf extract: Antimicrobial, antioxidant and photocatalytic dye degradation activitie. *Trop. J. Pharm. Res.* (2017) *16*, 743, doi:10.4314/tjpr.v16i4.2.

85. Scimeca M., Bischetti S., Lamsira H.K., Bonfiglio R., Bonanno E., Energy Dispersive X-ray (EDX) microanalysis: A powerful tool in biomedical research and diagnosis. *Eur. J. Histochem.* (2018) *62*, 2841, doi:10.4081/ejh.2018.2841.

86. Koupaei M.H., Shareghi B., Saboury A.A., Davar F., Semnani A., Evini M., Green synthesis of zinc oxide nanoparticles and their effect on the stability and activity of proteinase K. *RSC Adv.* (2016) *6*, 42313–42323, doi:10.1039/c5ra24862k.

87. Hussein E.A.M., Mohammad A. A. H., Harraz F.A., Ahsan M.F., Biologically Synthesized Silver Nanoparticles for Enhancing Tetracycline Activity Against Staphylococcus aureus and Klebsiella pneumoniae. *Braz. Arch. Biol. Technol.* (2019) *62*, 19180266, doi:10.1590/1678-4324-2019180266.

88. Nandiyanto A. B. D., Oktiani R., Ragadhita R., How to Read and Interpret FTIR Spectroscope of Organic Material. *Indones. J. Sci. Technol.* (2019) *4*, 97–118, doi:10.17509/ijost.v4i1.15806.

89. Rajakumar G., Rahuman A. A., Roopan S. M., Chung I. M., Anbarasan K., Karthikeyan V., Efficacy of larvicidal activity of green synthesized titanium dioxide nanoparticles using Mangifera indica extract against blood-feeding parasites. *Parasitol. Res.* (2015) *114*, 571–581, doi:10.1007/s00436-014-4219-8.

90. Singh A., Singh N., Hussain I., Singh H., Yadav V., Singh S., Green synthesis of nano zinc oxide and evaluation of its impact ongermination and metabolic activity of *Solanum lycopersicum. J. Biotechnol.* (2016) *233*, 84–94, doi: 10.1016/j.jbiotec.2016.07.010.

91. Amargeetha A., Velavan S., X-ray Diffraction (XRD) and Energy Dispersive Spectroscopy (EDS) Analysis of Silver Nanopar-ticles Synthesized from Erythrina Indica Flowers. *Nanosci. & Technol.* (2018) *5*, 1–5.

92. Kihara K., Donnay G., Anharmonic thermal vibrations in ZnO, *The Canadian Mineralogist* (1985) *23*, 647–654, https://pubs.geoscienceworld.org/canmin/article-abstract/23/4/647/11836/Anharmonic-thermal-vibrations-in-ZnO.

93. Schulz H., Thiemann K., Crystal structure refinement of AlN and GaN. *Solid State Commun.* (1977) *23*, 815–819, doi:10.1016/0038-1098(77)90959-0.

94. Schiebold E., Zeitschrift fuer Kristallographie, Kristallgeometrie, Kristallphysik, *Kristallchemie.* (1927) *56*, 430, https://crystallography.io/catalog/44.

95. Owen E. I., Williams G., A low-temperature X-ray camera. *J. Sci. Instruments* (1954) *31*, 49–54, doi:10.1088/0950-7671/31/2/305.

96. Govrin E.M., Levine A., The hypersensitive response facilitates plant infection by the necrotrophic pathogen *Botrytis cinerea*. *Current biology* (2000) *10*, 13, 751-757, doi.org/10.1016/S0960-9822(00)00560-1.

97. Fernández-Ortuño D., Bryson P. K., Schnabel G., First Report of *Pilidium concavum* Causing Tan-brown Rot on Strawberry Nursery Stock in South Carolina. *Plant Dis* (2014) *98*, 7, 1010, doi: 10.1094/PDIS-01-14-0048-PDN. PMID: 30708876.

98. Moshayedi M., Rahanandeh H., Hamzeh, A., In vitro evaluation of some fungicides and tea extract against *Pestalotia sp.* and *Colletotrichum sp*., the causal agents of leaf spot and anthracnose of azalea. *Journal of Ornamental Plants* (2017) 7, 1, 45-51.

99. Karaman D.S., Manner S., Fallarero A., Jessica M., Current Approaches for Exploration of Nanoparticles as Antibacterial Agents. *Antibacterial agent* 2017, doi.org/10.5772/68138.

100. Okafor F., Janen A., Kukhtareva T., Edwards V., Curley M., Green Synthesis of Silver Nanoparticles, Their Characterization, Application and Antibacterial Activity. *Int. J. Environ. Res. Public Health* (2013) *10*, 5221-5238, doi:10.3390/ijerph10105221.

101. Patra J.K., Baek K.H., Antibacterial Activity and Synergistic Antibacterial Potential of Biosynthesized Silver Nanoparticles against Foodborne Pathogenic Bacteria along with its Anticandidal and Antioxidant Effects. *Frontiers in Microbiology* (2017) 8, 167, doi: 10.3389/fmicb.2017.00167.

102. Gorczyca A., Przemieniecki S.W., Kurowski T., Ocwieja M., Early plant growth and bacterial community in rhizoplane of wheat and flax exposed to silver and titanium dioxide nanoparticles. *Environmental Science and Pollution Research* (2018) *25*, 33820–33826.

103. Pandian S. R. K., Deepak V., Kalishwaralal K., Viswanathan P., Gurunathan S., Mechanism Of Bactericidal Activity Of Silver Nitrate – A Concentration Dependent Bifunctional Molecule, *Brazilian Journal of Microbiology* (2010) 41: 805-809

104. Hidalgo E., Bartolomé R., Barroso C., Moreno A., Domínguez C., Silver Nitrate: Antimicrobial Activity Related to Cytotoxicity in Cultured Human Fibroblasts, Skin Pharmacol Appl Skin Physiol (1998) 11:140–151 (DOI:10.1159/000029820)

105. Ebrahimi K., Shiravand S., Mahmoudvand H., Biosynthesis of copper nanoparticles using aqueous extract of *Capparis spinosa* fruit and investigation of its antibacterial activity. *Marmara Pharmaceutical Journal* (2017) *21*, 4, 866-871.

106. Kim S.W., Jung J. H., Lamsal K., Kim Y.S., Min J.S., Lee Y.S., Antifungal Effects of Silver Nanoparticles (AgNPs) against Various Plant Pathogenic Fungi. *Mycobiology* (2012) *40*, 1, 53-58.

107. Krutyakov Y., Kudrinskiy A., Zherebin P., Yapryntsev A., Pobedinskaya M., Elansky S., Denisov A., Mikhaylov D., Lisichkin G., Tallow amphopolycarboxyglycinate-stabilized silver nanoparticles: new frontiers in development of plant protection products with a broad spectrum of action against phytopathogens. *Materials Research Express* (2016) *3*, 1–9.

108. Min J.S., Kim K.S., Kim S.W., Jung J. H., Lamsal K., Kim S.B., Jung M., Lee Y.S., Effects of colloidal silver nanoparticles on sclerotium-forming phytopathogenic fungi. *J. Plant Pathol* (2009) *25*, 376–380.

109. Mishra S., Keswani C., Singh A., Singh B.R., Singh S.P., Singh H.B., Microbial nanoformulation: exploring potential for coherent nano-farming, *The Handbook of Microbial Bioresourses*. (2016) CABI, London, pp. 107–120.

110. Younes N. A., Hassan H. S., Elkady M. F., Hamed A. M., Mona F.A., Dawood, Impact of synthesized metal oxide nanomaterials on seedlings production of three Solanaceae crops, Heliyon 6 (2020) e03188

111. Szollosi R., Molnár A., Kondak S., Kolbert Z., Dual Effect of Nanomaterials on Germination and Seedling Growth: Stimulation vs. Phytotoxicity. *Plants*, (2020) 9, 1745-1776. doi:10.3390/plants9121745

112. Baddar Z. E., Unrine J. M., Functionalized-ZnO-Nanoparticle Seed Treatments to Enhance Growth and Zn Content of Wheat (Triticum aestivum) Seedlings, *J. Agric. Food Chem.*, (2018) 66, 12166−12178, DOI: 10.1021/acs.jafc.8b03277

113. Allaby M., A Dictionary of Plant Sciences (2 ed.), *Oxford University Press* (2006).

114. Zhao X., Joo J. C., Kim D., Lee J. K., Kim J. Y., Estimation of the Seedling Vigor Index of Sunflowers Treated with Various Heavy Metals, *J Bioremed Biodeg*, (2016) 7, 353-359. doi:10.4172/2155-6199.1000353

115. Ko K.S., Koh D. C., Kong I. C., Evaluation of the Effects of Nanoparticle Mixtures on Brassica Seed Germination and Bacterial Bioluminescence Activity Based on the Theory of Probability. *Nanomaterials*, (2017) 7, 344-344. doi:10.3390

116. Vanninia C., Domingoa G., Onellib E., De Mattiac F., Brunic I., Marsonia M., Bracale M., Phytotoxic and genotoxic effects of silver nanoparticles exposure on germinating wheat seedlings, *Journal of Plant Physiology*, (2014) 171, 1142–1148. DOI:10.1016/j.jplph.2014.05.002

117. Abbasi Khalaki M., Ghorbani A., Moameri M., Effects of Silica and Silver Nanoparticles on Seed Germination Traits of Thymus kotschyanus in Laboratory Conditions, *Journal of Rangeland Science*, (2016) 6 (3), 221-231.

118. Zakharova O. V., Kolesnikov E.A., Shatrova N., Gusev A., The effects of CuO nanoparticles on wheat seeds and seedlings and Alternaria solani fungi: in vitro

study, *FORESTRY, IOP Conf. Series: Earth and Environmental Science*, (2019) 226, 012036-012046. doi:10.1088/1755-1315/226/1/012036

119. Yasmeen F., Razzaq A., Iqbal M. N., Jhanzab H. M., Effect of silver, copper and iron nanoparticles on wheat germination, *International Journal of Biosciences*, (2015) 6(4), 112-117. DOI:10.12692/ijb/6.4.112-117

120. Du W., Sun Y., Ji R., Zhu J.,Wu J., Guo H., TiO_2 and C-ZnO nanoparticles negatively affect wheat growth and soil enzyme activities in agricultural soil, *Journal of Environmental Monitoring*, (2011) 13, 822–828. DOI:10.1039/c0em00611d

121. Plaksenkova I., Jermaļonoka M., Bankovska L., Gavarāne I., Gerbreders V., Sledevskis E., Sniķeris J., Kokina I., Effects of Fe3O4 Nanoparticle Stress on the Growth and Development of Rocket Eruca sativa, *Journal of Nanomaterials*, (2019) 4, 1-10. https://doi.org/10.1155/2019/2678247

122. Hao Y., Zhang Z., Rui Y., Ren J., Hou T., Wu S., Rui M., Jiang F., Liu L., Effect of Different Nanoparticles on Seed Germination and Seedling Growth in Rice, *2nd Annual International Conference on Advanced Material Engineering* (AME 2016) (2016), 166-173. DOI:10.2991/ame-16.2016.28

123. Mehtre A. S., Syed H. M. Agrawal R. S.. Extraction and chemical composition of flaxseed gum (mucilage) from different flaxseed varieties, *The Bioscan*, (2017) 12(1), 47-49.

124. Feizi H., Rezvani Moghaddam P., Shahtahmassebi N., Fotovat A., Impact of bulk and nanosized titanium dioxide (TiO_2) on wheat seed germination and seedling growth, *Biol. Trace Elem. Res*, (2012) 146(1),101-107. DOI: 10.1007/s12011-011-9222-7